THE UNIVERSITY OF ALBERTA

A NUMERICAL STUDY OF THE SEA-BREEZE

BY

© STEVEN J. LAMBERT

A THESIS

SUBMITTED TO THE FACULTY OF GRADUATE STUDIES AND RESEARCH

IN PARTIAL FULFILMENT OF THE REQUIREMENTS FOR THE DEGREE

OF MASTER OF SCIENCE

DEPARTMENT OF GEOGRAPHY

EDMONTON, ALBERTA

SPRING, 1973

ABSTRACT

The non-linear equations for an incompressible turbulent atmosphere are integrated numerically to investigate the sea-breeze circulation. Solutions are presented for various initial states of the atmosphere. In addition, liquid water and water vapour are incorporated to permit the study of the effect of the sea-breeze circulation on a coastal fog bank.

ACKNOWLEDGEMENTS

I wish to thank my supervisor, Dr. E. P. Lozowski, who was always willing to help when problems arose. I also thank him for his unique ability to quickly read and return the initial drafts of the thesis. In addition, I would like to thank Dr. J. Tartar and Professor R. W. Longley for serving on the examining committee.

I am deeply indebted to Dr. Y. Mahrer, Hebrew University of Jerusalem, for providing a listing of his sea-breeze computer program.

I am grateful to my wife, Joy, who typed the final draft of this thesis.

I appreciate Mr. J. Chesterman's excellent photographic reduction of most of the figures.

I wish to thank the people of Canada for their financial support while I was on Educational Leave from the Atmospheric Environment Service of the Department of the Environment.

TABLE OF CONTENTS

LIST OF TABLES

LIST OF FIGURES

CHAPTER 1

THE SEA-BREEZE

1.1 Introduction

In coastal areas, during conditions of strong insolation and nocturnal cooling, there is a marked local diurnal variation in the surface winds. During the day, a wind (called a sea-breeze) blows from sea to land and during the night, a reverse flow from land to sea (a land-breeze) is observed.

1.2 Description of the Circulation

During the day, along the sea coasts or shores of large lakes, a temperature gradient is established as a result of the differential warming of the land and sea by the same heat source. According to Defant (1951), the solar energy incident upon the water is distributed through a deep layer by conduction or turbulent mixing, resulting in a small temperature rise. The land, on the other hand, has only a shallow layer heated by the sun; hence, a relatively large temperature rise occurs. Observations by Hsu (1967) show that the surface temperature gradient is concentrated along the coast.

The heated land causes the temperature of the air above it to rise as a result of turbulent diffusion and thermal convection. In the warmed layer, a pressure drop occurs as the atmosphere attempts to establish hydrostatic equilibrium. Once the surface pressure gradient is established, a flow from over the cool water to the warm land begins.

Aloft, the situation is reversed. The heating of the layer near the ground causes convection over the land. At higher levels in the atmosphere, where a stable stratification exists, the convection will result in a slight cooling of a deep layer aloft. The cooling is so weak that the increase in density is not able to cancel the effect of decreased density at the surface. This also results in a pressure gradient but opposite in sense to that near the surface and a flow from land to sea occurs.

The circulation is completed with subsidence over the sea as a result of conservation of mass.

Detailed observations of the sea-breeze are very scarce and, as a result, only the broadscale features of this circulation are known. Hence, it is difficult to judge the performance of a numerical model in its simulation of this phenomenon.

1.3 The Calm Gradient Wind Case

The implication of calm gradient wind is that there is no atmospheric motion in areas not influenced by the sea-breeze. Conrad (1928), on five calm summer days, noticed that the sea-breeze began over the coast between 7:00 A.M. and 8:00 A.M. and by watching ruffling of the water surface, he observed its seaward progression until the sails of a boat, one kilometer offshore, were affected at 9:00 A.M. Thus, the sea-breeze circulation spreads slowly landward and seaward during the day.

Wexler (1946) cites several examples in the tropics where the landward penetration of the sea-breeze reached over 150 kilometers from shore and was detectable 125 kilometers out to sea. He states, however, that in temperate latitudes the landward penetration is limited to 30 or 40 kilometers. Hills and forests appear to obstruct the movement inland. The sea-breeze of Massachusetts is retarded by Blue Hill, 180 meters high and 12 kilometers from the sea, while farther north its penetration is greater.

The vertical structure of the sea-breeze circulation in the tropics from observations by van Bemmelen (1922) under calm gradient wind conditions is given in Figure (1-1).

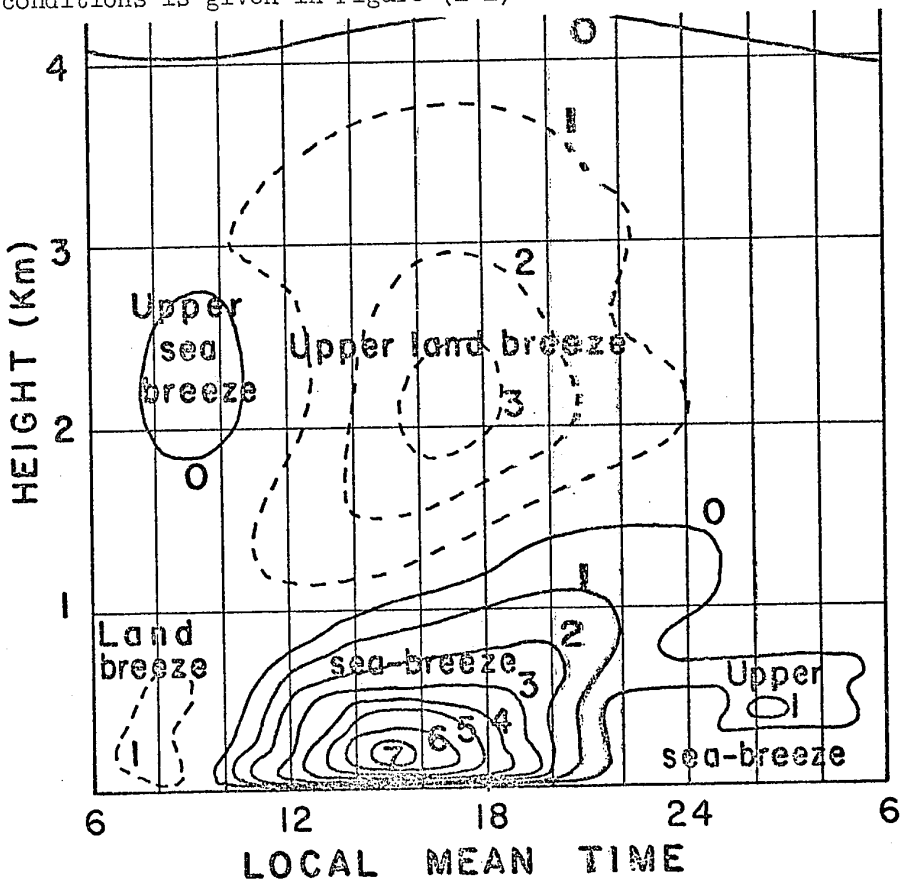

FIGURE (1-1) Vertical structure of the sea-breeze at Batavia. Velocities are given in m/sec.

Since the vertical structure depends on the solar heating, cloudiness, latitude, and season affect the results of Figure (1-1) by changing the vertical extent of the circulation and the strength of the winds.

As the day progresses, the sea-breeze and upper land-breeze are deflected by an ever-increasing amount from the action of the Coriolis force. The hourly variation of the wind during a sea-breeze situation at Hoek van Holland, as given by Bleeker and Schmidt (1947), is presented in Figure (1-2).

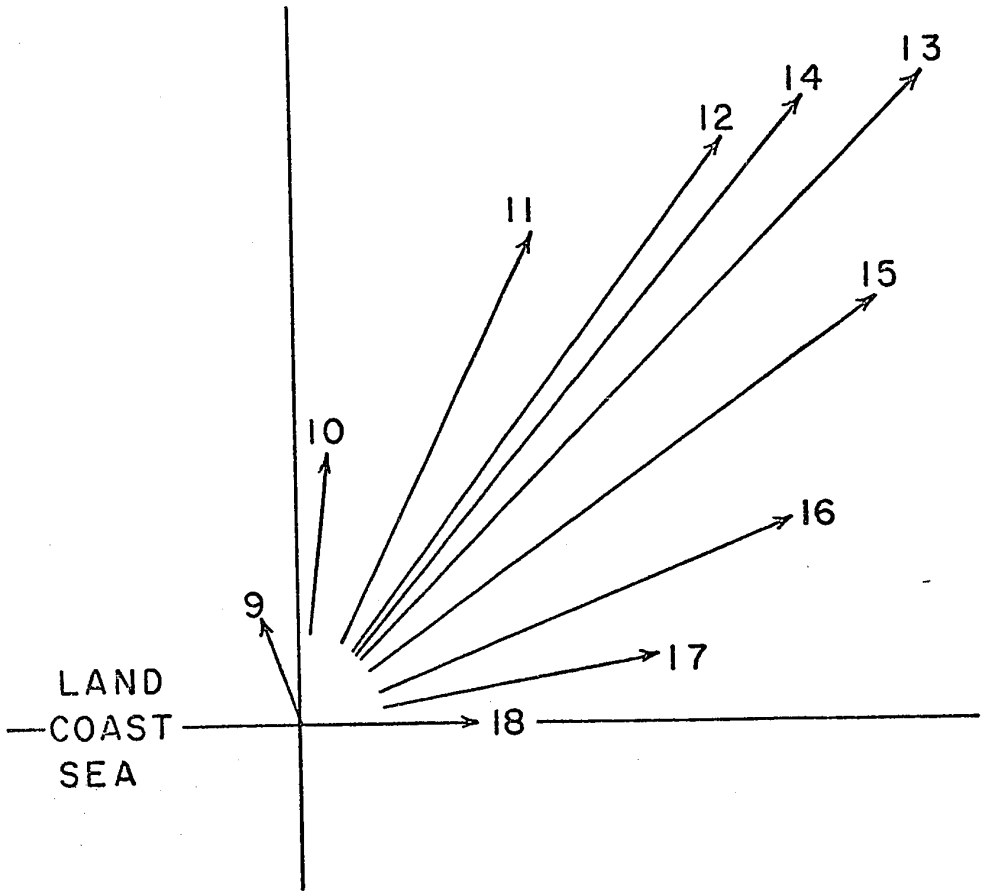

FIGURE (1-2) Hourly variation of the sea-breeze at a coastal station. (Hodograph)

1.4 The Sea-breeze with an Offshore Gradient Wind

The sea-breeze circulation is greatly modified by the presence of an offshore gradient wind. A sea-breeze which develops in opposition to the gradient wind is termed a "Cold Front-like" sea-breeze by Defant (1951). The development of this sea-breeze takes place several kilometers out at sea and then moves landward, often not reaching the coast until mid-afternoon. In the morning, the offshore gradient wind carries warmed air from the land out to sea and, as a result, the temperature gradient is displaced seaward causing the sea-breeze to develop out at sea. As the sea-breeze passes a given point on the land, that location experiences a marked windshift accompanied by a drop in temperature. Since these are the characteristics of a cold frontal passage, this form of the sea-breeze is well named.

The sea-breeze front does not move so far inland as the sea-breeze in the calm gradient wind case. In fact, the sea-breeze front may not even reach the land or if it does, it can be moved "backwards" by the opposing wind.

Observations by Koschmieder and Hornickel (1942) at Danzig indicate that the vertical extent of the frontal sea-breeze averaged 400 meters and occasionally reached 700 meters while, in the calm gradient wind case, the depth did not exceed 200 meters.

1.5 The Onshore Gradient Wind Case

When the gradient wind is onshore, a strong rise in temperature of the air over land is prevented and the sea-breeze component of the

wind is then very weak. Sutcliffe (1937) found statistically at Felixstowe, England, that with a gradient wind from the sea on clear days, the added sea-breeze effect from 6:00 A.M. to about 2:00 P.M. was approximately 1 m/sec in the lowest 300 meters.

1.6 The Land-breeze

As a result of increased stability over the land during the night, the land-breeze is weaker than its sea-breeze counterpart. The typical seaward range of the land-breeze, as determined by smoke observations off the coast of England, is ten to fifteen kilometers and eight kilometers off the Baltic coast.

The vertical extent of the land-breeze is considerably smaller than that of the sea-breeze. Zinner (1919) observed an average depth of 180 meters for the land-breeze at Burgas on the Black Sea and an average depth of 690 meters for the sea-breeze. The contrast between the sea-breeze regime and the land-breeze regime is also evident from Figure (1-1).

1.7 Previous Numerical Work

The first attempt to integrate the non-linear equations for the sea-breeze was that of Pearce (1955) but his model used an unrealistic mechanism for the input of heat to the atmosphere. In spite of this assumption, the sea-breeze circulation developed and the centre of the circulation moved inland during the day.

Using a sinusoidal variation with time for the land temperature and using diffusion to heat the atmosphere, Fisher (1961) modelled the sea-breeze but did not account for changes in stability in the low levels of the atmosphere. His results were in error after a few hours because of computational instability.

Estoque (1961) published solutions of the sea-breeze with a model that incorporated stability changes but assumed hydrostatic equilibrium and only approximate mass conservation. In spite of these restrictions, this model gave excellent results in that it essentially duplicated the observations for the sea-breeze perfectly but was unsuccessful in describing the land-breeze phase of the circulation. Estoque's model seems plagued by computational instability. The author's version of Estoque's model was stable only if strong smoothing was used and Moroz (1968) found Estoque's model to be unstable after ten hours.

McPherson (1970) used Estoque's model in three dimensions to study the affect of a coastal bay on the sea-breeze. The results of this model showed the distribution of vertical velocity around the bay. McPherson admits the use of a filter to keep the model stable but did not publish solutions after 12 hours of meteorological time.

The most significant contribution by Estoque is the method of computation near the ground and details of this are supplied in Chapter 2.

The model used by Neumann and Mahrer (1971) incorporates an improved sinusoidal heating function for the land, does not assume

hydrostatic equilibrium and gives essentially perfect mass conservation. This model is very successful in duplicating the existing sea-breeze observations. In addition, it is the first model to handle the land-breeze part of the circulation adequately. It is this model that forms the basis for the results presented in the present study.

CHAPTER 2

THE MODEL

2.1 Introduction

In this chapter, the equations which define the sea-breeze model are presented. Ultimately, this set of equations will be solved numerically by use of finite-differences on a network of grid points. Details of the grid will be given in Chapter 3.

In devising a model to study the sea-breeze circulation, one is faced with the problem of the strong vertical gradients of wind and temperature near the earth's surface. As a result of these rapid vertical changes, it is necessary to increase the number of vertical grid points in order to obtain satisfactory resolution near the ground in a study of this region using a grid point method.

Fisher (1961) placed the lower boundary of his grid at the earth's surface and used a large number of grid points to deal with the large vertical gradients of wind and temperature near the ground. However, Fisher made no attempt to include the effects of static stability.

In contrast, Estoque (1961) placed the lower boundary of his grid above the region of strong gradients and used an interpolation scheme to compute the profiles of temperature and wind in the boundary layer below the grid. With this method, Estoque was able to account for changes in the wind and temperature profiles as well as changes in

friction, resulting from changes in static stability in and below the grid. This interpolation method will be discussed fully in later sections.

In this study, Estoque's approach was used since it has the ability to distinguish between regimes of forced and free convection and because it requires fewer numerical computations.

2.2 Partitioning the Atmosphere

Following Estoque (1961), the region of the atmosphere that is influenced by the sea-breeze is divided into two sub-layers. The lower sub-layer extends from the earth's surface to the top of the constant flux layer which is assumed to be at a height of 50 meters. The upper sub-layer extends from 50 meters to a height where the effect of the sea-breeze vanishes. Estoque (1961) states that observations suggest a value of two kilometers for this height. For numerical convenience, a height of 1950 meters is used.

Estoque (1961) further states that the horizontal extent of the region influenced by the sea-breeze is about one hundred times its height. Again, for convenience, a value of 140 kilometers is used.

The upper sub-layer is divided into a network of grid points. The arrangement of the grid points is in equally spaced rows and columns with the lowest row at a height of 50 meters and the top row at 1950 meters. The columns are spaced so that the extreme left and right columns of the grid are coincident with the lateral boundaries

of the sea-breeze region outlined in Figure (2-1).

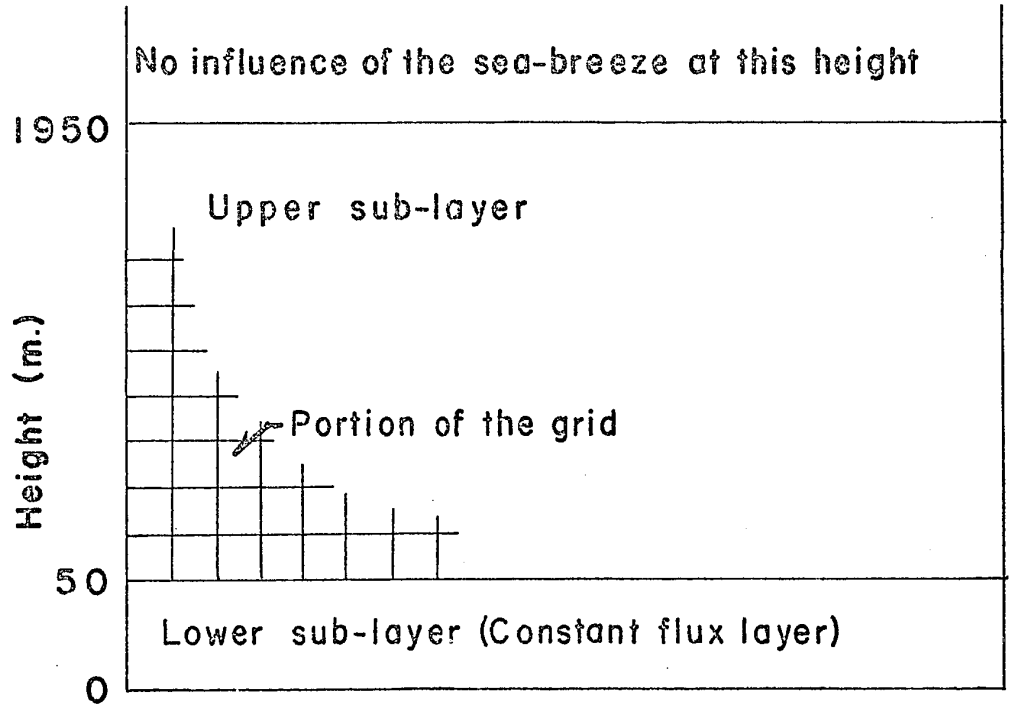

FIGURE (2-1) Partitions of the atmosphere.

2.3 The Co-ordinate System

The co-ordinate system used is a local tangent plane Cartesian system. It is assumed that the coastline is infinitely long and runs in a north-south direction with the land to the east and the sea to the west. The positive "x" axis points eastward (from sea to land), the positive "y" axis points northward and the positive "z" axis points vertically upward.

The above orientation of the coastline is chosen for convenience only and the sea-breezes described by the model are valid with any orientation of the coastline.

2.4 The Prediction Equations

The equations that are solved numerically to predict the sea-breeze circulation in the upper sub-layer are basically the Navier-Stokes equations for an incompressible turbulent atmosphere on the rotating earth plus the equation of continuity and the thermodynamic equation. To close this system of equations, it is necessary to use the equation of state for an ideal gas and Poisson's equation defining potential temperature. Since the horizontal extent of the sea-breeze region is small compared to the radius of the earth, the equations can be written in local tangent plane co-ordinates. Neglecting radiation and atmospheric moisture, these equations can be written as follows:

$$\frac{\partial \vec{V}}{\partial t} = -\vec{V}\cdot\nabla\vec{V} - \alpha\nabla p - 2\vec{\Omega}\times\vec{V} + \frac{\partial}{\partial z}\left(K_m \frac{\partial \vec{V}}{\partial z}\right) + \vec{g} \qquad (2.4.1)$$

$$\nabla\cdot\vec{V} = 0 \qquad (2.4.2)$$

$$\frac{\partial \theta}{\partial t} = -\vec{V}\cdot\nabla\theta + \frac{\partial}{\partial z}\left(K_h \frac{\partial \theta}{\partial z}\right) \qquad (2.4.3)$$

$$p\alpha = RT \qquad (2.4.4)$$

$$\theta = T\left(\frac{p_o}{p}\right)^{\frac{R}{c_p}} \qquad (2.4.5)$$

where $\vec{V}$ = three dimensional mean wind vector $(= \underline{i}u + \underline{j}v + \underline{k}w)$

α = specific volume for dry air

p = pressure

K_m = eddy diffusivity for momentum

θ = potential temperature

R = specific gas constant for dry air

T = temperature

$\vec{\Omega}$ = angular velocity of the earth

$\vec{g}$ = acceleration due to gravity

$\underline{i}, \underline{j}, \underline{k}$ = unit vectors

p_o = reference pressure (1000 mb)

K_h = eddy diffusivity for heat

2.5 The Eddy Diffusivities

From the mixing length theory, Hess (1959) states that Prandtl defines the turbulent shear stress:

$$\tau \equiv K_z \frac{\partial u}{\partial z}$$

and, as a result, the momentum transport by turbulence can be written:

$$\frac{\partial \tau}{\partial z} = \frac{\partial}{\partial z}\left(K_z \frac{\partial u}{\partial z}\right)$$

Sutton (1953) generalizes the above by stating that the transport of a scalar fluid property by eddies is given by:

$$\frac{d\chi}{dt} = \frac{\partial}{\partial x}\left(K_x \frac{\partial \chi}{\partial x}\right) + \frac{\partial}{\partial y}\left(K_y \frac{\partial \chi}{\partial y}\right) + \frac{\partial}{\partial z}\left(K_z \frac{\partial \chi}{\partial z}\right) \qquad (2.5.1)$$

where χ = scalar fluid property

K_x = eddy diffusivity in "x" direction

K_y = eddy diffusivity in "y" direction

K_z = eddy diffusivity in "z" direction

In this study, the quantities being transported by eddies are the horizontal momentum of the wind and the potential temperature. Outside the boundary layer, the changes in the horizontal gradients of these quantities are far less than those in the vertical and as a result, only the vertical term of (2.5.1) appears in the prediction equations.

From the expressions for the eddy diffusivities given by Lumley and Panofsky (1964), it can be seen that they are a maximum at the top of the constant flux layer. The magnitudes of the boundary layer eddy diffusivities drop to near zero at sufficiently great heights in the atmosphere where ground induced turbulence vanishes. The manner in which the diffusivities decrease with height is not known. Estoque (1961) used a linear decrease and McPherson (1970) assumed an exponential drop. In this study, a linear decrease is used yielding:

$$K(z) = K(h)\frac{H-z}{H-h} \qquad (2.5.2)$$

where K = eddy diffusivity

h = height of constant flux layer

H = height at which eddies vanish

It is required that the height at which the eddies vanish is the same as the height at which the influence of the sea-breeze is negligible. Hence, H is set equal to 1950 meters and as previously mentioned, the top of the constant flux layer is 50 meters.

Lumley and Panofsky (1964) state that over a large range of stabilities the diffusivity for heat, K_h, and the diffusivity for momentum, K_m, are not significantly different from each other. However, they also point out that this question is highly controversial. For the

lack of a better assumption, therefore, it will be assumed that K_h and K_m are equal.

2.6 The Assumption of Incompressibility

Batchelor (1967) derives the following three conditions necessary for air to behave as if incompressible:

$$\frac{U^2}{c^2} \ll 1 \qquad (2.6.1)$$

$$\frac{n^2 L^2}{c^2} \ll 1 \qquad (2.6.2)$$

$$\frac{\rho g L}{\gamma p} \ll 1 \qquad (2.6.3)$$

where γ = ratio of the specific heats for air

n = the dominant frequency of oscillations in the flow field

c = speed of sound

p = pressure

ρ = density

The spatial distributions of the wind vector $\vec{u}$ are characterized by a length scale L (meaning that in general $\vec{u}$ varies only slightly over distances small compared with L) and that the variations of the magnitude of $\vec{u}$ with respect to position and time have the magnitude U.

Equation (2.6.1) states that the flow velocity must be small compared to the speed of sound. The second equation (2.6.2) states the

frequency of any oscillatory motion in the air must be small compared to the frequency of sound and (2.6.3) restricts the vertical scale of motion to be much less than the "scale height" (defined as $\frac{p}{\rho g}$) of the atmosphere. It will be shown a posteriori that the model, outlined in this chapter, satisfies the above conditions.

2.7 The Lower Sub-layer

In the lower sub-layer, the vertical fluxes of heat and momentum are assumed to be constant in the vertical. Hence:

$$\frac{\partial}{\partial z}\left(K \frac{\partial \theta}{\partial z}\right) = 0 \qquad (2.7.1)$$

$$\frac{\partial}{\partial z}\left(K \frac{\partial U}{\partial z}\right) = 0 \qquad (2.7.2)$$

where K = eddy diffusivity

U = total horizontal wind $(U^2 = u^2 + v^2)$

θ = potential temperature

The purpose of the lower sub-layer equations is to provide the lower boundary conditions (necessary for computation of the vertical derivatives of the potential temperature and wind) for use by the prediction equations of the upper sub-layer.

In practice, the equations for the lower sub-layer are used to "adjust" the values of temperature and wind at the lower boundary of the grid (z=h) to ensure that these values are consistent with the profiles, the values present at the ground (z=0) and the values present at the second row of grid points (z=h+Δ z where Δ z is the spacing

between the grid rows).

In order for the prediction equations in the upper sub-layer to use the values produced by the boundary layer equations, continuity in the wind and temperature and their vertical first derivatives is required. In order to accomplish this, the constancy of the heat and momentum flux is extended from the top of the lower sub-layer to the first interior grid row of the upper sub-layer, that is, to a height of $h+\Delta z$.

Since both statically stable and unstable regimes may exist in the lower sub-layer, two sets of boundary layer equations are required. The gradient Richardson number is used as the indicator of stability. The transition from stable to unstable and from unstable to stable is assumed to occur at a critical Richardson number Ri_c. The unstable regime is assumed to occur with:

$$Ri \leq Ri_c \qquad (2.7.3)$$

and the stable regime with:

$$Ri > Ri_c \qquad (2.7.4)$$

where the Richardson number is evaluated at $z=(h+\Delta z)/2$ and defined as:

$$Ri = \frac{g}{\bar{\theta}}\left(\frac{\partial \theta}{\partial z}\right)\left(\frac{\partial U}{\partial z}\right)^{-2} \qquad (2.7.5)$$

where $\bar{\theta}$ = average potential temperature in lower sub-layer

U = total horizontal wind

g = acceleration due to gravity

Following Priestley (1959), the critical value of the Richardson number is taken to be -0.03.

2.8 The Unstable Regime

Using dimensional analysis and the assumption of a constant heat flux, Lumley and Panofsky derive the following equations for determining the temperature profile and eddy diffusivity in an unstable boundary layer:

$$\frac{\partial \theta}{\partial z} = C \left(\frac{H}{c_p \rho}\right)^{\frac{2}{3}} \left(\frac{g}{\bar{\theta}}\right)^{-\frac{1}{3}} z^{-\frac{4}{3}} \qquad (2.8.1)$$

$$\theta = B + 3C \left(\frac{H}{c_p \rho}\right)^{\frac{2}{3}} \left(\frac{g}{\bar{\theta}}\right)^{-\frac{1}{3}} z^{-\frac{1}{3}} \qquad (2.8.2)$$

$$K = C^{-1} \left(\frac{g H}{\bar{\theta} c_p \rho}\right)^{\frac{1}{3}} z^{\frac{4}{3}} \qquad (2.8.3)$$

where $\bar{\theta}$ = average potential temperature in the constant flux layer

C = a non-dimensional constant

B = an integration constant

ρ = air density

g = acceleration due to gravity

H = heat flux

c_p = specific heat of air at constant pressure

K = eddy diffusivity

Starting from these equations, Mahrer (personal communication) derives an expression for the eddy diffusivity at the top of the lower sub-layer in terms of the values at the ground and those at the second

row of grid points.

Although Priestley (1959) states that (2.8.3) is not valid below one meter, it will be assumed to be valid at $z=z_o$ where z_o is the roughness height. The potential temperature at the roughness height is set equal to the surface temperature. In addition, since Lumley and Panofsky state that the value of the constant C is near unity, it was set equal to one.

From (2.8.3) it can be written that:

$$\theta_{h+\Delta z} = B + 3\left(\frac{H}{c_p\rho}\right)^{\frac{2}{3}}\left(\frac{g}{\bar{\theta}}\right)^{-\frac{1}{3}}\left(h+\Delta z\right)^{-\frac{1}{3}} \qquad (2.8.4)$$

$$\theta_o = B + 3\left(\frac{H}{c_p\rho}\right)^{\frac{2}{3}}\left(\frac{g}{\bar{\theta}}\right)^{-\frac{1}{3}} z_o^{-\frac{1}{3}} \qquad (2.8.5)$$

where the subscript $h+\Delta z$ refers to values at the second grid row and the subscript o refers to values at the ground. Subtraction of (2.8.4) and (2.8.5) gives:

$$\left(\frac{H}{c_p\rho}\right)^{\frac{2}{3}} = \left(\frac{g}{\bar{\theta}}\right)^{\frac{1}{3}}\left\{3\left(\left[\Delta z+h\right]^{-\frac{1}{3}} - z_o^{-\frac{1}{3}}\right)\right\}\left(\theta_{h+\Delta z}-\theta_o\right) \qquad (2.8.6)$$

and substitution into (2.8.3) yields the diffusivity at z=h:

$$K = \left(h+z_o\right)^{\frac{4}{3}}\sqrt{\frac{g}{\bar{\theta}}\,\delta\left(\theta_{h+\Delta z}-\theta_o\right)} \qquad (2.8.7)$$

where

$$\delta = \left\{3\left(\left[\Delta z+h\right]^{-\frac{1}{3}} - z_o^{-\frac{1}{3}}\right)\right\}$$

To determine the values of u, v, and θ at the lower boundary of the upper sub-layer (z=h), the one-third power law of (2.8.2) is used in the form:

$$\theta = \overset{*}{A} z^{-\frac{1}{3}} + \overset{*}{B} \qquad (2.8.8)$$

The two constants $\overset{*}{A}$ and $\overset{*}{B}$ can be determined from:

$$\theta = \theta_{h+\Delta z} \quad \text{at} \quad z = h+\Delta z$$

$$\theta = \theta_o \quad \text{at} \quad z = z_o$$

which yields the following result for the potential temperature at z=h:

$$\theta_h = \alpha \theta_{h+\Delta z} + (1-\alpha)\theta_o \qquad (2.8.9)$$

where

$$\alpha = \frac{h^{-\frac{1}{3}} - z_o^{-\frac{1}{3}}}{\left((h+\Delta z)^{-\frac{1}{3}} - z_o^{-\frac{1}{3}}\right)}$$

If it is assumed the profiles of wind and temperature are similar, then:

$$U_h = \alpha U_{h+\Delta z} \qquad (2.8.10)$$

since the wind at $z=z_o$ is zero. The components of the wind follow logically from (2.8.10):

$$u_h = u_{h+\Delta z} \frac{U_h}{U_{h+\Delta z}} \qquad (2.8.11)$$

$$v_h = v_{h+\Delta z} \frac{U_h}{U_{h+\Delta z}} \qquad (2.8.12)$$

2.9 The Stable Regime

Estoque (1959) derived the following expressions for the wind, temperature and diffusivity at the lower boundary of the upper sub-layer:

$$K = \left[k_0(h+z_0)(1+\alpha Ri)\right]^2 \frac{U_{h+\Delta z}}{h+\Delta z} \qquad (2.9.1)$$

$$U_h = A_1 U_{h+\Delta z} \qquad (2.9.2)$$

$$\theta_h = A_1 \theta_{h+\Delta z} + (1-A_1)\theta_0 \qquad (2.9.3)$$

where k_0 = von Karman's constant = 0.4

Ri = Richardson number

α = a constant = -0.03

$$A_1 = \frac{\beta_1 + \frac{\Delta z}{h+\Delta z}(\beta_1 - \beta_2 h)\alpha Ri}{\beta_1 + \beta_2 \Delta z}$$

$$\beta_2 = \left[k_0(h+z_0)\right]^{-1}$$

$$\beta_1 = \frac{1}{k_0} \ln\left(\frac{h+z_0}{z_0}\right)$$

The values of the u and v components at z=h are computed from (2.8.11) and (2.8.12).

There is a marked discontinuity in the results for the stable and unstable regimes at the critical Richardson number (Ri_c).

2.10 The Boundary Conditions

Following Neumann and Mahrer (1971), the following boundary conditions are used. Since the sea-breeze has no influence on the top boundary of the upper sub-layer, the meteorological variables will not change with time at this point. As a result for the top boundary (z=H):

$$\frac{\partial}{\partial t}(u, v, p, \theta) = 0 \qquad (2.10.1)$$

$$w = 0 \qquad (2.10.2)$$

On the lateral boundaries, the conditions that exist at a large distance from the coastline (where the influence of the sea-breeze is negligible) are approximated. At the lateral boundaries:

$$\frac{\partial}{\partial x}(u, v, p, \theta) = 0 \qquad (2.10.3)$$

$$w = 0 \qquad (2.10.4)$$

On the lower boundary, the conditions are generated by the equations for the lower sub-layer discussed previously, using the boundary conditions at the earth's surface. At $z=z_o$:

$$u = v = w = 0 \qquad (2.10.5)$$

T_o = sea temperature

$T(t)$ = land temperature

$\frac{1}{2}(T(t)+T_o)$ = coast temperature

The coast is given the average of the land and sea temperatures to better represent Hsu's (1967) observations.

The form of the temperature wave is given by the first four

harmonics of Kuo's (1968) results for temperature change at five millimeters below the land surface on a clear summer's day. Kuo's results were scaled to give a peak-to-peak temperature change of about 25 C. The surface temperature of the land as a function of time[1] is:

$$T(t) = T_o + 12 \sin(15t - 110^\circ) + 3.5 \sin(30t + 75^\circ) + 0.5 \sin(45t + 66^\circ) + 0.6 \sin(60t - 115) \qquad (2.10.7)$$

where t is the time measured in hours from the time of equal land and sea temperatures (= 8:00 A.M.).

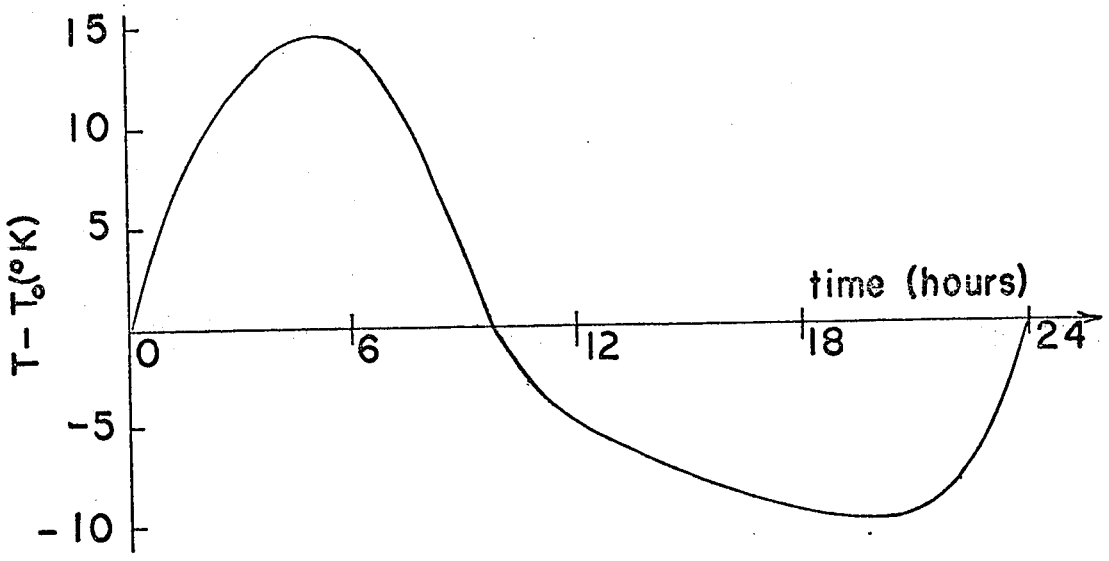

FIGURE (2-2) Form of the temperature wave applied to the land surface.

[1] the argument of the sine function is in angular degrees

CHAPTER 3

THE COMPUTER MODEL

3.1 Introduction

In the previous chapter, the theoretical model for the sea-breeze circulation was presented. In this chapter, the method used for solution by computer of the equations of Chapter 2 is outlined.

3.2 The Prediction Equations

In order to reduce the number of significant figures required during numerical computation, one can express the horizontal velocity components and potential temperature as the sum of an initial value and a "small" perturbation, i.e.:

$$u = u_0 + u' \qquad (3.2.1)$$

$$v = v_0 + v' \qquad (3.2.2)$$

$$\theta = \theta_0 + \theta' \qquad (3.2.3)$$

where the primed quantities are the perturbations and the subscripted quantities refer to the initial state.

Further, it is convenient to split the pressure into three parts as follows:

$$p = p_0 + p' + \overset{*}{p} \qquad (3.2.4)$$

where p_0 = initial pressure

p' = hydrostatic perturbation pressure

$\overset{*}{p}$ = non-hydrostatic perturbation pressure

The sum $(p + p')$ satisfies the hydrostatic equation:

$$\frac{\partial}{\partial z}(p_0 + p') = -\frac{p}{RT} g \qquad (3.2.5)$$

The initial horizontal wind field is assumed to be geostrophic and as a result, the initial horizontal pressure gradient terms can be approximated by:

$$\alpha_0 \frac{\partial p_0}{\partial x} = f v_0 \cong \alpha \frac{\partial p_0}{\partial x} \qquad (3.2.6)$$

$$\alpha_0 \frac{\partial p_0}{\partial y} = -f u_0 \cong \alpha \frac{\partial p_0}{\partial y} \qquad (3.2.7)$$

where $f = 2\Omega \sin\phi$

ϕ = latitude

α_0 = initial specific volume

α = specific volume

The initial temperature field is a function of height only and is of the form:

$$T_{0z} = T_{00} - \gamma_0 z \qquad (3.2.8)$$

where T_{0z} = temperature at height z

T_{00} = initial temperature at z=0

γ_0 = initial lapse rate (the initial rate of decrease of the temperature with height)

If it is further assumed that the initial horizontal wind field is a function of height only, the prediction equations of Section 2.4 become, upon incorporation of the assumptions stated above:

$$\frac{\partial u'}{\partial t} = -(u_o+u')\frac{\partial u'}{\partial x} - w\frac{\partial u'}{\partial z} + \frac{\partial K}{\partial z}\frac{\partial u'}{\partial z} + K\frac{\partial^2 u'}{\partial z^2} + \frac{\partial K}{\partial z}\frac{\partial u_o}{\partial z} \tag{3.2.9}$$

$$+K\frac{\partial^2 u_o}{\partial z^2} - \frac{RT}{\bar{p}}\frac{\partial p'}{\partial x} - \frac{RT}{\bar{p}}\frac{\partial p^*}{\partial x} + fv' - 2\Omega\cos\phi\, w$$

$$\frac{\partial v'}{\partial t} = -(u_o+u')\frac{\partial v'}{\partial x} - w\frac{\partial v'}{\partial z} + \frac{\partial K}{\partial z}\frac{\partial v'}{\partial z} + K\frac{\partial^2 v'}{\partial z^2}$$

$$- fu' + \frac{\partial K}{\partial z}\frac{\partial v_o}{\partial z} + K\frac{\partial^2 v_o}{\partial z^2} - w\frac{\partial v_o}{\partial z} \tag{3.2.10}$$

$$\frac{\partial w}{\partial t} = -(u_o+u')\frac{\partial w}{\partial x} - w\frac{\partial w}{\partial z} - \frac{RT}{\bar{p}}\frac{\partial p^*}{\partial z} + 2\Omega\cos\phi\, u' \tag{3.2.11}$$

$$\frac{\partial u'}{\partial x} + \frac{\partial w}{\partial z} = 0 \tag{3.2.12}$$

$$\frac{\partial \theta'}{\partial t} = -(u_o+u')\frac{\partial \theta'}{\partial x} - w\frac{\partial}{\partial z}(\theta_o+\theta') + \frac{\partial K}{\partial z}\frac{\partial}{\partial z}(\theta_o+\theta')$$

$$+K\frac{\partial^2}{\partial z^2}(\theta_o+\theta') \tag{3.2.13}$$

where ϕ = latitude of the point

Ω = angular velocity of the earth

T = temperature

K = eddy diffusivity

R = specific gas constant for dry air

f = Coriolis parameter

$\bar{p}$ = total pressure

The total pressure above is defined as:

$$\bar{p} = \bar{p}_o + p' + p^* \qquad (3.2.13)$$

Since it has been assumed that the initial pressure may be a function of all three space variables, it is convenient to define an average initial pressure which is a function of height only, using the hydrostatic equation for a constant lapse rate atmosphere:

$$\bar{p}_o(z) = \bar{p}_o(0)\left(\frac{T_{oz}}{T_{oo}}\right)^{\frac{g}{\gamma_o R}} \qquad (3.2.14)$$

where $\bar{p}_o(z)$ = average initial pressure at height z

$\bar{p}_o(0)$ = initial pressure at height $z=z_o$

The average pressure is used only to compute the specific volume in the prediction equations and as a result, the error introduced is less than one percent.

3.3 The Grid

As mentioned previously, the upper sub-layer is covered with a network of grid points in the form of equally spaced rows and columns. The lowest grid row is coincident with the lower boundary of the upper sub-layer (at z=h). The highest row of the grid is located at z=H where the influence of the sea-breeze is assumed to be negligible. The first and last columns of the grid are placed at the lateral boundaries

of the sea-breeze region described previously.

The grid rows are numbered consecutively upward, starting from one at the lowest row to M at the top row, where M is the total number of rows. Similarly, the columns are numbered consecutively, starting at one at seaward lateral boundary to L at the landward lateral boundary, where L is the total number of columns.

The notation used to refer to the value of a variable χ at a given grid point is $\chi_{i,j}$ where the grid point in question is located at the intersection of the i^{th} column and the j^{th} row.

To refer to the surrounding points of a given grid point, (i,j) , the notation as outlined in Figure (3-1) is used.

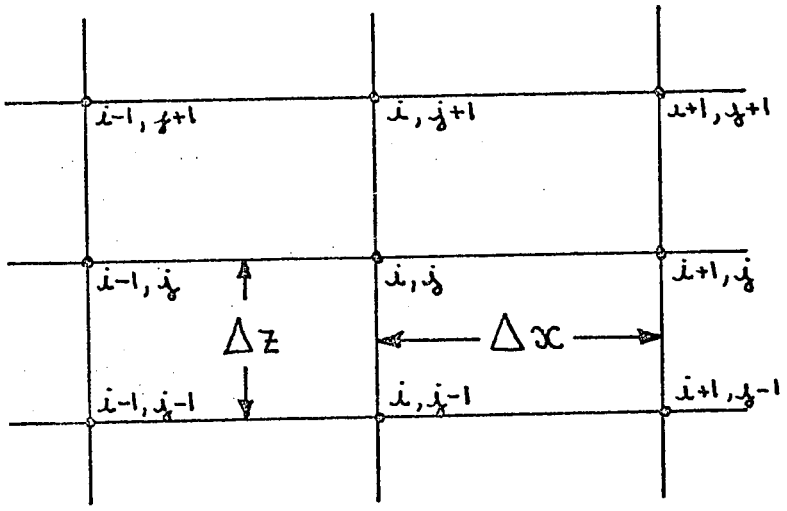

FIGURE (3-1) Indexing of the grid.

The equal spacing between the rows is Δz and that between the columns is Δx where Δx and Δz refer to distances measured in the real atmosphere.

3.4 Computation of the Hydrostatic Pressure Perturbation Field

If the initial pressure field is assumed to be hydrostatic, then from (3.2.5) the following can be written :

$$\frac{\partial p'}{\partial z} = \frac{g}{R}\left(\frac{\bar{p}_o}{T_o} - \frac{\bar{p}_o + p'}{T}\right) \qquad (3.4.1)$$

The derivative is approximated by a one-sided finite-difference scheme:

$$\left(\frac{\partial p'}{\partial z}\right)_{i,j} \cong \frac{1}{\Delta z}\left(p'_{i,j+1} - p'_{i,j}\right) \qquad (3.4.2)$$

This is substituted into (3.4.1) to give:

$$p'_{i,j} = \left\{\frac{\Delta z g}{R}\left(\frac{\bar{p}_{oj}}{T_{oj}} - \frac{\bar{p}_{oj}}{T_{i,j}}\right) - p'_{i,j+1}\right\}\left(\frac{\Delta z g}{R T_{i,j}} - 1\right)^{-1} \qquad (3.4.3)$$

This equation is used in succession on each column of the grid where the equation is integrated downward, using $p'_{i,j}$ equal to zero on the top row.

3.5 The Finite-difference Equations for v' and θ'

The finite-difference equations for v' and θ' are written with forward differences for the time derivatives:

$$\frac{\partial \theta'_{i,j}}{\partial t} \cong \frac{1}{\Delta t}\left(\theta'^{n+1}_{i,j} - \theta'^{n}_{i,j}\right) \qquad (3.5.1)$$

$$\frac{\partial v'_{i,j}}{\partial t} \cong \frac{1}{\Delta t}\left(v'^{n+1}_{i,j} - v'^{n}_{i,j}\right) \qquad (3.5.2)$$

where n = the index of the time step

Δt = time increment

The advection terms use "upstream" differencing:

$$-(u_o+u')\frac{\partial v'}{\partial x} \cong -\frac{1}{\Delta x}(u_o+u'_{i,j})(v'_{i,j}-v'_{i-1,j}) \quad (3.5.3)$$

for (u_o+u') greater than or equal to zero and:

$$-(u_o+u')\frac{\partial v'}{\partial x} \cong -\frac{1}{\Delta x}(u_o+u'_{i,j})(v'_{i+1,j}-v'_{i,j}) \quad (3.5.4)$$

for (u_o+u') less than zero. Similar expressions are used to replace the advection term in the θ' equation.

According to Haltiner (1971), the upstream difference approximation is computationally stable for a linear equation containing only this term if:

$$\Delta t < \frac{\Delta x}{u_o+u'} \quad (3.5.5)$$

and it is used with a forward time difference. It is difficult to determine the stability criteria for a complete set of non-linear equations; hence, it will be assumed that the above linear stability criteria provide a close stability approximation when applied to the prediction equations.

The convection terms use "upstream" differencing as well giving:

$$-w\frac{\partial v'}{\partial z} \cong -\frac{1}{\Delta z}w_{i,j}(v'_{i,j}-v'_{i,j-1}) \quad w_{i,j} \geq 0 \quad (3.5.6)$$

$$\cong -\frac{1}{\Delta z}w_{i,j}(v'_{i,j+1}-v'_{i,j}) \quad w_{i,j} < 0 \quad (3.5.7)$$

The linear stability criterion for the above is:

$$\Delta t < \frac{\Delta z}{w_{i,j}} \qquad (3.5.8)$$

The diffusivity terms are approximated by:

$$\frac{\partial K}{\partial z}\frac{\partial v'}{\partial z} + K\frac{\partial^2 v'}{\partial z^2} \cong \frac{1}{2\Delta z} K_i' \left(v'_{i,j+1} - v'_{i,j-1}\right)$$

$$+ K_i \frac{1}{\Delta z^2}\left(v'_{i,j+1} + v'_{i,j-1} - 2v'_{i,j}\right) \qquad (3.5.9)$$

where $K_i' = \partial K_i / \partial z$

From Haltiner, the linear stability criterion for the above is:

$$\Delta t < \frac{\Delta z^2}{2K_i} \qquad (3.5.10)$$

By use of the preceding approximations, the finite-difference prediction equations for the v -component of the wind and the potential temperature become:

$$v'^{n+1}_{i,j} = v'^{n}_{i,j} - \frac{\Delta t}{\Delta x}\left(u_{oj} + u'^{n}_{i,j}\right)\left(v'^{n}_{i+1,j} - v'^{n}_{i,j}\right) - \frac{\Delta t}{\Delta z} w^{n}_{i,j}$$

$$\left(v_{oj+1} - v_{oj}\right) - \frac{\Delta t}{\Delta z} w^{n}_{i,j}\left(v'^{n}_{i,j+1} - v'^{n}_{i,j}\right) - f u'^{n}_{i,j}\Delta t$$

$$+ \frac{\Delta t}{2\Delta z} K'^{n}_{i}\left(v'^{n}_{i,j+1} - v'^{n}_{i,j-1}\right) + \frac{\Delta t}{\Delta z^2} K^{n}_{i}\left(v'^{n}_{i,j+1} + v'^{n}_{i,j-1} - 2v'^{n}_{i,j}\right)$$

$$+ \frac{\Delta t}{2\Delta z} K'^{n}_{i}\left(v_{oj+1} - v_{oj}\right) + \frac{\Delta t}{\Delta z^2} K^{n}_{i}\left(v_{oj+1} + v_{oj-1} - 2v_{oj}\right)$$

(3.5.11)

$$\theta'^{n+1}_{i,j} = \theta'^{n}_{i,j} - \frac{\Delta t}{\Delta x}(u_o + u'^{n}_{i,j})(\theta'^{n}_{i+1,j} - \theta'^{n}_{i,j}) - \frac{\Delta t}{\Delta z} w^{n}_{i,j}$$

$$(\theta_{oj+1} - \theta_{oj} + \theta'^{n}_{i,j+1} - \theta'^{n}_{i,j}) + \frac{\Delta t}{2\Delta z} K'^{n}_{i}(\theta_{oj+1}$$

$$- \theta_{oj-1} + \theta'^{n}_{i,j+1} - \theta'^{n}_{i,j-1}) + \frac{\Delta t}{\Delta z^2} K^{n}_{i}(\theta_{oj+1} + \theta_{oj-1}$$

$$- 2\theta_{oj} + \theta'^{n}_{i,j+1} + \theta'^{n}_{i,j-1} - 2\theta'^{n}_{i,j}) \qquad (3.5.12)$$

where θ_{oj} = initial potential temperature of the j th row.

The above equations assume $(u_o + u'^{n}_{i,j})$ and $w^{n}_{i,j}$ are both negative. If either or both of the above are positive or zero, it is necessary to change the corresponding advection term according to (3.5.3) and/or (3.5.6).

3.6 Chorin's Method for the u' and w Equations

The method originated by Chorin (1968) is used to predict the u' and w fields. His method allows the equations of motion to be used in component form instead of resorting to the vorticity-stream function method.

In Chorin's scheme, an auxiliary velocity field is defined by removing the non-hydrostatic pressure terms from the u' and w equations and writing them in finite-difference form similar to the v' and θ' equations previously described. Approximating the pressure gradient term in the u' equation by a centred difference, the auxiliary velocities are:

$$u^{aux}_{i,j} = -\frac{\Delta t}{\Delta x}(u_o+u'^{n}_{i,j})(u'^{n}_{i+1,j}-u'^{n}_{i,j}) + f\Delta t v'^{n}_{i,j} - \frac{\Delta t}{\Delta z} w^{n}_{i,j}(u_{oj+1}-$$

$$u_{oj}) - \frac{\Delta t}{\Delta z} w^{n}_{i,j}(u'^{n}_{i,j+1}-u'^{n}_{i,j}) - \frac{\Delta t R T^{n}_{i,j}}{2\Delta x \bar{p}^{n}_{i,j}}(p'^{n}_{i+1,j} - p'^{n}_{i-1,j})$$

$$+ K'^{n}_{i2}\frac{\Delta t}{2\Delta z}(u'^{n}_{i,j+1} - u'^{n}_{i,j-1}) + K^{n}_{i}\frac{\Delta t}{\Delta z^2}(u'^{n}_{i,j+1}+u'^{n}_{i,j-1} - 2u'^{n}_{i,j})$$

$$+ K'^{n}_{i}\frac{\Delta t}{2\Delta z}(u_{oj+1} - u_{oj-1}) + K^{n}_{i}\frac{\Delta t}{\Delta z^2}(u_{oj+1} + u_{oj-1} - 2u_{oj})$$

$$- 2\Omega\Delta t\cos\phi\, w^{n}_{i,j} + u'^{n}_{i,j} \qquad (3.6.1)$$

$$w^{aux}_{i,j} = -\frac{\Delta t}{\Delta x}(u_o+u'^{n}_{i,j})(w^{n}_{i+1,j} - w^{n}_{i,j}) + 2\Omega\cos\phi\,\Delta t\, u'^{n}_{i,j}$$

$$- \frac{\Delta t}{\Delta z} w^{n}_{i,j}(w^{n}_{i,j+1} - w^{n}_{i,j}) + w^{n}_{i,j} \qquad (3.6.2)$$

The non-hydrostatic pressure terms are reintroduced and the following are obtained from the equations of motion:

$$u'^{n+1}_{i+1,j} = u^{aux}_{i+1,j} - \frac{\Delta t\alpha_{i+1,j}}{2\Delta x}(P^{*n+1}_{i+2,j} - P^{*n+1}_{i,j}) \qquad (3.6.3)$$

$$u'^{n+1}_{i-1,j} = u^{aux}_{i-1,j} - \frac{\Delta t\alpha_{i-1,j}}{2\Delta x}(P^{*n+1}_{i,j} - P^{*n+1}_{i-2,j}) \qquad (3.6.4)$$

$$w^{n+1}_{i,j+1} = w^{aux}_{i,j+1} - \frac{\Delta t\alpha_{i,j+1}}{2\Delta z}(P^{*n+1}_{i,j+2} - P^{*n+1}_{i,j}) \qquad (3.6.5)$$

$$w^{n+1}_{i,j-1} = w^{aux}_{i,j-1} - \frac{\Delta t \alpha_{i,j-1}}{2\Delta z}\left(P^{*n+1}_{i,j} - P^{*n+1}_{i,j-2}\right) \qquad (3.6.6)$$

The first pair of the above equations is divided by $2\Delta x$ and the second pair by $2\Delta z$. After subtracting and making the approximation that:

$$\alpha_{i+1,j} = \alpha_{i-1,j} = \alpha_{i,j+1} = \alpha_{i,j-1} = \alpha_{i,j}$$

the following is obtained:

$$\frac{u'^{n+1}_{i+1,j} - u'^{n+1}_{i-1,j}}{2\Delta x} + \frac{w^{n+1}_{i,j+1} - w^{n+1}_{i,j-1}}{2\Delta z} = \frac{u^{aux}_{i+1,j} - u^{aux}_{i-1,j}}{2\Delta x}$$

$$+ \frac{w^{aux}_{i,j+1} - w^{aux}_{i,j-1}}{2\Delta z} - \frac{\Delta t}{4\Delta x^2}\alpha_{i,j}\left(P^{*n+1}_{i+2,j} - 2P^{*n+1}_{i,j} + P^{*n+1}_{i-2,j}\right)$$

$$+ \frac{\Delta t}{4\Delta z^2}\alpha_{i,j}\left(P^{*n+1}_{i,j+2} - 2P^{*n+1}_{i,j} + P^{*n+1}_{i,j-2}\right) \qquad (3.6.7)$$

where $\alpha_{i,j} = \frac{RT_{i,j}}{\bar{P}_j}$

The left side of the above equation is the divergence of the wind field at the (n+1)th time step which, in accordance with the equation of continuity, is assumed to be zero. The first two terms of the right-hand side form the divergence of the auxiliary velocity field. The remaining two terms are a finite-difference Laplacian whose nodes are separated by two grid lengths. By defining:

$$\frac{u^{aux}_{i+1,j} - u^{aux}_{i-1,j}}{2\Delta x} + \frac{w^{aux}_{i,j+1} - w^{aux}_{i,j-1}}{2\Delta z} \equiv DV^{aux}_{i,j} \qquad (3.6.8)$$

equation (3.6.7) can be written:

$$\frac{4\Delta z^2}{\Delta t \alpha_{i,j}} DV^{aux}_{i,j} = \frac{\Delta z^2}{\Delta x^2}\left(P^{*n+1}_{i+2,j} - 2P^{*n+1}_{i,j} + P^{*n+1}_{i-2,j}\right)$$

$$+\left(P^{*n+1}_{i,j+2} - 2P^{*n+1}_{i,j} + P^{*n+1}_{i,j-2}\right) \qquad (3.6.9)$$

Chorin solves (3.6.9) for the pressure field, using an iteration procedure and by setting u^{aux} on the lateral boundaries equal to u'^{n+1} and setting w^{aux} on the top and bottom boundaries equal to w^{n+1} in (3.6.8). Hence, it is required that u'^{n+1} and w^{n+1} are known on the boundaries specified above. In this work, a sequential relaxation method is used, setting $P^{*n+1}=0$ at the boundaries for all time steps.

3.7 The Relaxation Procedure

Equation (3.6.9) is solved by iteration. At each step in the iteration procedure, (3.6.9) is evaluated with the pressures from the previous step and in the case of the first iteration step, the values calculated at the previous time step are used. In general, these will not satisfy (3.6.9) and a residual pressure term will remain defined by:

$$\frac{\Delta z^2}{\Delta x^2} P^{*m,n+}_{i+2,j} + \frac{\Delta z^2}{\Delta x^2} P^{*m,n+1}_{i-2,j} + P^{*m,n+1}_{i,j+2} + P^{*m,n+1}_{i,j-2}$$

$$-2\left(\frac{\Delta z^2}{\Delta x^2}+1\right)P^{*m,n+1}_{i,j} - \frac{4\Delta z^2}{\Delta t \alpha_{i,j}} DV^{aux}_{i,j} = R^m_{i,j} \qquad (3.7.1)$$

where $R^m_{i,j}$ = residual

m = iteration index

The value of the pressure at the point (i, j) is adjusted so that the residual vanishes. This new pressure is the (m+1)th iterate:

$$\frac{\Delta z^2}{\Delta x^2} P^{*m,n+1}_{i+2,j} + \frac{\Delta z^2}{\Delta x^2} P^{*m,n+1}_{i-2,j} + P^{*m,n+1}_{i,j+2} + P^{*m,n+1}_{i,j-2} - 2\left(\frac{\Delta z^2}{\Delta x^2} + 1\right) P^{*m+1,n+1}_{i,j} - \frac{4\Delta z^2}{\Delta t \alpha_{i,j}} DV^{aux}_{i,j} = 0 \quad (3.7.2)$$

Subtraction of (3.7.2) from (3.7.1) gives the iteration equation:

$$P^{*m+1,n+1}_{i,j} = P^{*m,n+1}_{i,j} + R^m_{i,j} \Big/ 2\left(\frac{\Delta z^2}{\Delta x^2} + 1\right) \quad (3.7.3)$$

This equation can only be used in the area of the grid which is two or more columns or rows from the boundaries. To derive the iteration equation for the region one grid length away from the boundary, we make use of the fact that the appropriate component of the auxiliary velocity on the boundaries stated in Section (3.7) is replaced by the appropriate component of the "n+1" velocity field, which forces the normal derivative of the pressure across the boundaries equal to zero. Hence, every pressure at a point one grid length from a boundary has an equal image pressure lying outside the boundary.

On Figure (3-2), the following pressures are equal:

$$IP_{j+1} = P^{*m+1}_{2,j+1}$$

$$IP_{j} = P^{*n+1}_{2,j}$$

$$IP_{j-1} = P^{*n+1}_{2,j-1}$$

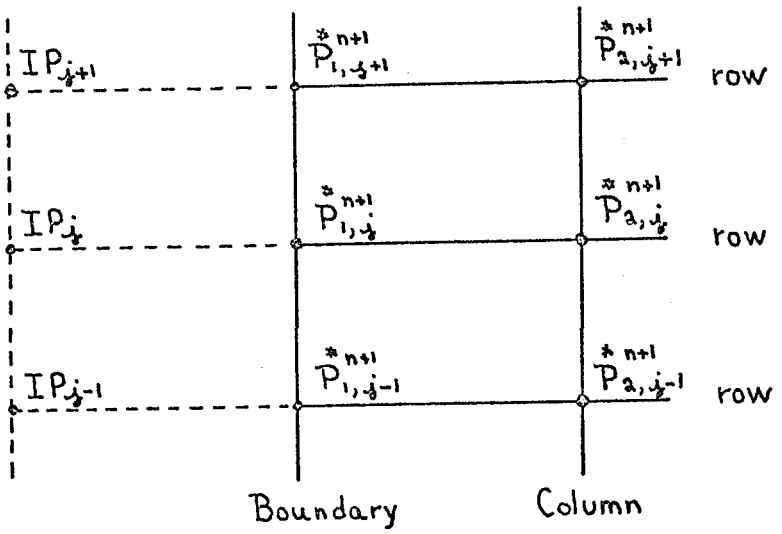

FIGURE (3-2) The image pressures.

Using the above, (3.7.1) and (3.7.3) can be used one grid length from the boundary. The iteration equation for the column $i=2$ is:

$$\overset{*}{P}{}^{m+1,n+1}_{2,j} = \overset{*}{P}{}^{m,n+1}_{2,j} + \frac{R^m_{2,j}}{\frac{\Delta z^2}{\Delta x^2}+2} \qquad (3.7.4)$$

$$R^m_{2,j} = \frac{\Delta z^2}{\Delta x^2}\overset{*}{P}{}^{m,n+1}_{4,j} + \overset{*}{P}{}^{m,n+1}_{2,j+2} + \overset{*}{P}{}^{m,n+1}_{2,j-2} - \left(\frac{\Delta z^2}{\Delta x^2}+2\right)\overset{*}{P}{}^{n+1}_{2,j} - \frac{4\Delta z^2}{\Delta t\,\alpha_{i,j}} DV^{aux}_{2,j} \qquad (3.7.5)$$

Similar expressions are used at other grid points lying one grid length from the boundary.

There are four points in the corners of the above region which require a third iteration equation derived also by the use of images:

$$P^{*m+1,n+1}_{2,2} = P^{*m,n+1}_{2,2} + \frac{R^{m}_{2,2}}{\frac{\Delta z^2}{\Delta x^2} + 1} \qquad (3.7.6)$$

$$R^{m}_{2,2} = \frac{\Delta z^2}{\Delta x^2} P^{*m,n+1}_{4,2} + P^{*m,n+1}_{2,4} - \left(\frac{\Delta z^2}{\Delta x^2} + 1\right) P^{*m,n+1}_{2,2} - \frac{4\Delta z^2}{\Delta t \alpha_{i,j}} DV^{aux}_{2,2} \qquad (3.7.7)$$

A similar expression is used for the other three corners. Figure (3-3) shows a corner of the grid and indicates which iteration equation is used for each of the grid points.

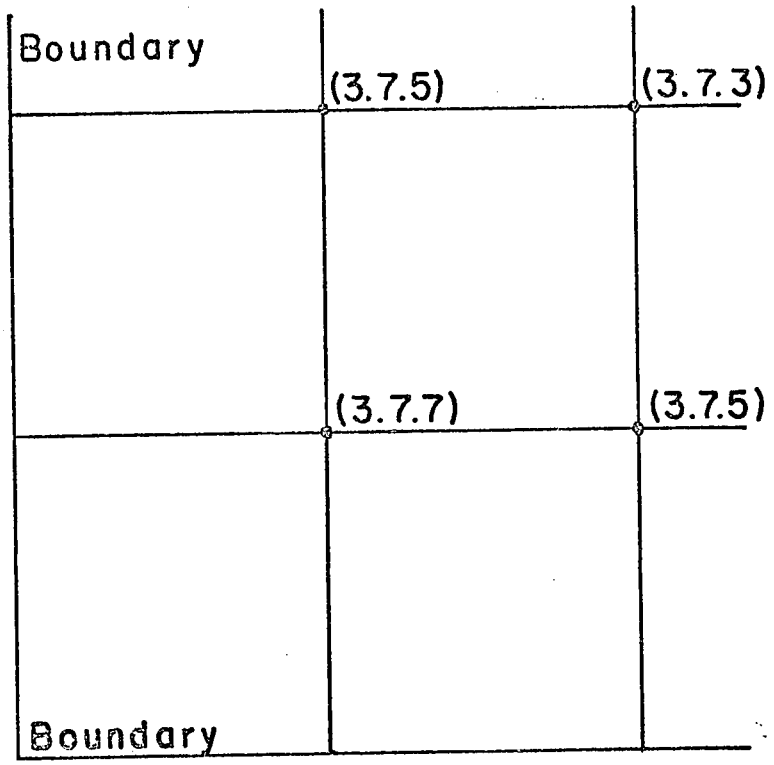

FIGURE (3-3) Use of the three iteration equations.

The iteration procedure is applied sequentially to each point of the grid as many times as necessary to reduce the residual at every point to less than some pre-determined maximum error. In practice, the iteration procedure converges more rapidly if an over-relaxation is

used at each grid point. If such a procedure is used, (3.7.3), (3.7.5) and (3.7.7) respectively become:

$$P^{*\,m+1,n+1}_{i,j} = P^{*\,m,n+1}_{i,j} + \frac{\lambda R^{m}_{i,j}}{2\left(\frac{\Delta z^2}{\Delta x^2}+1\right)} \qquad (3.7.8)$$

$$P^{*\,m+1,n+1}_{2,j} = P^{*\,m,n+1}_{2,j} + \frac{\lambda R^{m}_{2,j}}{\left(\frac{\Delta z^2}{\Delta x^2}+2\right)} \qquad (3.7.9)$$

$$P^{*\,m+1,n+1}_{2,2} = P^{*\,m,n+1}_{2,2} + \frac{\lambda R^{m}_{2,2}}{\left(\frac{\Delta z^2}{\Delta x^2}+1\right)} \qquad (3.7.10)$$

where λ = over-relaxation factor

The value of λ which gives the most rapid convergence is most accurately determined by experiment and was found to be 1.7.

Once the values of $P^{*\,n+1}$ have been determined, (3.6.3) to (3.6.6) are used to find $u'^{\,n+1}$ and w^{n+1}.

3.8 Computation of the Vertical Velocity at the Lower Sub-layer Boundary

Figure (3-4) shows a portion of the grid near the lower boundary.

The equation of continuity written in centered differences for the point P is:

$$\frac{u'^{\,n+1}_{i+1,\frac{h}{2}} - u'^{\,n+1}_{i-1,\frac{h}{2}}}{2\Delta x} = -\frac{w_{i,1}}{h} \qquad (3.8.1)$$

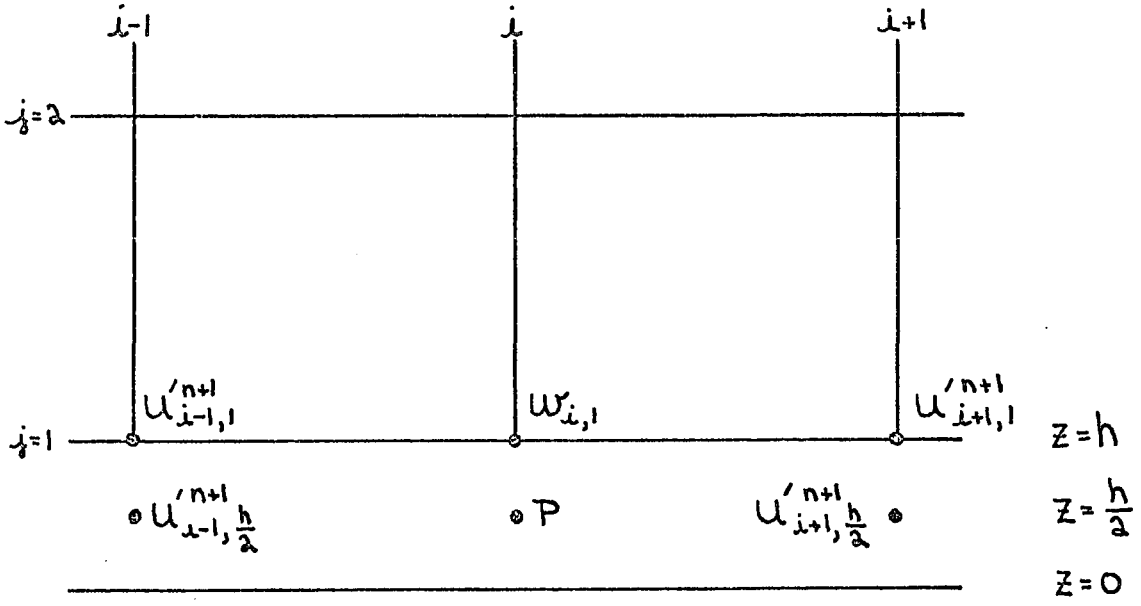

FIGURE (3-4) Boundary value of the vertical velocity.

since the vertical velocity is zero at the earth's surface. If a linear increase in the wind is assumed in lower sub-layer, then:

$$u'^{n+1}_{i+1,\frac{h}{2}} = \frac{1}{2} u'^{n+1}_{i+1,1} \qquad (3.8.2)$$

$$u'^{n+1}_{i-1,\frac{h}{2}} = \frac{1}{2} u'^{n+1}_{i-1,1} \qquad (3.8.3)$$

Even if this assumption is in error, the vertical velocity field is hardly affected since it is not too sensitive to the values of $w_{i,1}$ Substitution of the above into (3.8.1) gives the result:

$$w^{n+1}_{i,1} = \frac{h}{4\Delta x}\left(u'^{n+1}_{i-1,1} - u'^{n+1}_{i+1,1} \right) \qquad (3.8.4)$$

3.9 Filtering the Velocity Fields

A one dimensional three-point filter is applied at each time step to all three components of the velocity field. The form of the filter is:

$$\overline{F}_i = (1-S)F_i + \frac{S}{2}(F_{i+1} + F_{i-1}) \qquad (3.9.1)$$

where F_i = unfiltered values

$\overline{F}_i$ = filtered value

S = a constant which determines the response of the filter

To control non-linear instability, it is necessary to remove two to three gridlength waves with the filter. According to Haltiner (1971), the response of (3.9.1) with S=0.5 is:

$$R = \cos^2 \frac{\pi \Delta x}{L}$$

where R = response

L = wavelength of a wave in units of Δx

The response is the amplitude of a given wave after application of the filter divided by its amplitude before filtering. Clearly for a two gridlength wave, the response is zero. Figure (3-5) shows the response

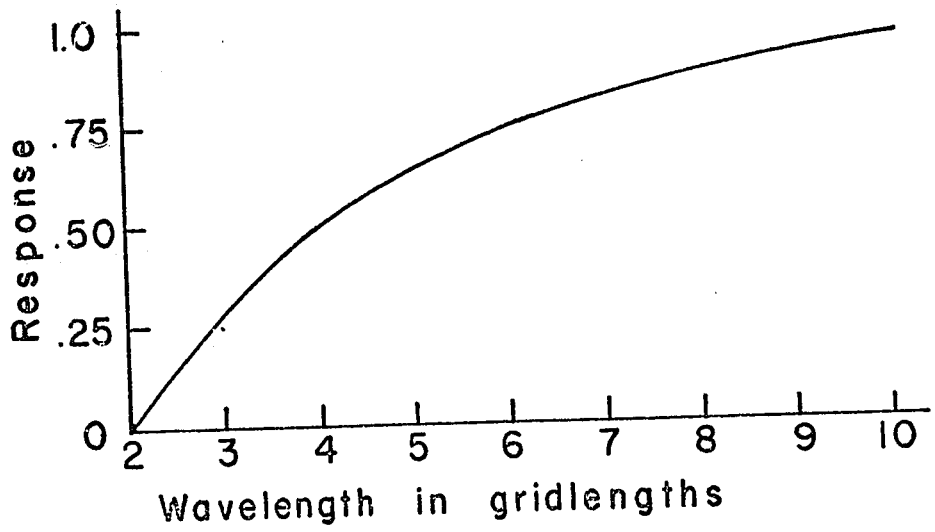

FIGURE (3-5) Filter response.

for other wavelengths.

3.10 Ordering of the Steps

To help clarify what has been presented so far, it is helpful to show the steps followed in the computer model.

a) determine initial values

b) compute θ', v' and u' at z=h using the lower sub-layer equations of Sections (2.8) and (2.9)

c) filter u', v' and w fields using (3.9.1)

d) apply $\frac{\partial}{\partial x}=0$ boundary condition to u', v' and θ' fields

e) compute temperature using (2.4.5)

f) compute hydrostatic pressure perturbation from (3.4.3)

g) compute u^{aux} and w^{aux} fields using (3.6.1) and (3.6.2)

h) compute θ'^{n+1} and v'^{n+1} from (3.5.11) and (3.5.12)

i) apply temperature wave to land surface (2.10.7)

j) calculate DV^{aux} from (3.6.8)

k) determine non-hydrostatic pressure perturbation using equations of Section (3.7)

l) compute u'^{n+1} and w^{n+1} using (3.6.3) and (3.6.5)

m) repeat steps b) to l) until desired length of forecast is achieved

n) display results

A fully documented listing of the computer program is included in Appendix A.

CHAPTER 4

THE RESULTS OF AN INTEGATION WITH THE ATMOSPHERE INITIALLY AT REST - THE COMPARISON MODEL

4.1 Introduction

The computer program, used by Neumann and Mahrer (1971), was modified by including the vertical Coriolis term, changing some of the lower sub-layer equations and increasing the peak-to-peak amplitude of the temperature wave applied to the land from 20 C to 25 C.

The purpose of duplicating Neumann's and Mahrer's results is to provide a standard by which to compare the results that are presented in succeeding chapters and for this reason, the model will be referred to as the "Comparison Model".

4.2 Initial Conditions and Fields

The model was integrated for a period of twelve hours starting at 8:00 A.M., using a 20 row by 29 column grid. In the computer program, an extra row is added to the grid to store the data for z=0, making the grid 21 rows by 29 columns. The finite-difference data concerning the grid as well as the initial lapse rate, horizontal wind components, surface temperature and surface pressure are presented in Table (4-1). From these data, the initial fields of Table (4-2) were computed.

The size of the time step was chosen to satisfy (3.5.5),

(3.5.8) and (3.5.10). The largest expected values of the u component, w component and eddy diffusivity were:

$$u_{max} \sim 5 \text{ m/sec}$$

$$w_{max} \sim 0.25 \text{ m/sec}$$

$$K_{max} \sim 30 \text{ m}^2/\text{sec}$$

Hence, the restriction on the time step for each of these values was:

$$\Delta t \leq \frac{\Delta x}{u_{max}} = 1000 \text{ sec}$$

$$\Delta t \leq \frac{\Delta z}{w_{max}} = 400 \text{ sec}$$

$$\Delta t \leq \frac{(\Delta z)^2}{2K_{max}} = 166 \text{ sec}$$

To have a margin of safety, the time step used was 150 seconds.

NUMBER OF HORIZONTAL GRID POINTS	29
NUMBER OF VERTICAL GRID POINTS	21
HORIZONTAL SPACE INCREMENT (m)	5000.0
VERTICAL SPACE INCREMENT (m)	100.0
TIME STEP (sec)	150.0
LAPSE RATE (deg/m)	0.0065
U COMPONENT (m/sec)	0.0
V COMPONENT (m/sec)	0.0
SURFACE TEMPERATURE (K)	299.0
SURFACE PRESSURE (mb)	1000.0

TABLE (4-1) Grid data and initial conditions.

ROW	TEMPERATURE (K)	POTENTIAL TEMPERATURE (K)	PRESSURE (mb)	HEIGHT (m)
1	299.0	299.0	1000.0	0.0
2	298.7	299.2	994.3	50.0
3	298.0	299.5	983.0	150.0
4	297.4	299.8	971.8	250.0
5	296.7	300.1	960.7	350.0
6	296.1	300.5	949.7	450.0
7	295.4	300.8	938.8	550.0
8	294.8	301.1	928.0	650.0
9	294.1	301.5	917.3	750.0
10	293.5	301.8	906.7	850.0
11	292.8	302.2	896.2	950.0
12	292.2	302.5	885.8	1050.0
13	291.5	302.8	875.5	1150.0
14	290.9	303.2	865.3	1250.0
15	290.2	303.5	855.2	1350.0
16	289.6	303.8	845.2	1450.0
17	288.9	304.2	835.2	1550.0
18	288.3	304.5	825.4	1650.0
19	287.6	304.9	815.7	1750.0
20	287.0	305.2	806.0	1850.0
21	286.3	305.6	796.5	1950.0

TABLE (4-2) Initial fields.

A latitude of 43 N was chosen for the integration since this allowed the Coriolis parameter to be set equal to 10^{-4} sec^{-1}. Because the sea-breeze does not depend strongly on the latitude, this choice of latitude does not severely restrict the applicability of the results.

4.3 Results

The computer program displayed the wind and temperature fields every two hours of meteorological time, that is, after 48 time steps.

The results of the model at 10:00 A.M. showed that the centre of a weak negative circulation (negative in the mathematical sense) was evident at a height of about 350 meters above the coastline. At this time, the strongest onshore wind of about 0.5 m/sec was at the coast and a weaker flow of larger vertical extent was present aloft. The turning effect of the Coriolis force was beginning to be felt since a small v -component was present.

The noon results (Figure (4-1)), as expected, showed that the circulation had strengthened. The centre of the circulation, located 3 km inland was at a height of nearly 500 meters. As was previously the case, a weaker return flow existed aloft. The maximum ascent velocity was 3 cm/sec with the maximum descent about the same. The action of the Coriolis force continued to strengthen the v -component of the wind and as well, a striking vertical temperature gradient was present near the ground.

At 2:00 P.M., which was shortly after the time of maximum temperature of land surface, the results (Figure (4-2)) showed that

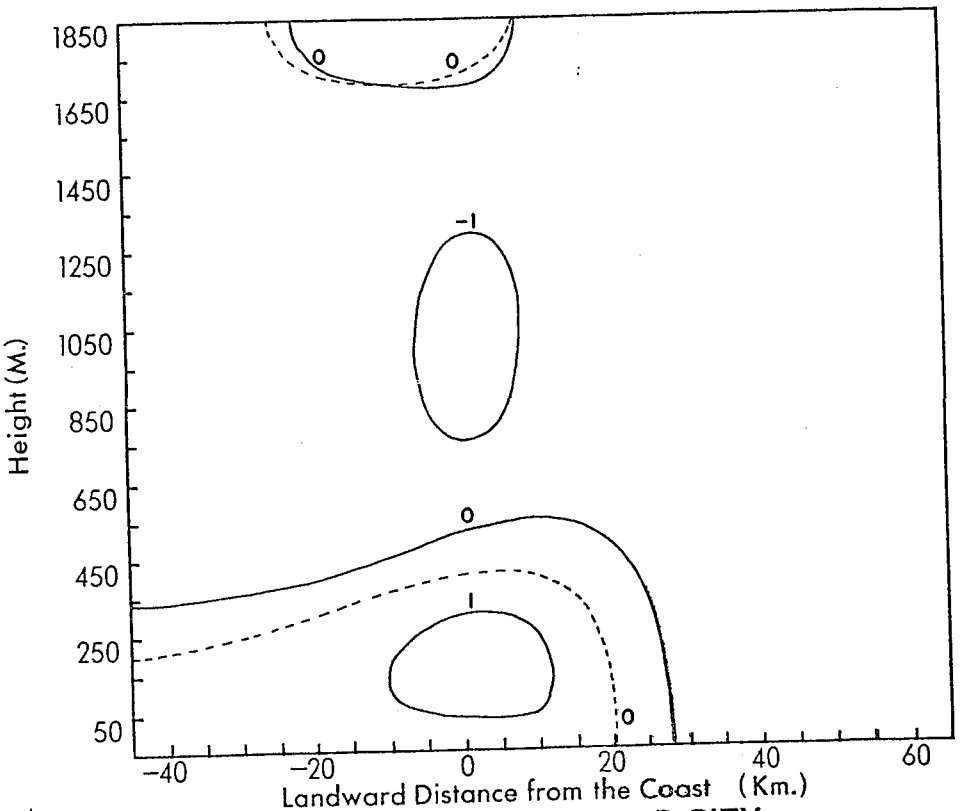

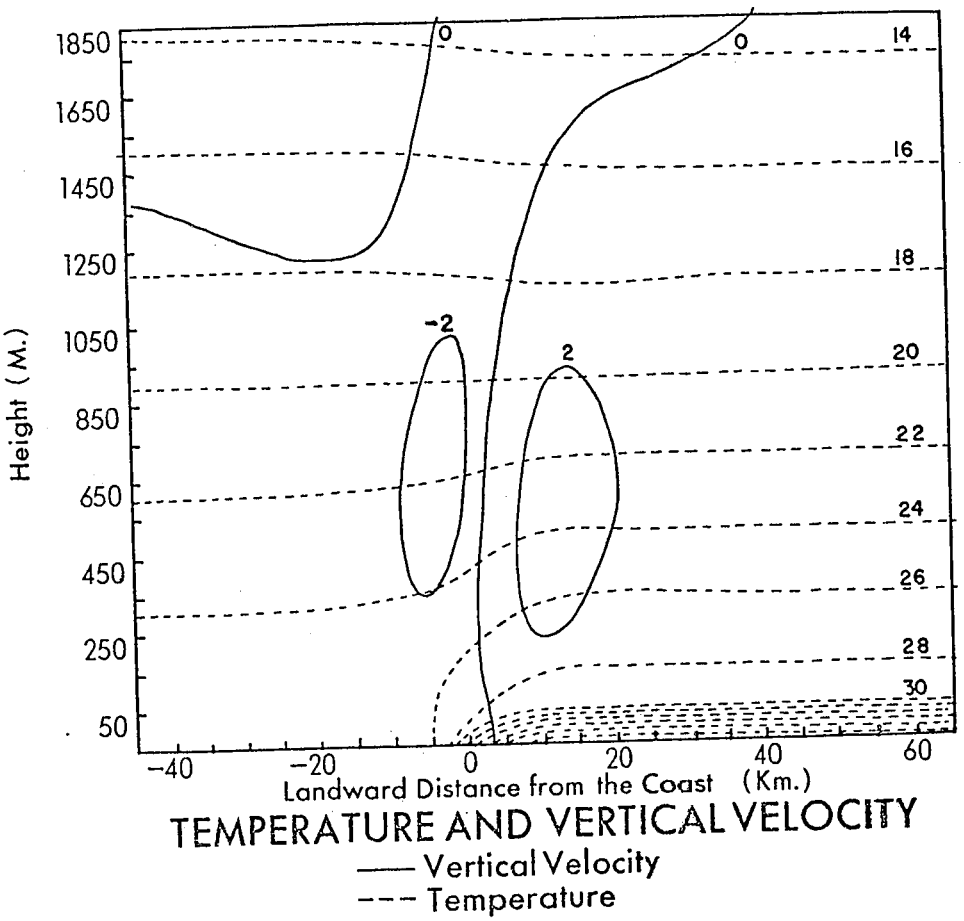

FIGURE (4-1) Results for noon. Horizontal velocities are given
[illegible] vertical velocities in cm/sec and temperatures in C.

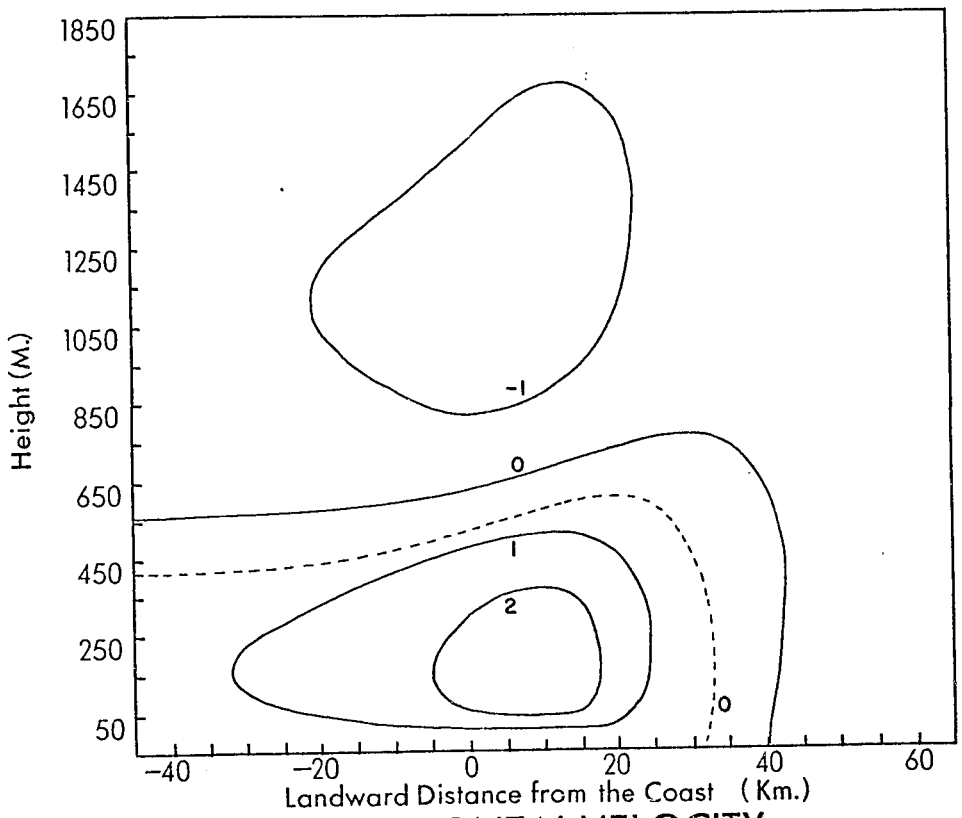

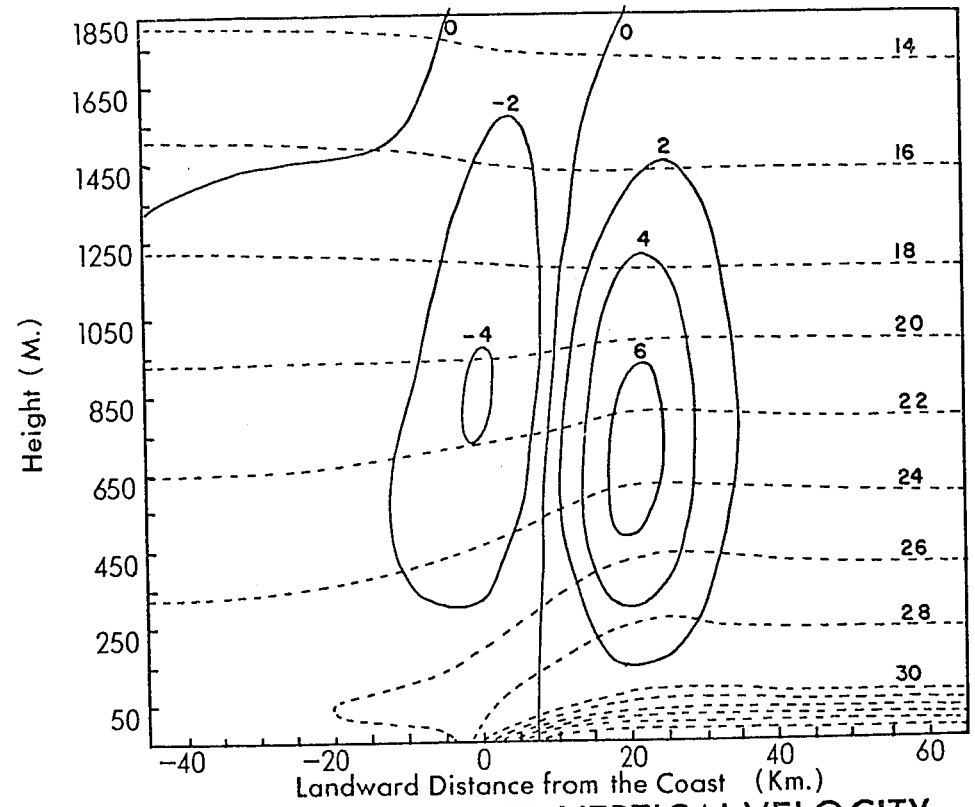

FIGURE (4-2) Results for 2:00 P.M. Horizontal velocities are given in m/sec, vertical velocities in cm/sec and temperatures in C.

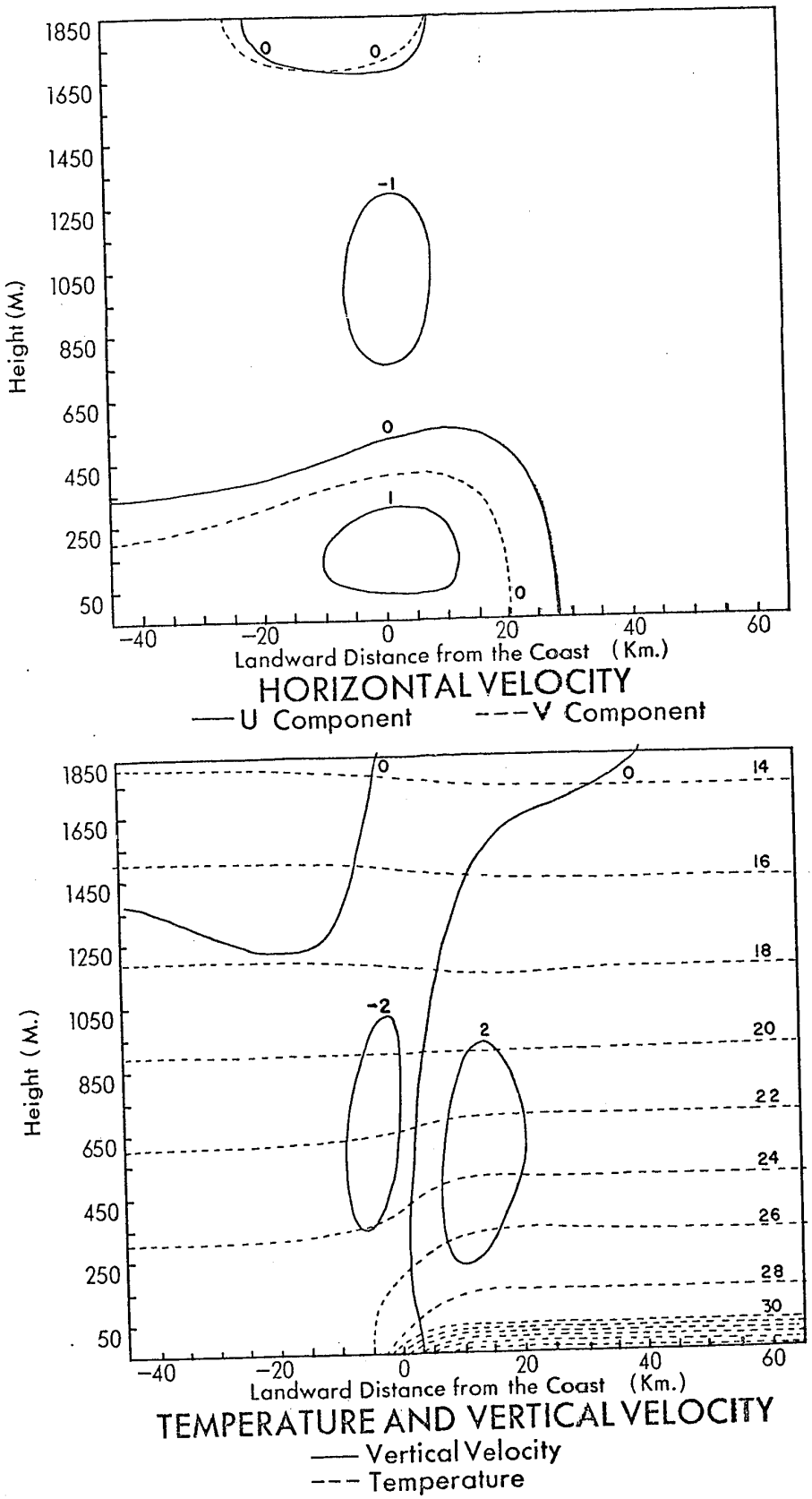

FIGURE (4-1) Results for noon. Horizontal velocities are given in m/sec, vertical velocities in cm/sec and temperatures in C.

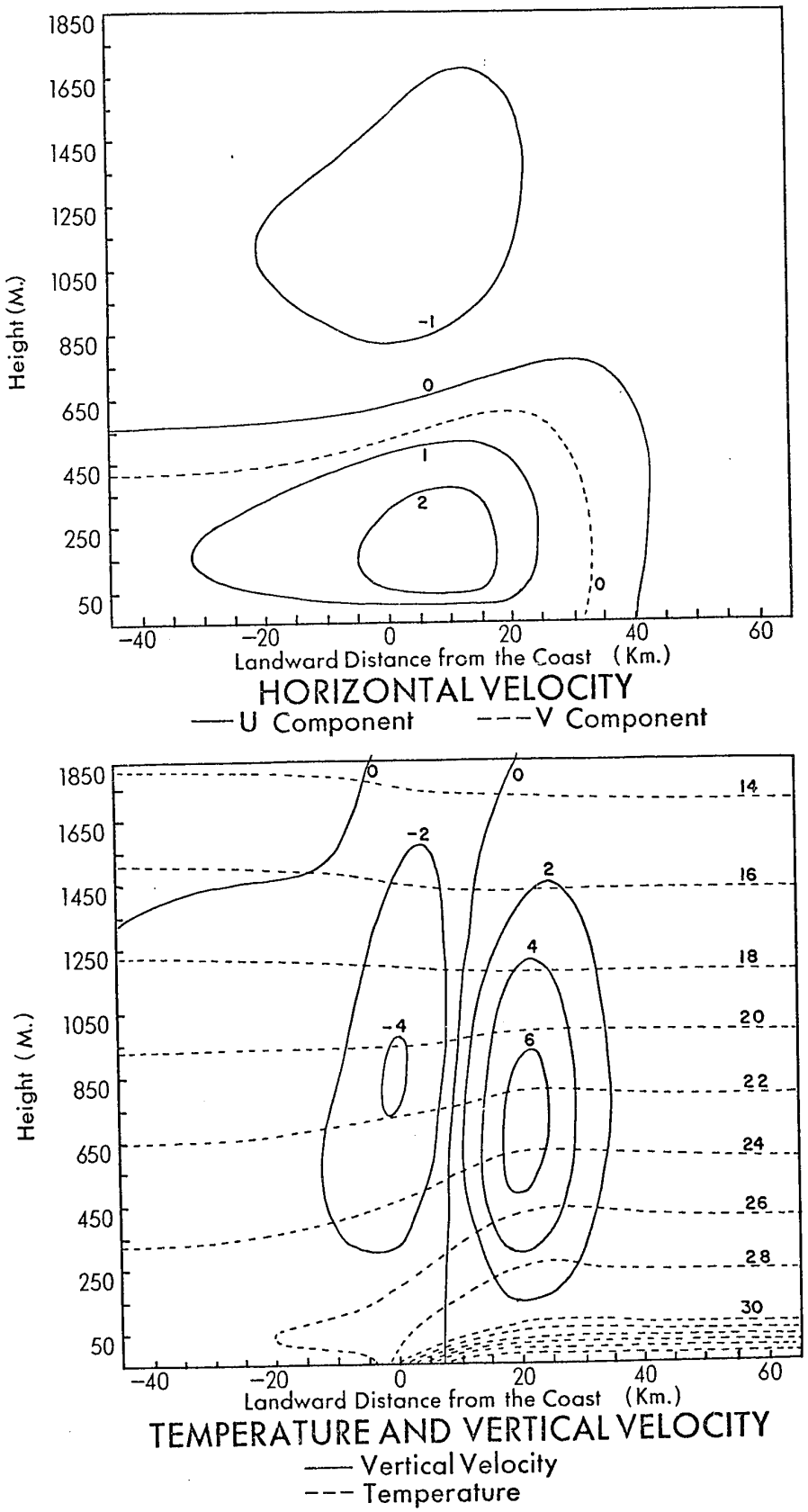

FIGURE (4-2) Results for 2:00 P.M. Horizontal velocities are given in m/sec, vertical velocities in cm/sec and temperatures in C.

the onshore flow had reached nearly 3 m/sec. The centre of the circulation was now 8 km inland at a height of about 600 m. At this time, the maximum descent was slightly over 4 cm/sec with the maximum ascent about 50 percent larger. Because of the distorted scale of the diagrams, continuity may not appear to be satisfied, i.e. it is not necessary to have large vertical velocities in order to have large horizontal velocities. The temperature field showed a slight upward bulging of the isotherms near the region of greatest upward motion.

Although the land had been cooling for nearly three hours, the results for 4:00 P.M. (Figure (4-3)) showed that the sea-breeze continued to intensify. The strongest onshore wind was about 4.5 m/sec. By this time, the Coriolis force had turned the onshore flow nearly 15 degrees from a line perpendicular to the coast. The effect of the high turbulent friction over the land was clearly shown by the strong horizontal gradients of the u -component of the wind. This effect via continuity was responsible for increased ascent over the land. The centre of the circulation which continued to accelerate inland was located 20 kilometers from the coast at a height of 800 meters. The bulging of the isotherms in the region of strongest ascent continued to increase although the vertical temperature gradient near the ground had weakened with the continued cooling of the land.

Figure (4-4) gives the results for 6:00 P.M. which showed that the sea-breeze had started to decrease in strength. The wind had been turned by 30 degrees from the action of the Coriolis force. The enhancement of the ascent by friction was even more striking than in

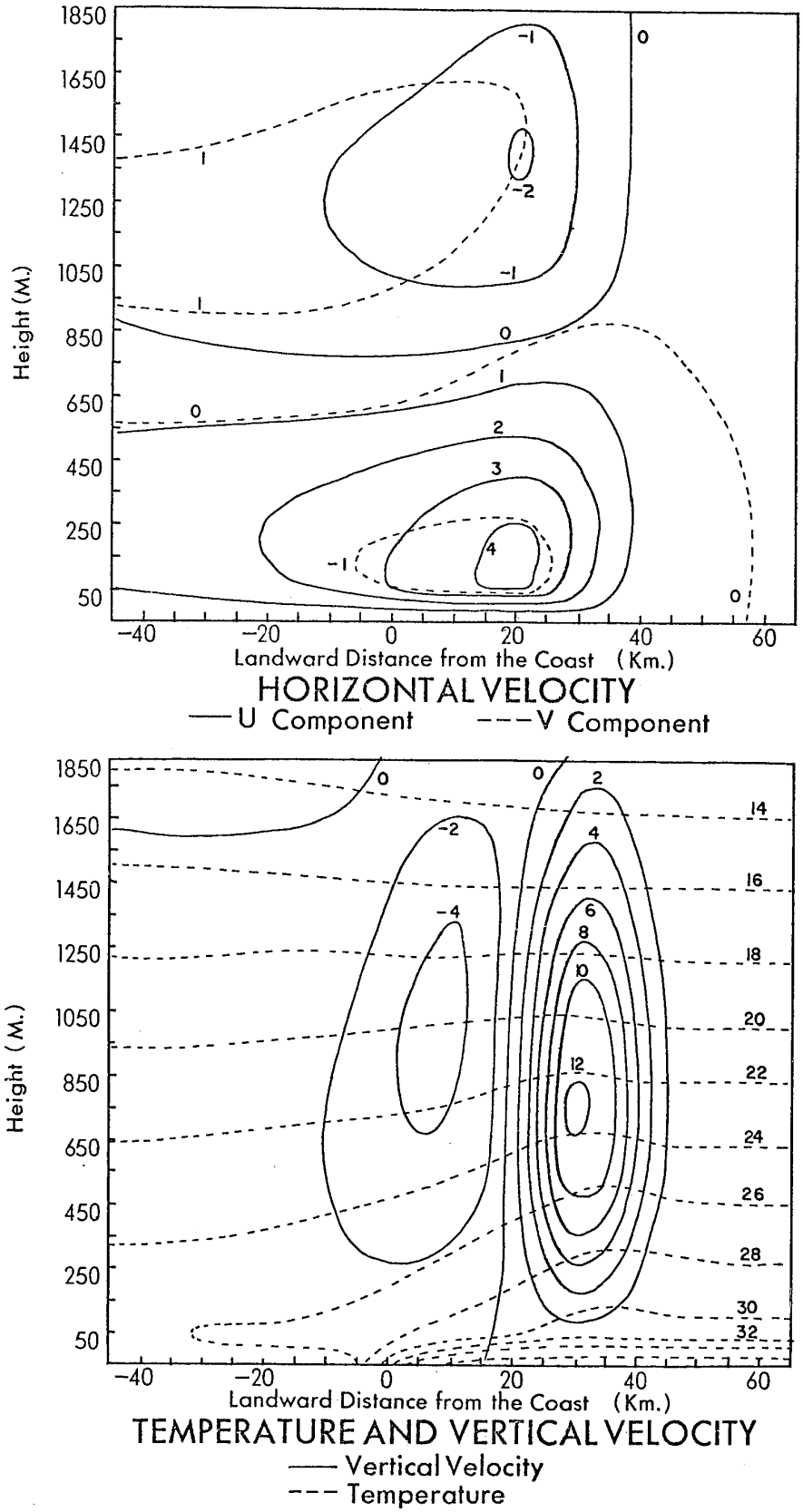

FIGURE (4-3) Results for 4:00 P.M. Horizontal velocities are given in m/sec, vertical velocities in cm/sec and temperatures in C.

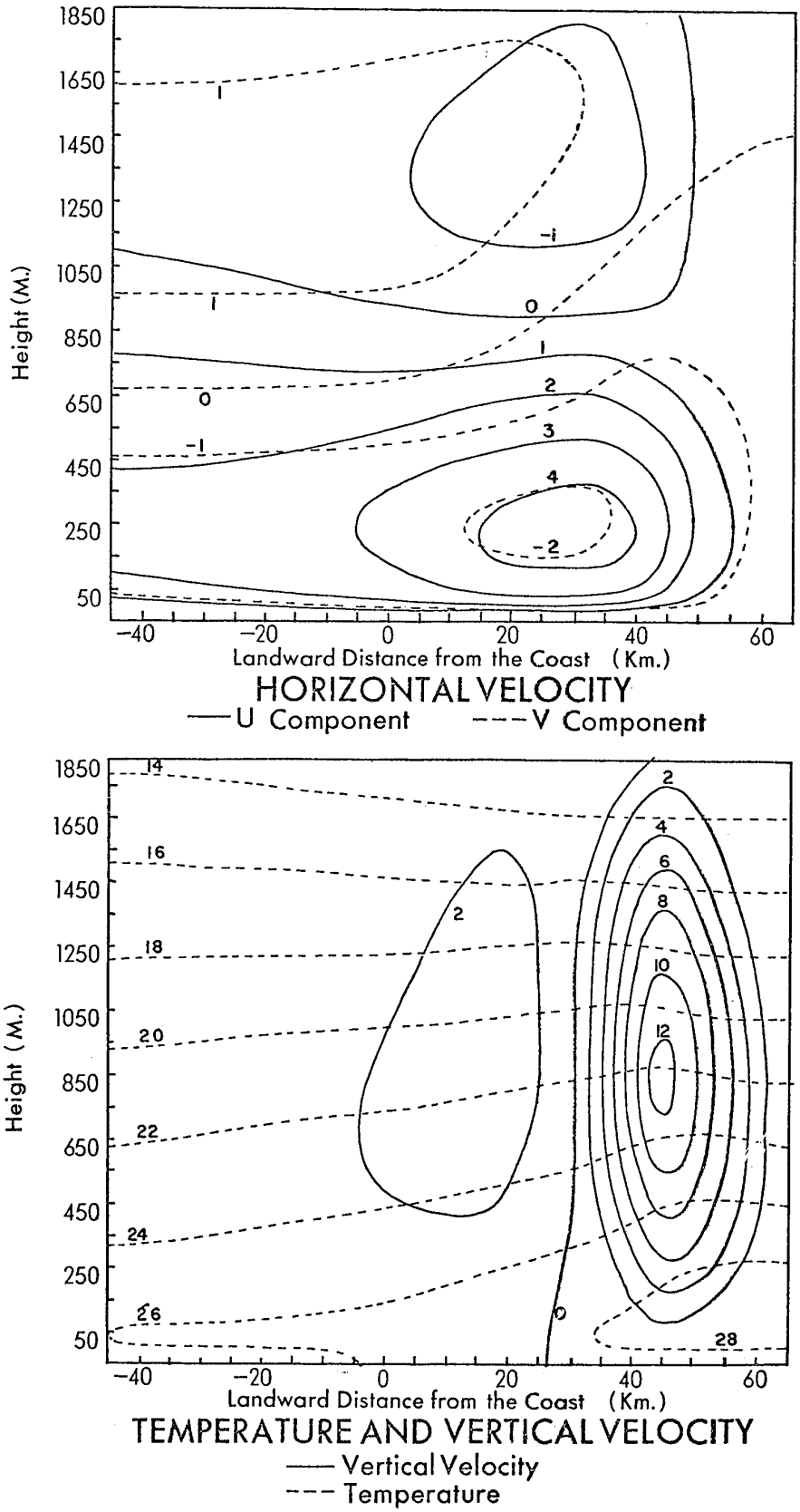

FIGURE (4-4) Results for 6:00 P.M. Horizontal velocities are given in m/sec, vertical velocities in cm/sec and temperatures in C.

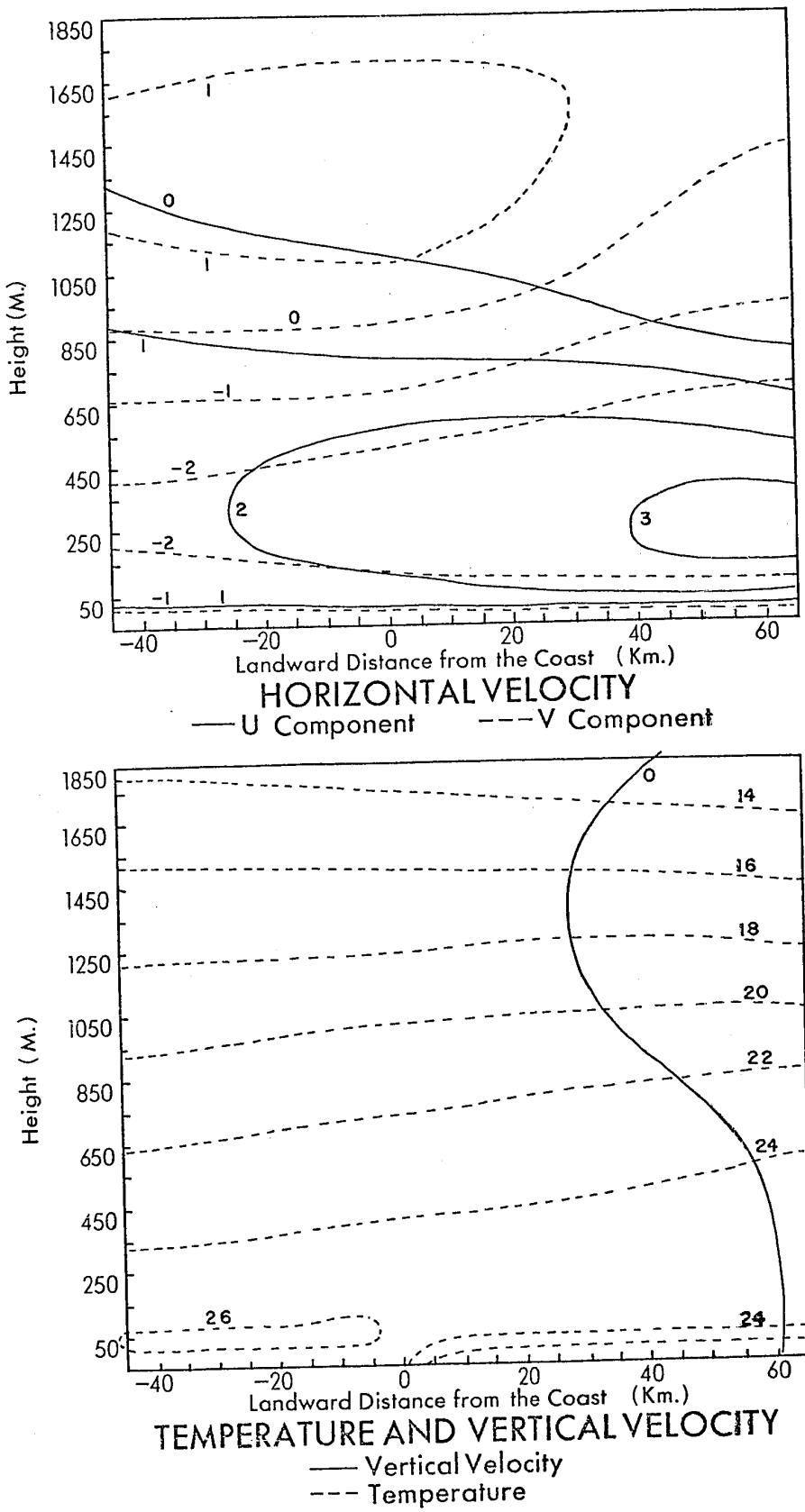

FIGURE (4-5) Results for 8:00 P.M. Horizontal velocities are given in m/sec, vertical velocities in cm/sec and temperatures in C.

the previous results. There had been so much cooling over the land that an inversion was present. Although the horizontal and vertical velocities had decreased only slightly, the core of the circulation was 30 kilometers inland at a height of approximately 900 meters.

The results for 8:00 P.M. (Figure (4-5)) showed that the sea-breeze was dissipating with an onshore flow of nearly 4.5 m/sec, turned 40 degrees by the action of the Coriolis force. The vertical velocities are probably in error since the core was near the lateral boundary. The temperature field showed a strengthened inversion over land and an isothermal layer above it to a height of 400 to 500 meters.

Figure (4-6) gives the hourly variation of the wind at the coastline for the twelve hour period of integration (cf. Figure (1-2)).

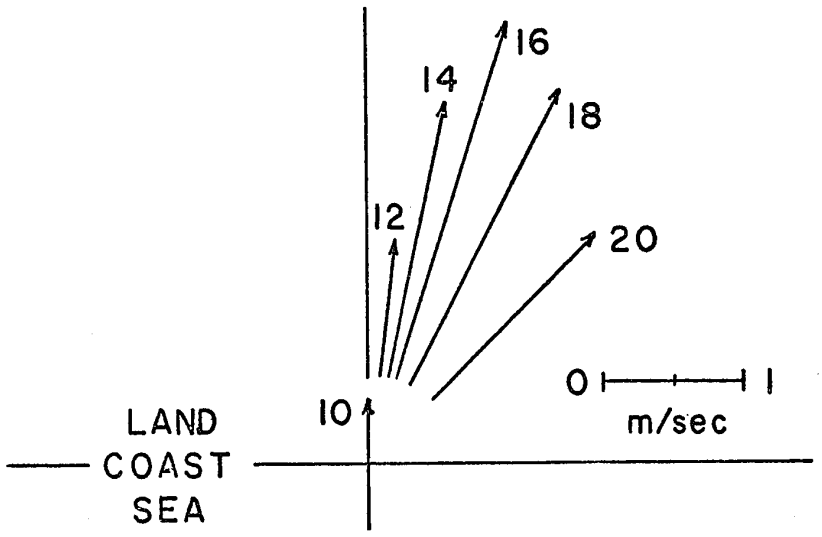

FIGURE (4-6) Predicted hourly variation of the wind.

4.4 Verification of the Incompressibility Assumption

Batchelor's criteria were applied to the results given by the Comparison Model. Condition (2.6.1) states that:

$$\frac{U^2}{c^2} << 1$$

Since the strongest wind was about 5 m/sec, (2.6.1) is verified. Since the smallest time scale that could be resolved in this model is:

$$2\Delta t = 300 \text{ sec} \cong \frac{1}{n}$$

the inequality (2.6.2) is satisfied. The most stringent condition is (2.6.3):

$$\frac{\rho g L}{\gamma p} << 1 \qquad (4.4.1)$$

It is first necessary to determine the scale length L:

$$L \sim \frac{w}{\left|\frac{\partial w}{\partial z}\right|}$$

Evaluating (4.4.1) at 4:00 P.M. gives:

$$L \sim 800 \text{ m}$$

Hence, (2.6.3) becomes:

$$\frac{\rho g L}{\gamma p} = 0.06 << 1$$

From the application of Batchelor's criteria, it can be seen that the assumption of incompressibility is reasonable.

4.5 The Energy Equation

A check was made to see whether the model conserves energy. The first law of thermodynamics in the form:

$$\frac{dQ}{dt} = c_p \frac{dT}{dt} - \alpha \frac{dp}{dt} \qquad (4.5.1)$$

where Q = heat input

T = temperature

c_p = specific heat at constant pressure

α = specific volume

p = pressure

t = time

was integrated over the entire grid with the exception of the boundary points. Equation (4.5.1) can be rewritten in terms of potential temperature as:

$$\frac{dQ}{dt} = \frac{T}{\theta} c_p \frac{d\theta}{dt} \qquad (4.5.2)$$

and upon substitution of (2.4.3) becomes:

$$\frac{dQ}{dt} = \frac{T}{\theta} c_p \frac{\partial}{\partial z}\left(K \frac{\partial \theta}{\partial z}\right) \qquad (4.5.3)$$

Substitution of (4.5.3) into (4.5.1) and expansion of the total derivatives gives:

$$\frac{T}{\theta} c_p \frac{\partial}{\partial z}\left(K \frac{\partial \theta}{\partial z}\right) = c_p \frac{\partial T}{\partial t} + c_p u \frac{\partial T}{\partial x} + c_p w \frac{\partial T}{\partial z}$$

$$- \alpha \frac{\partial p}{\partial t} - \alpha u \frac{\partial p}{\partial x} - \alpha w \frac{\partial p}{\partial z} \qquad (4.5.4)$$

Equation (4.5.4) integrated over the grid yields:

$$\sum_{i=2}^{L-1}\sum_{j=2}^{M-1}\frac{T}{\theta}c_p\frac{\partial}{\partial z}\left(K\frac{\partial\theta}{\partial z}\right)\Delta x\,\Delta z\,\Delta t \overset{(1)}{=}$$

$$\sum_{i=2}^{L-1}\sum_{j=2}^{M-1}c_p\frac{\partial T}{\partial t}\Delta x\Delta z\Delta t \overset{(2)}{+} \sum_{i=2}^{L-1}\sum_{j=2}^{M-1}c_p u\frac{\partial T}{\partial x}\Delta x\Delta z\Delta t \overset{(3)}{+}$$

$$\sum_{i=2}^{L-1}\sum_{j=2}^{M-1}c_p w\frac{\partial T}{\partial z}\Delta x\Delta z\Delta t \overset{(4)}{-} \sum_{i=2}^{L-1}\sum_{j=2}^{M-1}\alpha\frac{\partial p}{\partial t}\Delta x\Delta z\Delta t \overset{(5)}{-}$$

$$-\sum_{i=2}^{L-1}\sum_{j=2}^{M-1}\alpha u\frac{\partial p}{\partial x}\Delta x\Delta z\Delta t \overset{(6)}{-} \sum_{i=2}^{L-1}\sum_{j=2}^{M-1}\alpha w\frac{\partial p}{\partial z}\Delta x\Delta z\Delta t \overset{(7)}{} \qquad (4.5.5)$$

where Δt = time step

Δx = horizontal space increment

Δz = vertical space increment

M = number of grid rows

L = number of grid columns

Term (1) of the above is the heat entering the grid through the lower boundary by turbulent diffusion, term (2) is the increase in enthalpy, term (3) is the heat leaving the grid through the lateral boundaries, term (4) is the heat leaving the lower boundary of the grid by convection, term (5) is the change in potential energy in the pressure field and term (6) is the production of mean and turbulent kinetic energy via the action of the pressure field. The

major part of term (7) is the increase in potential energy and the rest of this term is the production of kinetic energy.

Figure (4-7) gives the cumulative magnitude of each of the terms of (4.5.5) since 8:00 A.M. Terms (5) and (6) are not included since they are small. The maximum imbalance of equation (4.5.5) occurred at the twelfth hour when the right hand side was six percent larger than the left hand side.

---

[1] The centre of the circulation is located at the intersection of the zero isopleth of the u-component and the zero isopleth of the vertical velocity.

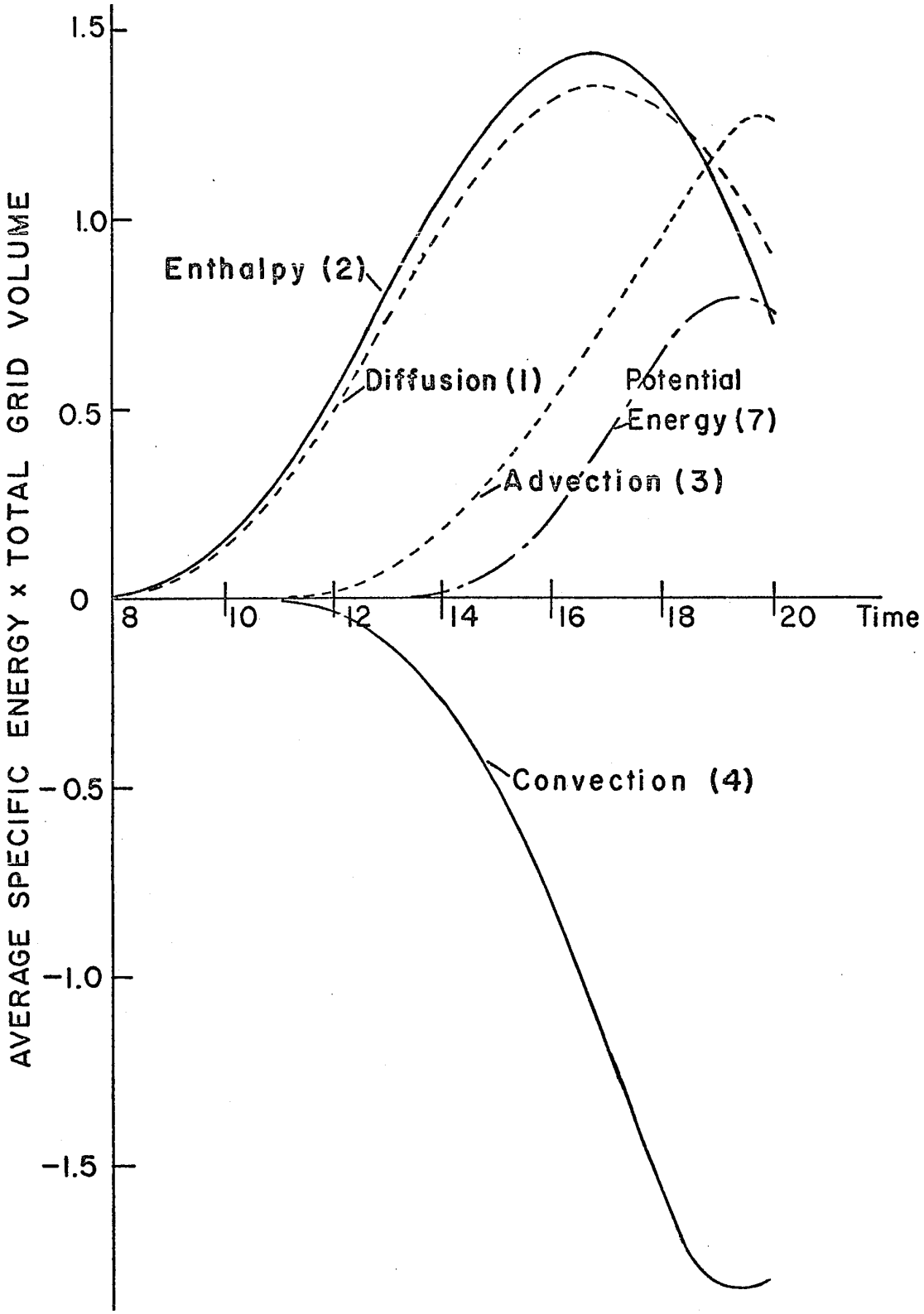

FIGURE (4-7) Cumulative magnitudes of the terms of the energy equation. The units of energy are 10^{11} J m^{3} Kg^{-1}.

CHAPTER 5

SYNOPTIC CONTROL OF THE SEA-BREEZE

5.1 Introduction

The motionless atmosphere in which the sea-breeze of the previous chapter occurred is rarely observed. In an attempt to approach physical reality more closely, the effects of initial atmospheric motion, initial lapse rate and ground heating on the sea-breeze circulation were studied.

Estoque (1962) presented the results of similar solutions using a model which assumed hydrostatic equilibrium and which also used only an approximation to the incompressible continuity equation.

5.2 The Effects of Increased Stability

The initial conditions and grid parameters used for this integration are given in Table (5-1). These data were the same as those for the Comparison Model except that the initial lapse rate had been made more stable. From the initial conditions, the initial fields of Table (5-2) were computed. To prevent an inordinate number of figures, only the results for 10:00 A.M. and 4:00 P.M. are presented.

The results of this solution parallel those of the previous chapter except for a few interesting details. The 10:00 A.M. results (Figure (5-1)) were rather unexpected since they showed that the increased stability had strengthened both the onshore wind and the

NUMBER OF HORIZONTAL GRID POINTS	29
NUMBER OF VERTICAL GRID POINTS	21
HORIZONTAL SPACE INCREMENT (m)	5000.0
VERTICAL SPACE INCREMENT (m)	100.0
TIME STEP (sec)	150.0
LAPSE RATE (deg/m)	0.0010
U COMPONENT (m/sec)	0.0
V COMPONENT (m/sec)	0.0
SURFACE TEMPERATURE (K)	299.0
SURFACE PRESSURE (mb)	1000.0

TABLE (5-1) Initial conditions and grid parameters for the stable lapse rate case.

return flow aloft. The stable air above the unstable layer near the ground produced a sharp vertical change in the lapse rate in the low levels. Due to the $K \frac{\partial^2 \theta}{\partial z^2}$ term in the thermodynamic equation, a relatively strong rise in temperature occurred, which resulted in an increased onshore flow. Aloft, the stable stratification produced strong cooling thus causing an increased return flow as well. However, the vertical penetration of the landward flow had been reduced.

In contrast, the 4:00 P.M. results (Figure (5-2)) showed that the intensity of the sea-breeze had been diminished by the increased initial stability. The centre of the circulation was located 9 km from the coast at a height of approximately 500 meters. The strength of the sea-breeze and vertical velocity were less while

ROW	TEMPERATURE (K)	POTENTIAL TEMPERATURE (K)	PRESSURE (mb)	HEIGHT (m)
1	299.0	299.0	1000.0	0.0
2	298.9	299.4	994.3	50.0
3	298.8	300.3	983.0	150.0
4	298.7	301.2	971.8	250.0
5	298.6	302.1	960.8	350.0
6	298.5	303.0	949.9	450.0
7	298.4	303.9	939.1	550.0
8	298.3	304.8	928.4	650.0
9	298.2	305.7	917.8	750.0
10	298.1	306.6	907.4	850.0
11	298.0	307.5	897.0	950.0
12	297.9	308.4	886.8	1050.0
13	297.8	309.3	876.7	1150.0
14	297.7	310.2	866.7	1250.0
15	297.6	311.1	856.8	1350.0
16	297.5	312.0	847.0	1450.0
17	297.4	312.9	837.4	1550.0
18	297.3	313.9	827.8	1650.0
19	297.2	314.8	818.4	1750.0
20	297.1	315.7	809.0	1850.0
21	297.0	316.6	799.8	1950.0

TABLE (5-2) Initial fields for the stable lapse rate case.

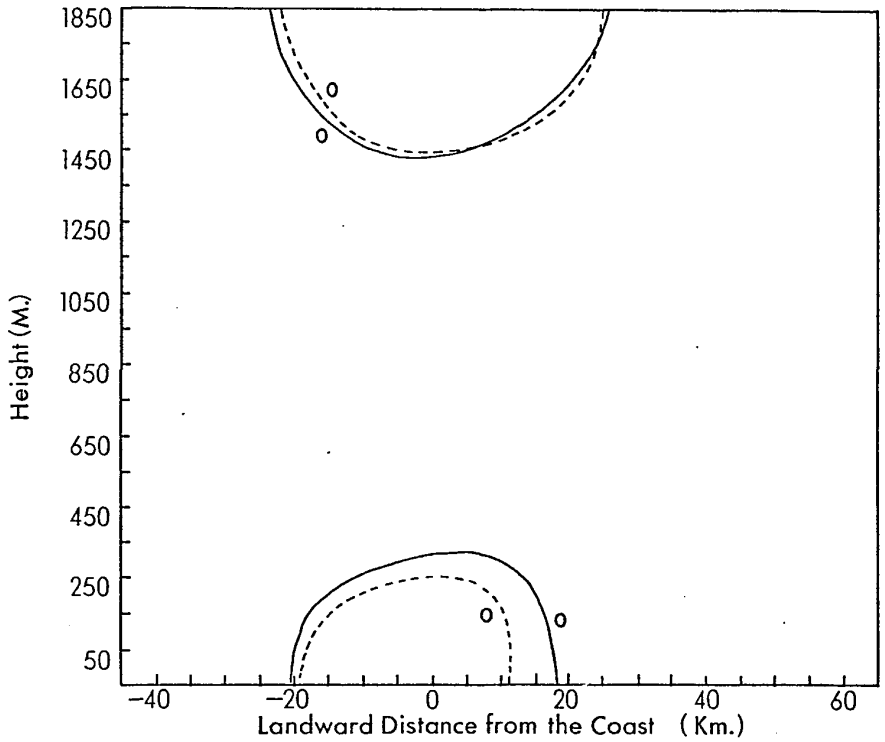

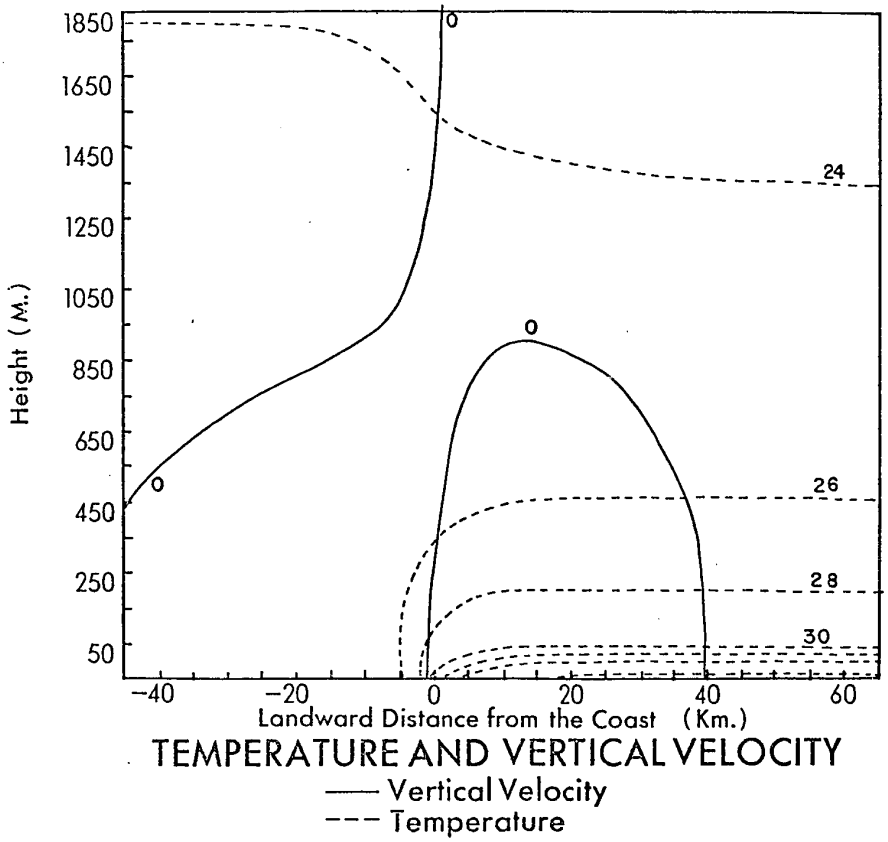

FIGURE (5-1) 10:00 A.M. results for the stable case. Horizontal velocities are given in m/sec, vertical velocities in cm/sec and temperatures in C.

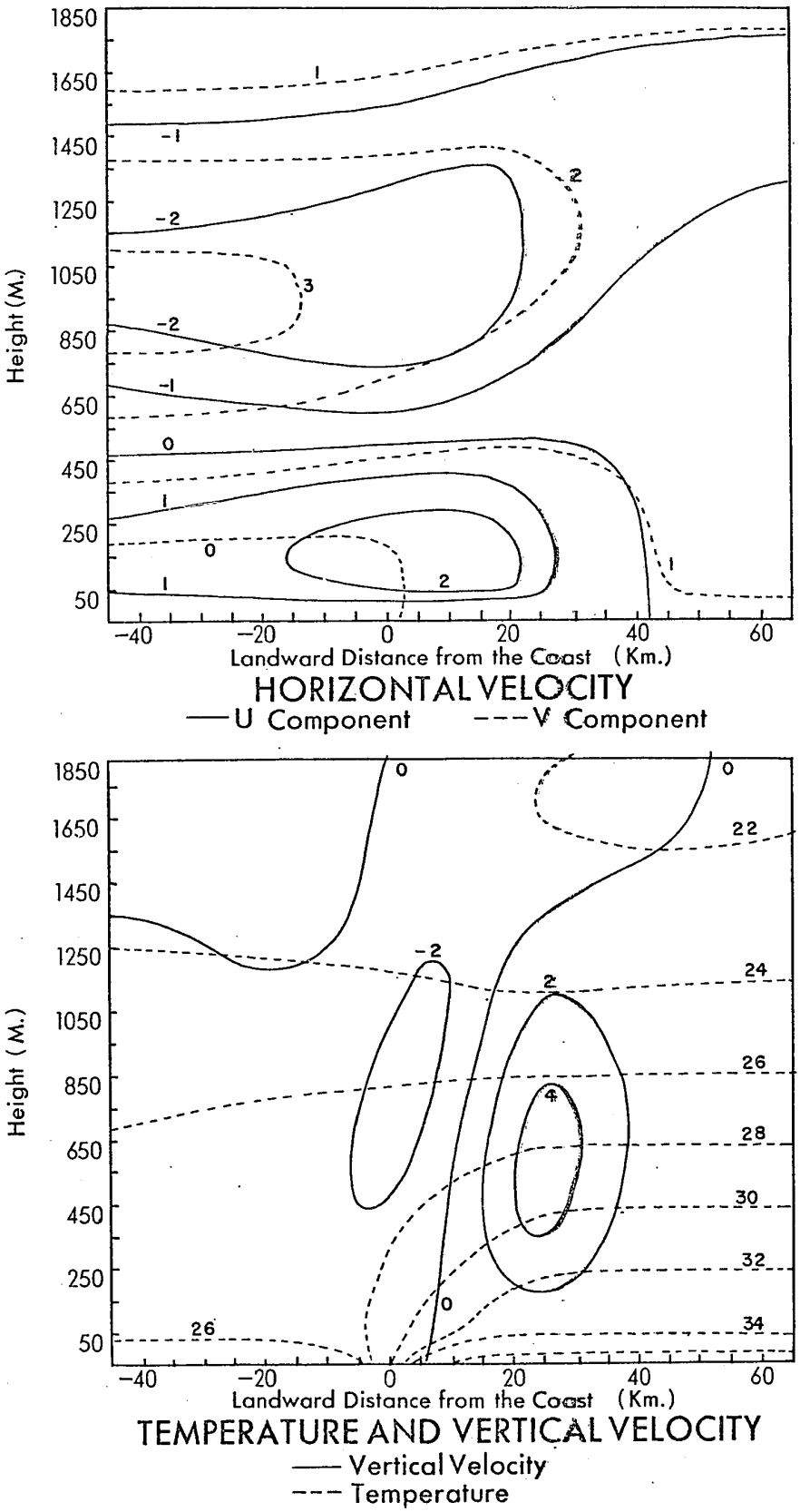

FIGURE (5-2) 4:00 P.M. results for the stable case. Horizontal velocities are given in m/sec, vertical velocities in cm/sec and temperatures in C.

the return flow aloft was greater than in the results for a less stable atmosphere. The flow was less than in the Comparison Model because the rapid vertical change in the lapse rate had been removed by diffusion. In addition, the heat input to the atmosphere was used to overcome the increased density aloft, produced by the strong cooling which resulted from the stable lapse rate. This effect via the hydrostatic equation caused a relatively weak onshore flow.

5.3 An Offshore Flow of 3 m/sec

NUMBER OF HORIZONTAL GRID POINTS	29
NUMBER OF VERTICAL GRID POINTS	21
HORIZONTAL SPACE INCREMENT (m)	5000.0
VERTICAL SPACE INCREMENT (m)	100.0
TIME STEP (sec)	150.0
LAPSE RATE (deg/m)	0.0065
U COMPONENT (m/sec)	-3.0
V COMPONENT (m/sec)	0.0
SURFACE TEMPERATURE (K)	299.0
SURFACE PRESSURE (mb)	1000.0

TABLE (5-3) Initial conditions and grid data for the offshore gradient wind case.

Table (5-3) gives the grid parameters and initial conditions used for this solution. The initial fields were the same as those given in Table (4-2). Only the results for 10:00 A.M. and 4:00 P.M. are included.

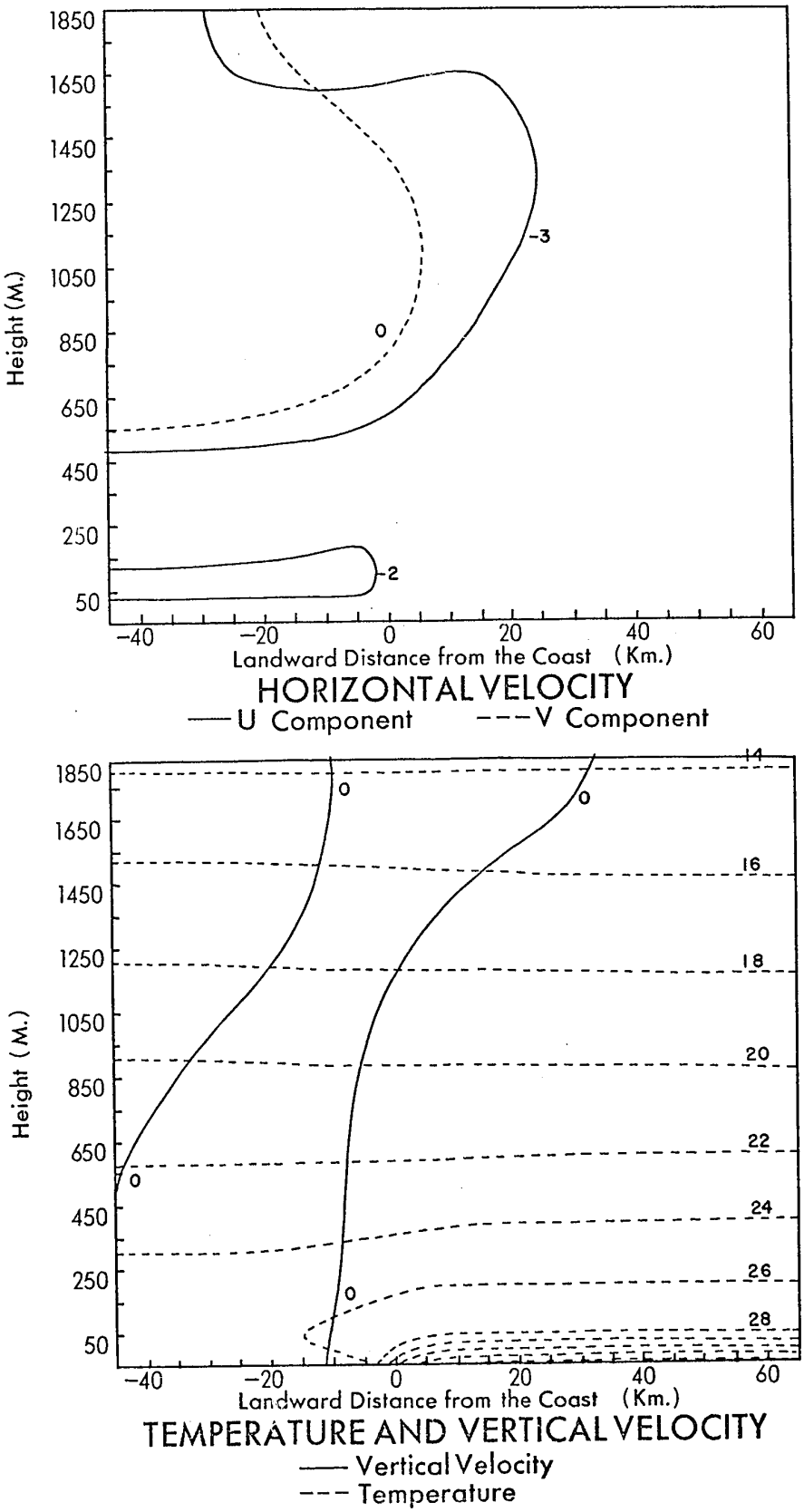

FIGURE (5-3) 10:00 A.M. results for an offshore wind. Horizontal velocities are given in m/sec, vertical velocities in cm/sec and temperatures in C.

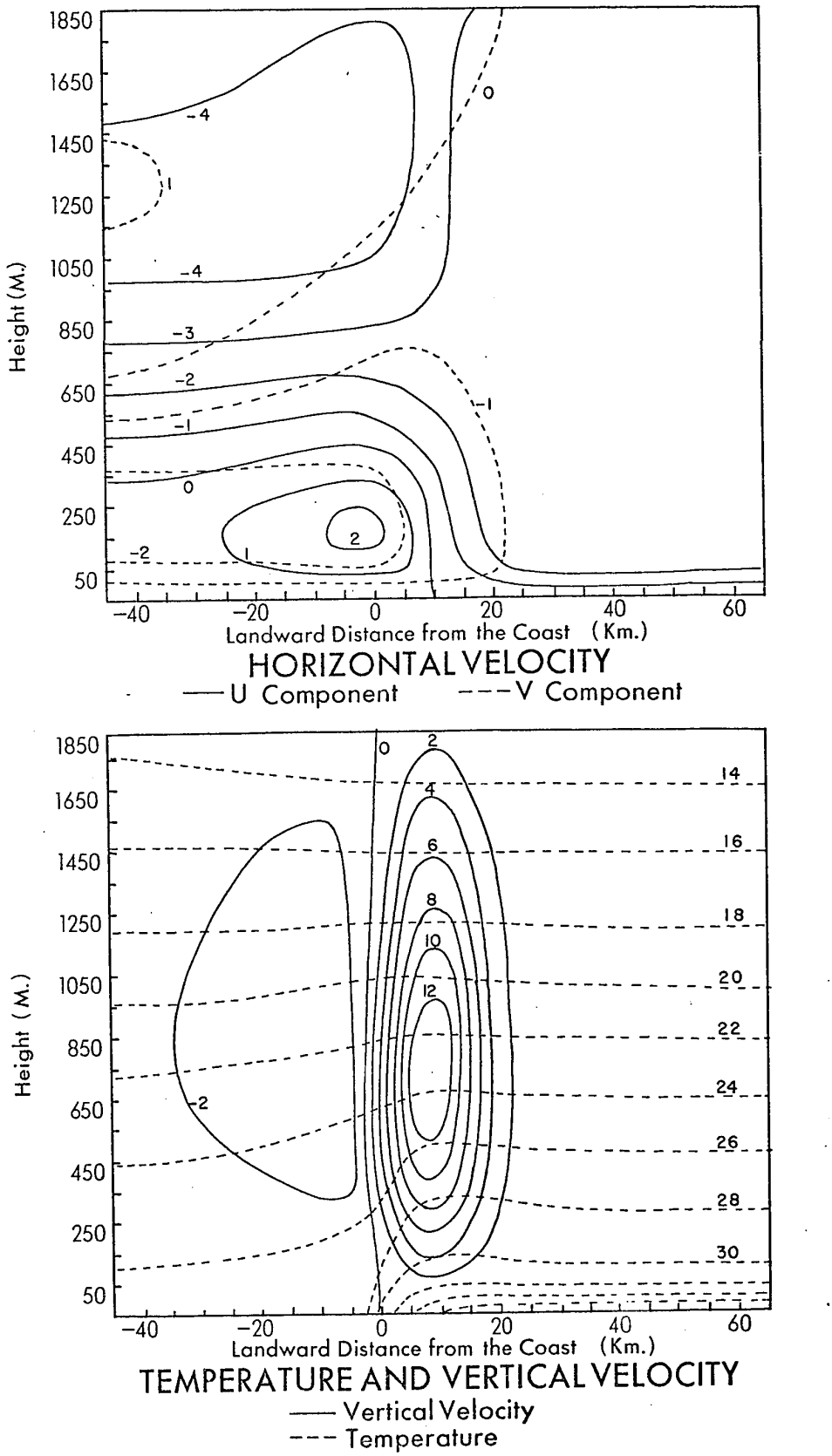

FIGURE (5-4) 4:00 P.M. results for an offshore wind. Horizontal velocities are given in m/sec, vertical velocities in cm/sec and temperatures in C.

The results for 10:00 A.M. (Figure (5-3)) showed that the sea-breeze had not yet been able to counteract the offshore flow. The vertical velocities, however, had a similar spatial distribution to those of the Comparison Model with the exception that the line of zero vertical velocity had been displaced nearly 10 km seaward.

Shortly after 12:00 A.M., a landward flow began over the sea 5 km from the coast and at approximately 1:00 P.M., the sea-breeze reached the coast.

Figure (5-4) gives the results for 4:00 P.M. A sea-breeze front, similar to that described in Chapter 1, was located nearly 10 km inland from the coast. The combined effects of turbulent friction and convergence at the front produced an area of strong ascent while only weak subsidence occurred over the sea. As expected, the landward penetration, vertical extent and strength of the sea-breeze were retarded by the offshore flow but the ascent and return flow aloft were strengthened by the opposing wind.

5.4 An Onshore Flow of 3 m/sec

With the exception of the initial u -component, the initial conditions, initial fields and grid parameters were the same as the offshore case. The initial conditions and grid data are given in Table (5-4).

The results for 10:00 A.M. (Figure (5-5)) showed that a weak sea-breeze circulation had begun but the vertical velocity pattern was

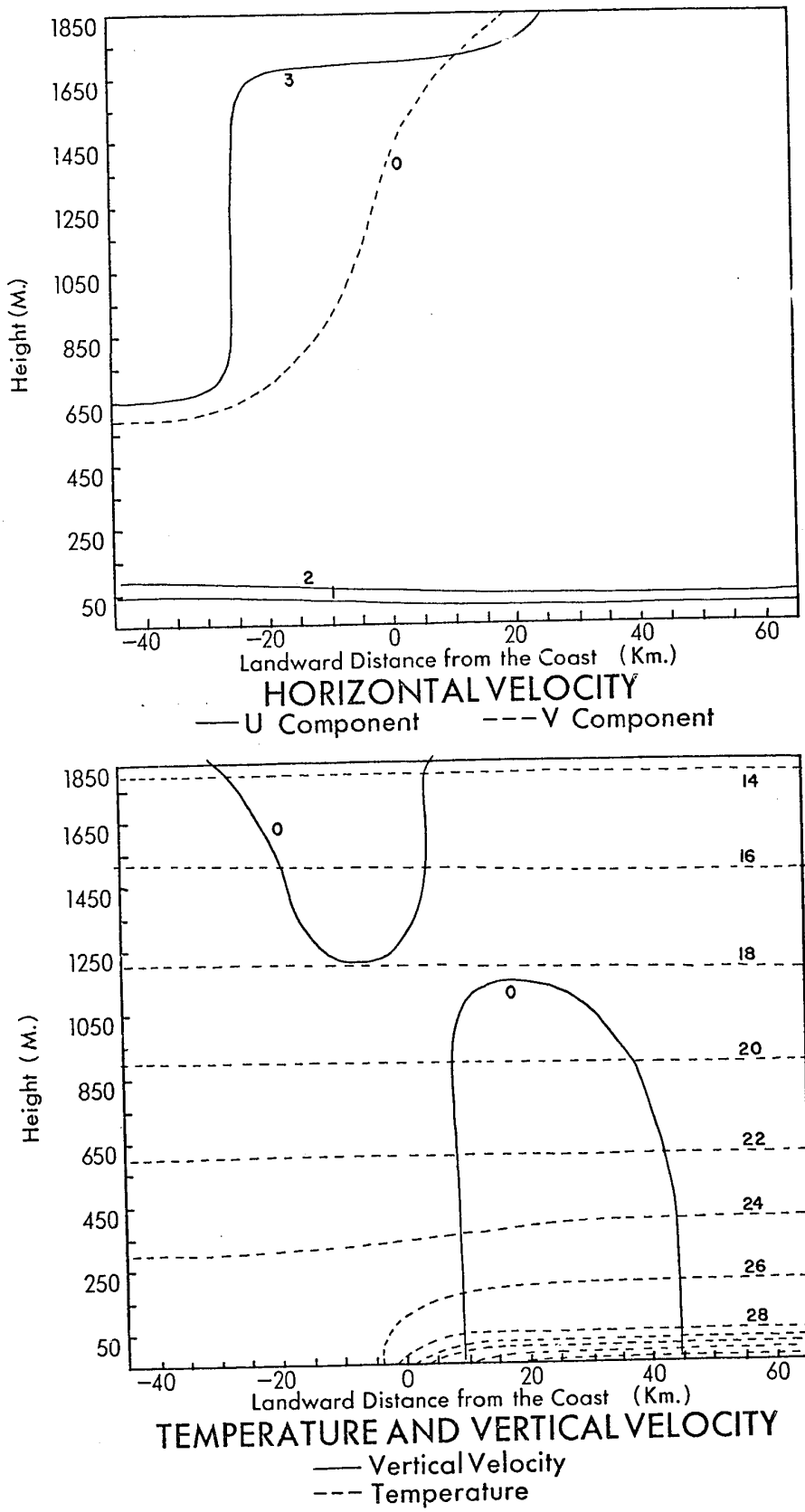

FIGURE (5-5) 10:00 A.M. results for an onshore wind. Horizontal velocities are given in m/sec, vertical velocities in cm/sec and temperatures in C.

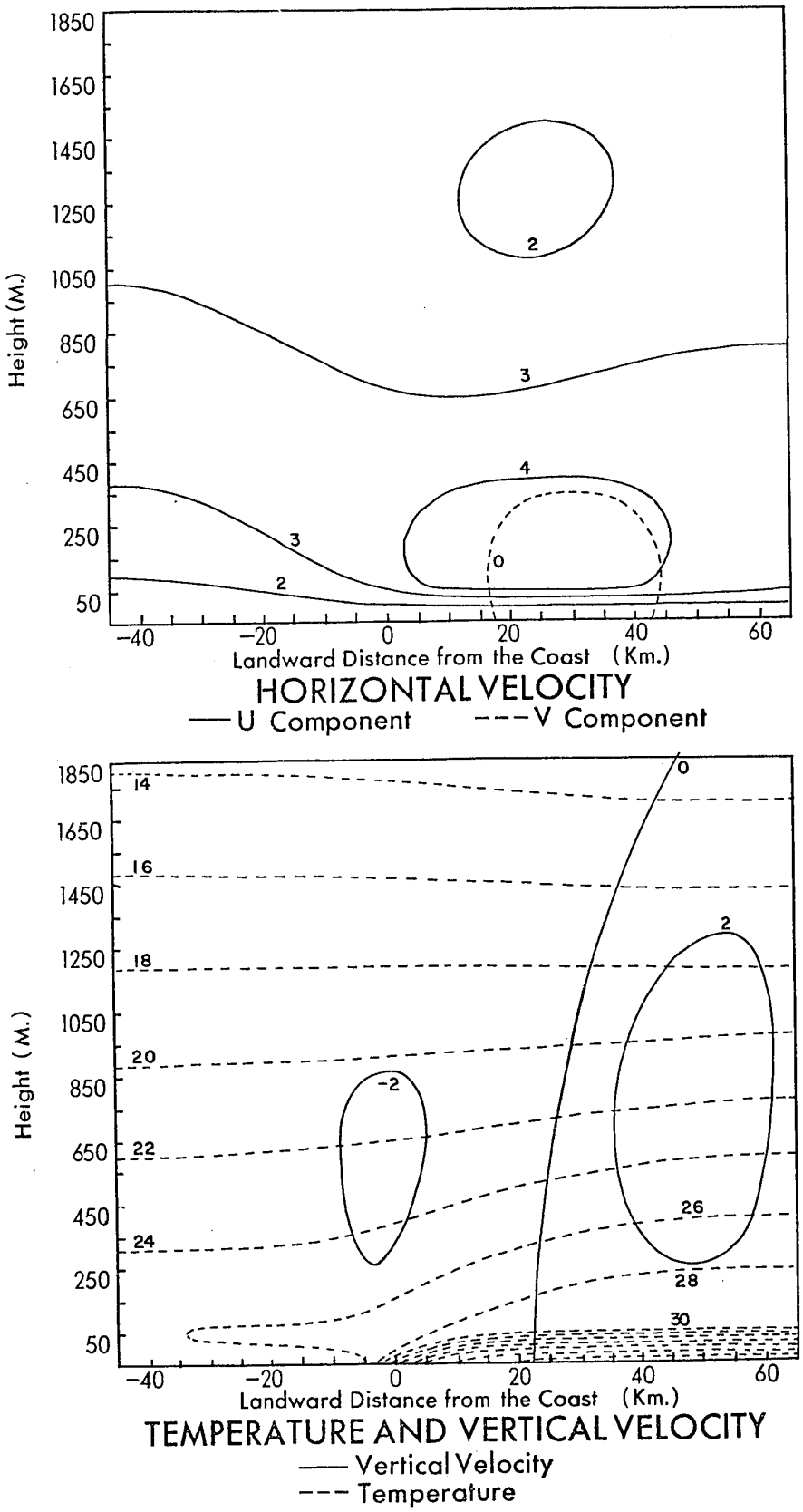

FIGURE (5-6) 2:00 P.M. results for an onshore wind. Horizontal velocities are given in m/sec, vertical velocities in cm/sec and temperatures in C.

displaced landward by the onshore gradient wind.

NUMBER OF HORIZONTAL GRID POINTS	29
NUMBER OF VERTICAL GRID POINTS	21
HORIZONTAL SPACE INCREMENT (m)	5000.0
VERTICAL SPACE INCREMENT (m)	100.0
TIME STEP (sec)	150.0
LAPSE RATE (deg/m)	0.0065
U COMPONENT (m/sec)	3.0
V COMPONENT (m/sec)	0.0
SURFACE TEMPERATURE (K)	299.0
SURFACE PRESSURE (mb)	1000.0

TABLE (5-4) Initial conditions and grid data for the onshore gradient wind case.

The results for 2:00 P.M. (Figure (5-6)) showed that the familiar pattern of vertical velocity was displaced far inland. In addition, vertical velocity over the sea was nearly of the same magnitude as that over land. The maximum onshore flow at 2:00 P.M. was about 4.5 m/sec and was located over 20 km inland. After 2:00 P.M., the results were probably in error due to the approach of the circulation to the landward lateral boundary where w is constrained to be zero.

5.5 The Effect of Reduced Insolation

Since radiation is implied in this model through the temperature wave applied to the land, it is possible to study the effect of reduced heating by decreasing the amplitude of the temperature

displaced landward by the onshore gradient wind.

NUMBER OF HORIZONTAL GRID POINTS	29
NUMBER OF VERTICAL GRID POINTS	21
HORIZONTAL SPACE INCREMENT (m)	5000.0
VERTICAL SPACE INCREMENT (m)	100.0
TIME STEP (sec)	150.0
LAPSE RATE (deg/m)	0.0065
U COMPONENT (m/sec)	3.0
V COMPONENT (m/sec)	0.0
SURFACE TEMPERATURE (K)	299.0
SURFACE PRESSURE (mb)	1000.0

TABLE (5-4) Initial conditions and grid data for the onshore gradient wind case.

The results for 2:00 P.M. (Figure (5-6)) showed that the familiar pattern of vertical velocity was displaced far inland. In addition, vertical velocity over the sea was nearly of the same magnitude as that over land. The maximum onshore flow at 2:00 P.M. was about 4.5 m/sec and was located over 20 km inland. After 2:00 P.M., the results were probably in error due to the approach of the circulation to the landward lateral boundary where w is constrained to be zero.

5.5 The Effect of Reduced Insolation

Since radiation is implied in this model through the temperature wave applied to the land, it is possible to study the effect of reduced heating by decreasing the amplitude of the temperature

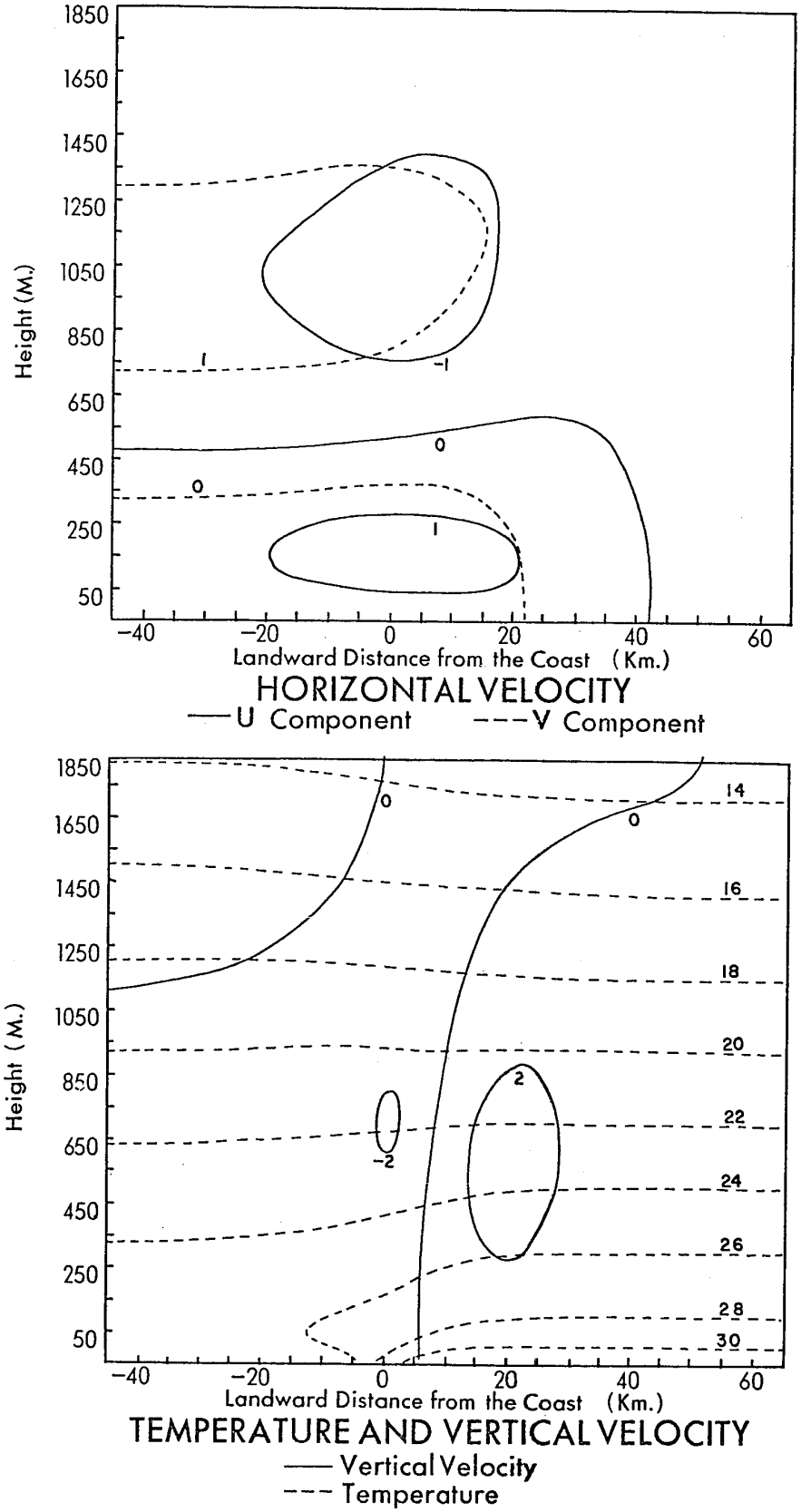

FIGURE (5-7) 4:00 P.M. results for reduced heating. Horizontal velocities are given in m/sec, vertical velocities in cm/sec and temperatures in C.

wave.

The model was run with the same initial conditions and grid data as the integration of Chapter 4 with the exception that the heating of the land was halved. The results for 4:00 P.M. are given in Figure (5-7). Although the strength of the horizontal wind field was approximately half that of the full heating case, the vertical velocities are greatly reduced as a consequence of the much lower turbulent friction which has a non-linear temperature dependence.

5.6 Summary

Increased stability generally decreases the strength of the sea-breeze since stability inhibits the diffusion of heat energy into the atmosphere. Similarly, decreasing the ground heating reduces the influence of the sea-breeze since less heat energy is available for conversion into mechanical energy. The results show also that a linear relation between heating and stability and the strength of the circulation does not exist.

The complex non-linear relation between the prevailing synoptic wind pattern and the sea-breeze circulation is shown by the results for offshore and onshore initial winds.

CHAPTER 6

THE INCLUSION OF MOISTURE IN THE MODEL

6.1 Introduction

Since water can exist in two states at above freezing temperatures considered in this study, it is necessary to use two additional equations in the model; one for water vapour and the other for liquid water. In addition, it is necessary to modify the thermodynamic equation to account for the transfer of latent heat produced during phase changes.

6.2 The Prediction Equations for Water Vapour and Liquid Water

The quantity used to describe the concentration of both the vapour and liquid is the maxing ratio which is defined as the ratio of the mass of liquid or vapour to the mass of dry air containing the vapour or liquid:

$$r_w = \frac{\text{mass of liquid water}}{\text{mass of dry air}}$$

$$r_v = \frac{\text{mass of water vapour}}{\text{mass of dry air}}$$

where r_w = mixing ratio for liquid water

r_v = mixing ratio for water vapour

The rate of change of the mixing ratio with time following the air motion (neglecting the fall-out of water droplets since this is small) is caused by diffusion and condensation/evaporation, resulting

from vertical motion and a correction term for ensuring that the air does not become supersaturated or subsaturated with liquid water present. The correction terms result from the fact that the time step used is too large to adequately represent the processes of evaporation and condensation. Hence:

$$\frac{Dr_v}{Dt} = D_v + W_v + C_v \qquad (6.2.3)$$

$$\frac{Dr_w}{Dt} = D_w + W_w + C_v \qquad (6.2.4)$$

where D = rate of change due to diffusion

W = rate of change due to vertical velocity

C = correction term

If it is assumed that the eddy diffusivities for heat, water vapour and liquid water are equal, then the diffusion terms are:

$$D_v = \frac{\partial}{\partial z}\left(K \frac{\partial r_v}{\partial z}\right) \qquad (6.2.5)$$

$$D_w = \frac{\partial}{\partial z}\left(K \frac{\partial r_w}{\partial z}\right) \qquad (6.2.6)$$

The following shows that diffusion is more important than droplet fall-out. Figure (6-1) shows a grid box bounded on the top by a mixing ratio of 1 gm/kg and on the bottom by a mixing ratio of 0 gm/kg.

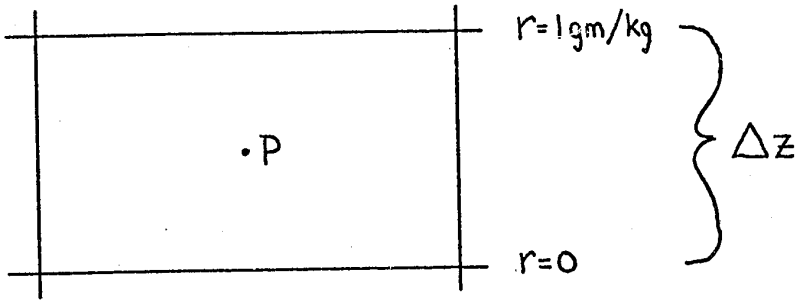

FIGURE (6-1) Grid box for diffusion/fall-out calculation.

The increase of the mixing ratio at the point P from diffusion is:

$$\left(\frac{\partial r_w}{\partial t}\right)_{diff} = \frac{\partial K}{\partial z}\frac{\partial r_w}{\partial z} + K\frac{\partial^2 r_w}{\partial z^2}$$

$$= \frac{5}{2000}\left[\frac{.001-0}{100}\right] + 5\left[\frac{.001+0-2(0)}{2500}\right] \quad (K=5)$$

$$= 2\times10^{-6}\ sec^{-1}$$

Petterssen (1959) gives the mean fog droplet size as 10-15 μ which have a terminal velocity of 3 mm/sec. The increase in the mixing ratio due to fall-out is:

$$\left(\frac{\partial r_w}{\partial t}\right)_{fall\text{-}out} = r_{top}\frac{V}{\Delta z} = .001\ \frac{.003}{100}$$

$$= 3\times10^{-8}\ sec^{-1}$$

Hence, diffusion is more important than fall-out.

In the atmosphere, the amount of water changing phase per unit time following the motion is the time rate of change of the saturation mixing ratio for water vapour. To account for mixing ratio changes resulting from vertical motion, it is necessary to express the rate of change of the saturation mixing ratio as a function of the vertical velocity:

$$\frac{dr_{vs}}{dt} = f(w, T, \bar{p}) = W_v \qquad (6.2.7)$$

where r_{vs} = saturation mixing ratio for water vapour

Since the total mass of water substance must be conserved:

$$W_w = -W_v \qquad (6.2.8)$$

From Hess (1959), the saturation mixing ratio is approximately related to the saturation vapour pressure by:

$$r_{vs} \cong \epsilon\frac{e_s}{\bar{p}} \qquad (6.2.9)$$

$$r_{vs} \cong \epsilon \frac{e_s}{\bar{p}} \qquad (6.2.9)$$

where r_{vs} = saturation mixing ratio

ϵ = ratio of molecular weight of water to the effective molecular weight of dry air

e_s = saturation vapour pressure

$\bar{p}$ = total pressure

Hess (1959) also gives the saturation vapour pressure as a function of temperature:

$$e_s = 6.11 \exp\left\{\frac{L}{R_v}\left(\frac{1}{273} - \frac{1}{T}\right)\right\} \qquad (6.2.10)$$

where e_s = saturation vapour pressure

L = latent heat of condensation (assumed constant)

R_v = specific gas constant for water vapour

T = absolute temperature

In order to begin to find an expression for (6.2.7), (6.2.9) is differentiated to obtain:

$$\frac{1}{r_{vs}}\frac{dr_{vs}}{dt} \cong \frac{1}{e_s}\frac{de_s}{dt} - \frac{1}{\bar{p}}\frac{d\bar{p}}{dt} \qquad (6.2.11)$$

Substitution of the hydrostatic equation in the form (ignoring pressure changes resulting from the weight of liquid water and water vapour) gives:

$$\frac{d\bar{p}}{dt} = -\rho g \frac{dz}{dt} \qquad (6.2.12)$$

$$= -\frac{\bar{p} g}{RT} w$$

Thus, (6.2.11) becomes:

$$\frac{1}{r_{vs}}\frac{dr_{vs}}{dt} \cong \frac{1}{e_s}\frac{de_s}{dt} + \frac{gw}{RT} \qquad (6.2.13)$$

Differentiating (6.2.10) yields the Clausius-Clapeyron relation:

$$\frac{1}{e_s}\frac{de_s}{dt} = \frac{L}{R_v T^2}\frac{dT}{dt} \qquad (6.2.14)$$

and substitution into (6.2.13) produces:

$$\frac{1}{r_{vs}}\frac{dr_{vs}}{dt} = \frac{L}{R_v T^2}\frac{dT}{dt} + \frac{gw}{RT} \qquad (6.2.15)$$

The first law of thermodynamics for an ideal gas (dry air) can be written:

$$\frac{dQ}{dt} = c_p\frac{dT}{dt} - \alpha\frac{dp}{dt} \qquad (6.2.16)$$

where Q = heat transferred to the gas

c_p = specific heat capacity of dry air at constant pressure

α = specific volume

Assuming that the condensation takes place as a result of saturated adiabatic expansion, (6.2.16) becomes:

$$-L\frac{dr_{vs}}{dt} = c_p\frac{dT}{dt} + gw \qquad (6.2.17)$$

Elimination of $\frac{dT}{dt}$ between (6.2.17) and (6.2.15) gives:

$$\frac{dr_{vs}}{dt} = -Sw \qquad (6.2.18)$$

where

$$S = \frac{r_{vs}g}{R}\left[\frac{LR - R_v T c_p}{R_v T^2 c_p + L^2 r_{vs}}\right]$$

Hence by (6.2.7) and (6.2.8)

$$W_v = -S_w \qquad (6.2.19)$$

$$W_w = S_w \qquad (6.2.20)$$

Because of the remarks prior to (6.2.17), equation (6.2.18) is valid only if a phase change takes place, that is, only if the air is already saturated. If the vertical motion does not result in a phase change, then S=0.

In order to correct the errors caused by the time step being too large, the values of r_v and r_w at each grid point are checked at every time step to ensure that:

a) the air is not supersaturated

b) the air is not subsaturated with liquid water present

If condition (a) is not satisfied, the value of r_v is lowered to r_{vs} and the liquid water mixing ratio is increased by the same amount. Since this correction is computed over a time interval, Δt, it is necessary to divide the above result by Δt in order to obtain the change in the mixing ratio per unit time. Hence, the correction term becomes for $r_v > r_{vs}$:

$$C_v = -(r_v - r_{vs}) / \Delta t \qquad (6.2.21)$$

$$C_w = -(r_{vs} - r_v) / \Delta t \qquad (6.2.22)$$

If condition (b) is not satisfied, the air is brought to saturation and the mixing ratio of the liquid water is lowered by the same amount; however, the total correction cannot be greater than the total amount

of liquid water present. The correction terms are for $r_v \leq r_{vs}$ and $r_w > 0$:

$$C_v = \min\left\{r_{vs} - r_v, r_w\right\} \qquad (6.2.23)$$

$$C_w = -\min\left\{r_{vs} - r_v, r_w\right\} \qquad (6.2.24)$$

where min = the smaller of the two arguments

The left-hand sides of (6.2.3) and (6.2.4) are expanded in a way analogous to (3.2.12) to obtain the prediction equations:

$$\frac{\partial r_v}{\partial t} = -(u_0+u')\frac{\partial r_v}{\partial x} - w\frac{\partial r_v}{\partial z} + \frac{\partial K}{\partial z}\frac{\partial r_v}{\partial z} + K\frac{\partial^2 r_v}{\partial z^2} - Sw + C_v \qquad (6.2.25)$$

$$\frac{\partial r_w}{\partial t} = -(u_0+u')\frac{\partial r_w}{\partial x} - w\frac{\partial r_w}{\partial z} + \frac{\partial K}{\partial z}\frac{\partial r_w}{\partial z} + K\frac{\partial^2 r_w}{\partial z^2} + Sw + C_w \qquad (6.2.26)$$

These equations, written in finite-difference form similar to (3.5.12), become:

$$\begin{aligned} r v_{i,j}^{n+1} = {} & r v_{i,j}^{n} - \frac{\Delta t}{\Delta x}(u_0+u'^{n}_{i,j})(r v^{n}_{i+1,j} - r v^{n}_{i,j}) \\ & - \Delta t\, S^{n}_{i,j} w^{n}_{i,j} + \frac{\Delta t}{2\Delta z} K'^{n}_{i}(r v^{n}_{i,j+1} - r v^{n}_{i,j-1}) \\ & - \frac{\Delta t}{\Delta z} w^{n}_{i,j}(r v^{n}_{i,j+1} - r v^{n}_{i,j}) + C^{n}_{v_{i,j}}\Delta t \\ & - \frac{\Delta t}{\Delta z^2} K^{n}_{i}(r v^{n}_{i,j+1} + r v^{n}_{i,j-1} - 2 r v^{n}_{i,j}) \end{aligned} \qquad (6.2.27)$$

$$rw_{i,j}^{n+1} = rw_{i,j}^{n} - \frac{\Delta t}{\Delta x}(u_o + u'^{n}_{i,j})(rw^{n}_{i+1,j} - rw^{n}_{i,j})$$

$$+ \Delta t\, S^{n}_{i,j}\, w^{n}_{i,j} + \frac{\Delta t}{2\Delta z} K'^{n}_{i}(rw^{n}_{i,j+1} - rw^{n}_{i,j-1})$$

$$- \frac{\Delta t}{\Delta z} w^{n}_{i,j}(rw^{n}_{i,j+1} - rw^{n}_{i,j}) + C^{n}_{w_{i,j}} \Delta t$$

$$- \frac{\Delta t}{\Delta z^2} K^{n}_{i}(rw^{n}_{i,j+1} + rw^{n}_{i,j-1} - 2rw^{n}_{i,j}) \qquad (6.2.28)$$

where $rv = r_v$

$rw = r_w$

The above equations assume $(u_o + u'^{n}_{i,j})$ and $w^{n}_{i,j}$ are both negative. If either or both of the above are positive or zero, the differencing scheme for the advection terms must be changed as stated in Section (3.5). In addition, the stability criteria (3.5.5), (3.5.8) and (3.5.10) are valid.

6.3 The Boundary Conditions for the Liquid Water and Water Vapour

For the reasons stated in Section (2.10), the boundary conditions are:

a) at the top boundary

$$\frac{\partial}{\partial t}(r_v, r_w) = 0 \qquad (6.3.1)$$

b) at the lateral boundaries

$$\frac{\partial}{\partial x}(r_v, r_w) = 0 \qquad (6.3.2)$$

c) since the total water is conserved and there is no advection, the boundary condition at the surface is

$$\frac{\partial}{\partial t}\left(r_v + r_w\right) = 0 \qquad (6.3.3)$$

hence

$$r_v + r_w = \text{const.} \qquad (6.3.4)$$

6.4 Modification of the Thermodynamic Equation

Writing (6.2.17) in terms of potential temperature gives:

$$LS_w = \frac{T}{\theta} c_p \frac{d\theta}{dt} \cong c_p \frac{d\theta}{dt} \qquad (6.4.1)$$

From equations (2.4.3) and (3.2.3):

$$\frac{d\theta'}{dt} = \frac{\partial}{\partial z}\left(K \frac{\partial \theta_0}{\partial z}\right) + \frac{\partial}{\partial z}\left(K \frac{\partial \theta'}{\partial z}\right) \qquad (6.4.2)$$

Substitution of (6.4.2) into (6.4.1) and expansion of the total derivative gives:

$$\frac{\partial \theta'}{\partial t} = -(u_0 + u')\frac{\partial \theta'}{\partial x} - w\frac{\partial \theta_0}{\partial z} - w\frac{\partial \theta'}{\partial z} + \frac{\partial}{\partial z}\left(K \frac{\partial \theta_0}{\partial z}\right) + \frac{\partial}{\partial z}\left(K \frac{\partial \theta'}{\partial z}\right) + \frac{LS_w}{c_p} \qquad (6.4.3)$$

which is the thermodynamic equation modified for latent heat released during vertical motion.

The following expression (which is a finite-difference approximation of the rate of change of the saturation mixing ratio for water vapour with temperature) is used to determine the effect

of the "correction" terms (C_v and C_w) on the thermodynamic equation:

$$\frac{\partial r_{vs}}{\partial t} = \frac{\Delta r_w}{\Delta \theta'} \qquad (6.4.4.)$$

where Δr_w = the change in the mixing ratio of liquid water resulting from the application of the correction terms

$\Delta \theta'$ = temperature change at a given grid point resulting from the change in liquid water mixing ratio

r_{vs} = saturation mixing ratio of water vapour

Differentiating (6.2.9) and (6.2.10) gives:

$$\frac{\partial r_{vs}}{\partial t} = \frac{r_{vs} L}{R_v T^2} \qquad (6.4.5)$$

Since $\Delta r_w = C_w$, equation (6.4.4) can be rewritten to obtain the expression for $\Delta \theta'$:

$$\Delta \theta' = \frac{R_v T^2 C_w}{r_{vs} L}$$

where $\Delta \theta'$ = change in potential temperature per unit time

After the inclusion of (6.4.6), equation (6.4.3) written in finite-difference form is:

$$\theta'^{n+1}_{i,j} = -\frac{\Delta t}{\Delta x}(u_{oj}+u'^{n}_{i,j})(\theta'^{n}_{i+1,j}-\theta'^{n}_{i,j}) + \frac{L}{C_p}\Delta t\, S^{n}_{i,j}\, w^{n}_{i,j}$$

$$- \frac{\Delta t}{\Delta z} w^{n}_{i,j}(\theta'^{n}_{i,j+1}-\theta'^{n}_{i,j}) + \frac{\Delta t}{2\Delta z} K'^{n}_{i}(\theta^{n}_{i,j+1}-\theta^{n}_{i,j-1})$$

$$+ \frac{\Delta t}{\Delta z^2} K^{n}_{i}(\theta^{n}_{i,j+1}+\theta^{n}_{i,j-1}-2\theta^{n}_{i,j}) + \Delta t \Delta \theta'^{n}_{i,j} + \theta'^{n}_{i,j}$$

where $\theta = \theta_0 + \theta'$

The advection terms in this equation have been written for negative $(u_0+u'^{n}_{i,j})$ and $w^{n}_{i,j}$.

Changes in the equation of state and Poisson's equation resulting from the inclusion of water vapour and liquid water are ignored in this study.

CHAPTER 7

THE DISSIPATION OF AN ALREADY EXISTING COASTAL FOG BANK BY THE SEA-BREEZE CIRCULATION

7.1 Introduction

So far, only the results of a "dry" model have been presented. If the moisture equations of Chapter 6 are introduced into this study, the investigation of many "practical" meteorological situations becomes possible. This chapter shows the influence of the sea-breeze circulation on coastal fog. The fog is assumed to be already in existence at the initial time and its subsequent dissipation is studied in the model.

7.2 Initial Conditions and Fields

The fact that this model does not deal explicitly with solar radiation presents many problems which must be rectified by the use of rather drastic assumptions.

The first problem that arises is the form of the temperature wave that is used to heat the land. Since the shape of the temperature wave depends on the amount of insolation reaching the ground, it is not possible to use Kuo's temperature wave because the fog reduces the amount of solar energy reaching the surface and also reduces the outgoing long wave radiation. Hence, as a first approximation, a simple sine wave of the following form is used to heat the land:

$$T_{land} = T_o + 5 \sin(15t)$$

where T_{land} = temperature of the land

T_o = initial surface temperature

t = time in hours measured from 8:00 A.M.

Geiger (1966) gives the variation of the sea temperature averaged over a depth of approximately one meter. The amplitude of the variation is about 0.1 C, is sinusoidal in character and reaches a maximum at 4:00 P.M. Since the amplitude above is the result of averaging over a depth of one meter, the temperature at the sea surface is much larger. As a result, the following wave of amplitude 1.0 C is used to heat the sea:

$$T_{sea} = T_o + 0.5 + \sin\{15(t-2)\}$$

where T_{sea} = sea surface temperature

T_o = initial surface temperature

t = time in hours measured from 8:00 A.M.

It will be assumed that none of the water vapour condensed falls but remains suspended in the air.

The fog bank at the initial time extended from seaward lateral boundary to landward lateral boundary and was topped at a height of 550 meters. The initial liquid water mixing ratio in the fog was set at 1 gm/kg and zero elsewhere.

The initial distribution of the water vapour mixing ratio was a function of height only:

$$r_v(z) = r_{vs} \qquad 0 \le z \le 550 \text{ m}$$

$$r_v(z) = r_v(550)\,\frac{2550-z}{2000} \qquad 550 \le z \le 1950 \text{ m}$$

where $r_v(z)$ = mixing ratio at height z

r_{vs} = saturation mixing ratio

This distribution gave saturation in the fog and a linear decrease of the mixing ratio above the fog.

To comply with observations, the initial temperature distribution was chosen to give a weak inversion in the fog bank and a stable lapse rate above it:

$$T(z) = T_o + 0.001\,z \qquad 0 \le z \le 550$$

$$T(z) = T(550) - .005\,(z-550) \qquad 550 \le z \le 1950$$

where $T(z)$ = temperature at height z

T_o = initial surface temperature

Using the same finite-difference parameters and number of grid points as in previous solutions, the initial fields of Table (7-1) were computed.

7.3 Results for the Atmosphere Initially at Rest

As a result of the assumptions mentioned above, it was felt that meaningful results would not be obtained after 8 hours. Results are given for the mid-point (12:00 noon) and the end of the period (4:00 P.M.).

The noon results (Figure (7-1)) showed that an offshore flow was present, resulting from the use of heat to evaporate the fog bank. The vertical velocity pattern showed weak subsidence over the sea and weak ascent over land. The fog bank over the sea was basically unchanged since the initial time while that over land had either cleared or "lifted" to form a stratus cloud.

By 4:00 P.M. (Figure (7-2)) a weak sea-breeze had formed and the vertical velocities had strengthened. The fog and stratus over land had completely dissipated. The fog was still present over the sea but its liquid water content was less than half its initial value.

7.4 Results for an Initial Onshore Flow of 3 m/sec

As before, only the noon and 4:00 P.M. results are presented.

The noon results (Figure (7-3)) for this case showed that the fog had either cleared or lifted to stratus. Although the configuration of the fog bank over the sea was not significantly different from the initial time, its liquid water content had been greatly reduced.

The 4:00 P.M. results (Figure (7-4)) showed that the fog had completely dissipated. Due to the increased forced convection resulting from the initial onshore wind, this case was more efficient in dissipating the fog bank than the case with no initial wind.

ROW	TEMPERATURE (K)	HEIGHT (m)	LIQUID WATER (gm/kg)	WATER VAPOUR (gm/kg)
1	299.0	0.0	1.0	20.07
2	299.0	50.0	1.0	20.25
3	299.1	150.0	1.0	20.60
4	299.2	250.0	1.0	20.96
5	299.3	350.0	1.0	21.32
6	299.4	450.0	1.0	21.69
7	299.5	550.0	1.0	22.07
8	299.0	650.0	0.0	20.97
9	298.5	750.0	0.0	19.86
10	298.0	850.0	0.0	18.76
11	297.5	950.0	0.0	17.66
12	297.0	1050.0	0.0	16.55
13	296.5	1150.0	0.0	15.45
14	296.0	1250.0	0.0	14.35
15	295.5	1350.0	0.0	13.24
16	295.0	1450.0	0.0	12.14
17	294.5	1550.0	0.0	11.04
18	294.0	1650.0	0.0	9.93
19	293.5	1750.0	0.0	8.83
20	293.0	1850.0	0.0	7.73
21	292.5	1950.0	0.0	6.62

TABLE (7-1) Initial fields for fog dissipation study.

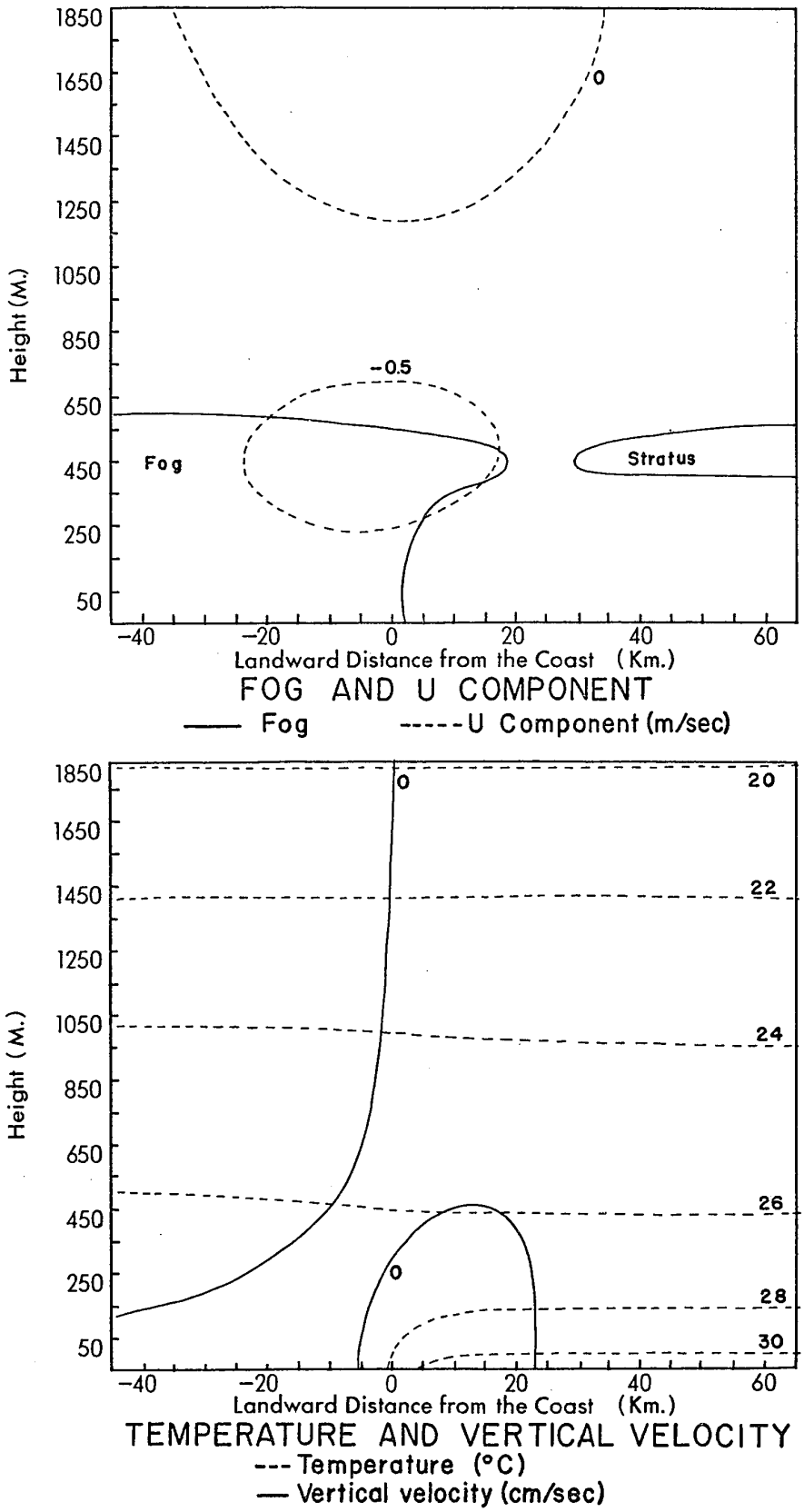

FIGURE (7-1) 12:00 A.M. results for the atmosphere initially at rest.

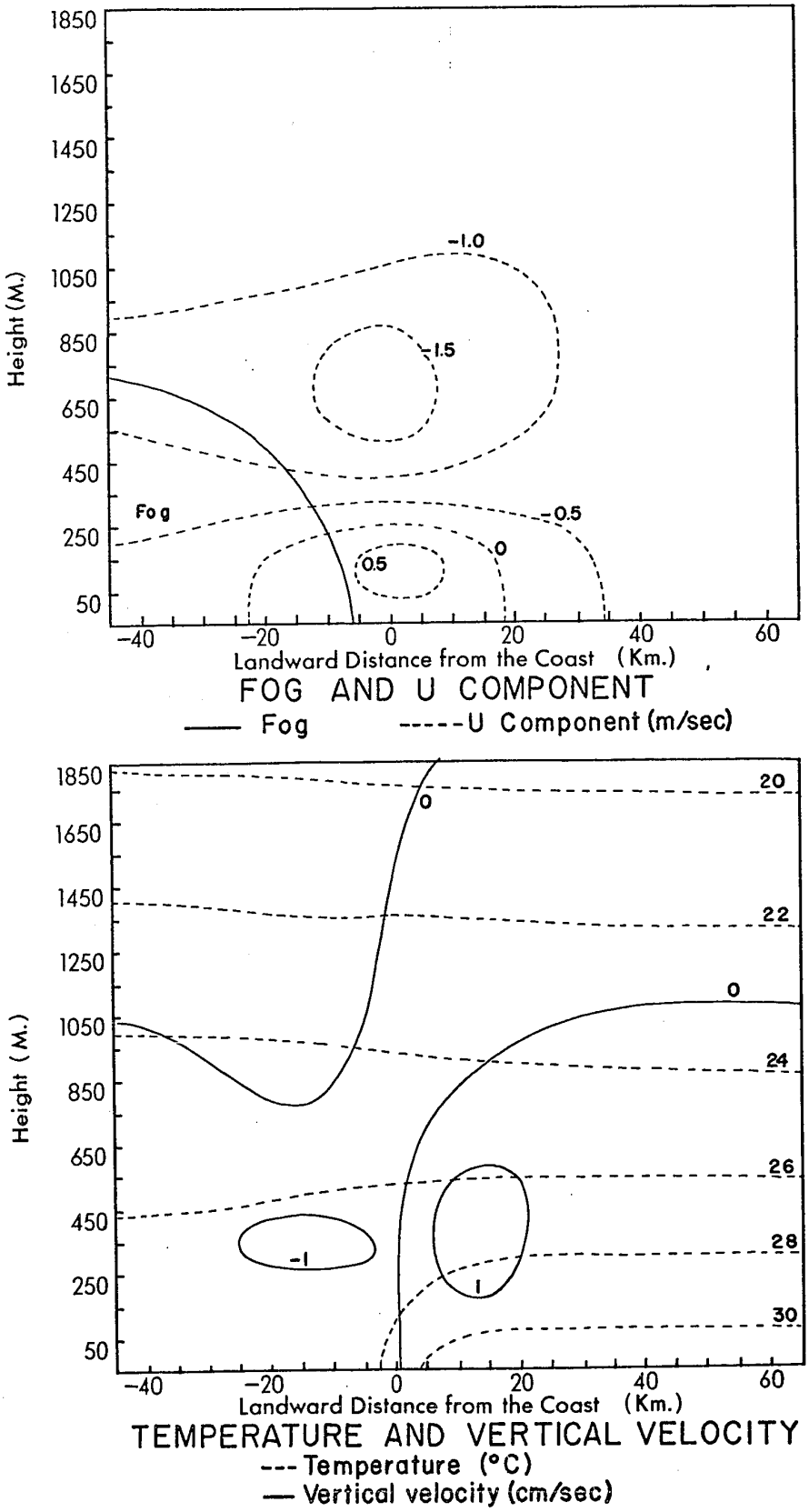

FIGURE (7-2) 4:00 P.M. results for the atmosphere initially at rest.

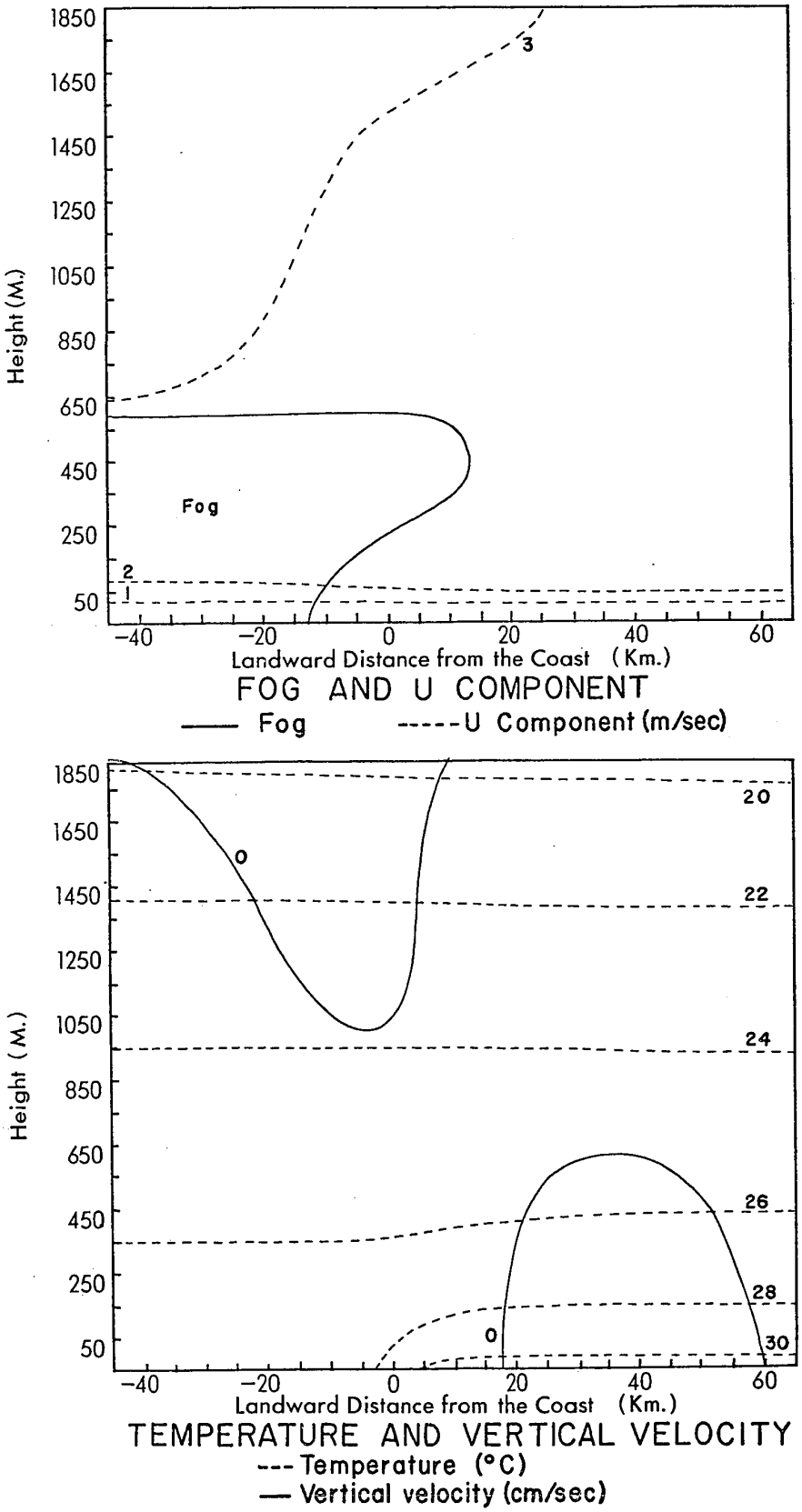

FIGURE (7-3) 12:00 A.M. results for an onshore wind.

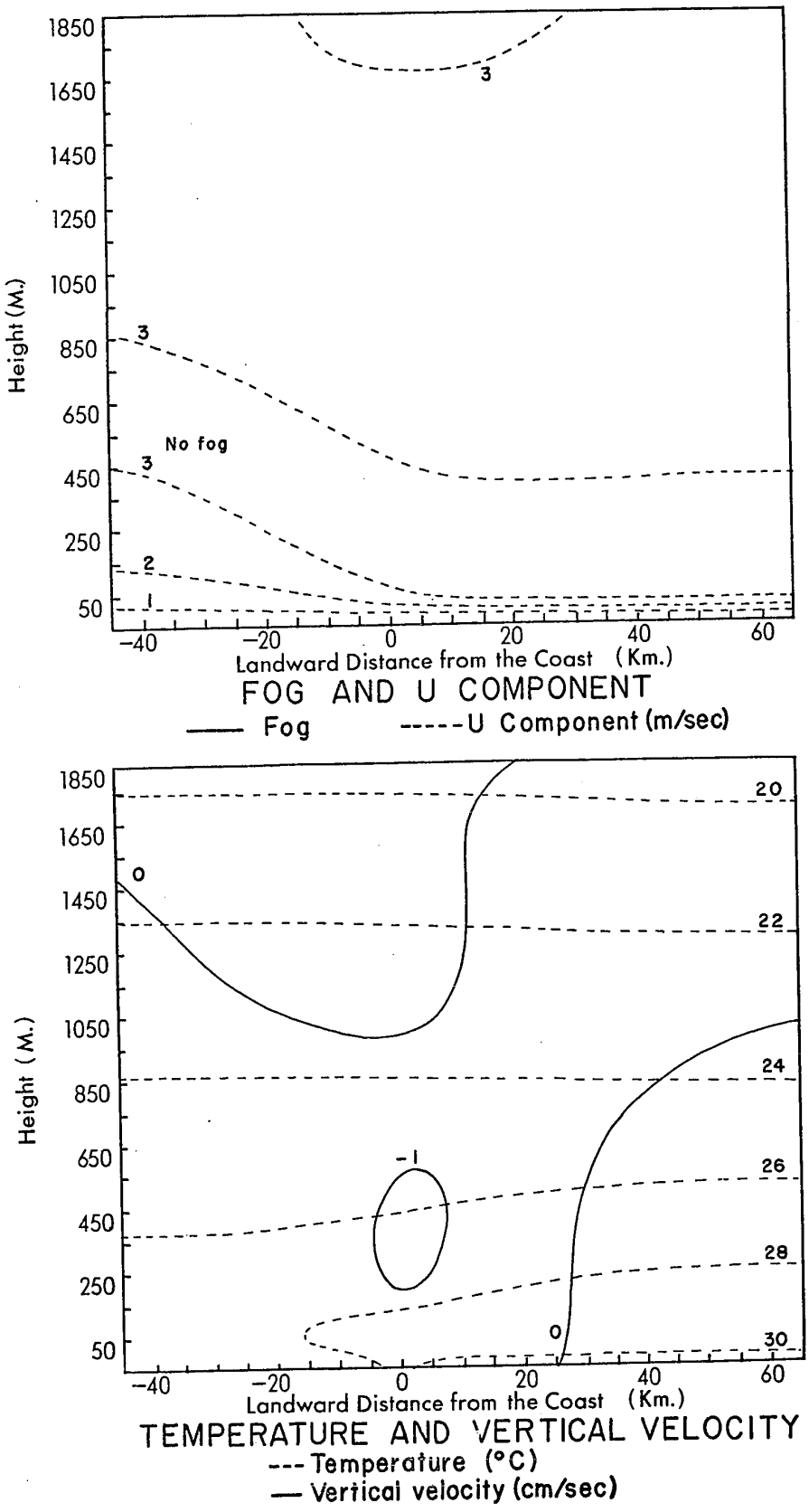

FIGURE (7-4) 4:00 P.M. results for an onshore wind.

CHAPTER 8

CONCLUSIONS

8.1 Contributions to Knowledge

The original work contained in this study is the inclusion of the Coriolis term in the vertical equation of motion, the use of a non-hydrostatic mass conserving model to study synoptic control of the sea-breeze and the inclusion of equations for moisture to study a practical meteorological problem.

8.2 Validity of the Model

In spite of all the assumptions made, a comparison of the results of this study with observations shows that the sea-breeze is well reproduced by this model. The greatest difference between the theoretical results and the observations is in the vertical extent of the sea-breeze. Koschmieder and Hornikel (1942) observed that the vertical penetration of the sea-breeze under calm gradient wind conditions was less than that under offshore gradient wind conditions. However, this study predicts the opposite. Table (8-1) summarizes the model's performance in representing the available observations.

8.3 Suggestions for Future Study

The energy equation should be used in each of the sea-breeze cases studied in order to fully understand the circulation.

CASE	OBSERVED FEATURES DESCRIBED BY MODEL	OBSERVED FEATURES NOT DESCRIBED BY MODEL
1) calm gradient wind	- hodograph - spreading out of wind from coast-line - weak reverse flow aloft	
2) offshore gradient wind case	- beginning at sea - front well represented - less landward penetration than calm wind case	- higher vertical penetration than calm wind case
3) onshore gradient wind case	- sea-breeze weak - average increase of wind 1 m/sec, model gives 1.5 m/sec	
4) fog dissipation	- no observations available	

TABLE (8-1) Performance of the model.

In the cases where a synoptic wind is used, the model should be allowed to reach a steady state, i.e. the synoptic wind should be allowed to produce an Ekman spiral before the temperature wave is applied to the land.

The most significant improvement that could be made is the inclusion of radiation in the model.

The model could also be improved by more accurate equations for the lower sub-layer. More realistic results could be obtained if Chorin's method is modified to use a compressible equation of continuity. With the shallow convection restriction removed, the number of meteorological problems that could be investigated is greatly increased, such as the enhancement of cumulus development by the sea-breeze.

BIBLIOGRAPHY

Batchelor, G. K., 1967: An Introduction to Fluid Dynamics. London, Cambridge University Press, 615 pp.

Chorin, A. J., 1968: Numerical Solution of the Navier-Stokes Equations. Math. Comput., 22, 745-762.

Conrad, V., 1928: Beobachtungen über den Seewind im einem Flachen Sandstrand. Ann. d. Hydr. usw., 56, 1-3.

Defant, F., 1951: Compendium of Meteorology. Amer. Met. Soc., 658-672.

Estoque, M. A., 1959: A Preliminary Report on a Boundary-layer Experiment. GRD Res. Notes, 20, AFCRC, Bedford, Mass.

_____, 1961: A Theoretical Investigation of the Sea Breeze. Quart. J. Roy. Meteor. Soc., 87, 136-146.

_____, 1962: The Sea Breeze as a Function of the Prevailing Synoptic Situation. J. Atmos. Sci., 19, 244-250.

Fisher, E. L., 1961: A Theoretical Study of the Sea Breeze. J. Meteor., 18, 216-233.

Geiger, R., 1966: The Climate Near the Ground. Cambridge, Harvard University Press. 611 pp.

Haltiner, G. J., 1971: Numerical Weather Prediction. New York, John Wiley and Sons, 317 pp.

Hess, S. L., 1959: Introduction to Theoretical Meteorology. New York, Holt, Rinehart, and Winston, 362 pp.

Hsu, S., 1968: Mesoscale Surface Temperature Characteristics of the Texas Coast Sea Breeze. Austin, Report No. 6, Atmospheric Science Group, University of Texas, 73 pp.

Koschmieder, H. and K. Hornickel, 1942: Danziger Seewind Studien III. Meteorol., Forschungsarbeiten, Heft 8.

Kuo, H. L., 1968: The Thermal Interaction Between the Atmosphere and the Earth and the Propagation of Diurnal Temperature Waves. J. Atmos. Sci., 25, 682-706.

Lumley, J. L. and H. A. Panofsky, 1964: The Structure of Atmospheric Turbulence. New York, Interscience Publishers, 239 pp.

McPherson, R. D., 1970: A Numerical Study of the Effect of a Coastal Irregularity on the Sea Breeze. J. Appl. Met., 9, 767-777.

Neumann, J. and Y. Mahrer, 1971: A Theoretical Study of the Land and Sea Breeze Circulation. J. Atmos. Sci., 28, 532-542.

Pearce, R. P., 1955: The Calculation of the Sea-breeze Circulation in Terms of the Differential Heating Across the Coast Line. Quart. J. Roy. Meteor. Soc., 81, 351-381.

Petterssen, S., 1956: Weather Analysis and Forecasting. New York, McGraw-Hill Book Co., Vol. 2, 2nd ed., 266 pp.

Priestley, C. H. B., 1959: Turbulent Transfer in the Lower Atmosphere. Chicago, Chicago University Press, 130 pp.

Schmidt, F. H., 1947: An Elementary Theory of the Land and Sea Breeze Circulation. J. Meteor., 4, 9-15.

Sutcliffe, R. C., 1937: The Sea Breeze at Felixstowe. A Statistical Investigation of Pilot Balloon Ascents up to 5,500 Feet. Quart. J. Roy. Meteor. Soc., 63, 134-142.

Van Bemmelen, W., 1922: Land und Seebrisen in Batavia. Beit. Z. Phy. d. fr. Atm., 10, 169-182.

Wexler, R., 1946: Theory and Observations of Land and Sea Breezes. Bull. Amer. Meteor. Soc., 27, 272-287.

Zinner, F., 1919: Der See und Landwinde zu Burgas. Met. Z., 36, 93-95.

APPENDIX A

The following is a listing of the computer program used in the fog dissipation study of Chapter 7.

SUBROUTINE MAPPA is courtesy of Y. Mahrer.

```
      DIMENSION Q1NEW(30,30), UN(21), Z(30), A(21), B(21), DZR(21), W1(3
     10,21), P1(30,21), G1(30,3), G2(30,21), C(30), D(30), U2(30,3), DTZ
     21(30), U(30,21), U1(30,21), V(30,21), V1(30,21), W(30,21), TE(30,2
     31), TE1(30,21), P(30,21), PL(30), T(30,21), TL(30), TEL(30), QWL(2
     41), QVL(21), QV(30,21), QV1(30,21), QW(30,21), QW1(30,21), S(30,21
     5), TR(30,3), RI(30)
      DATA QWL/1.,1.,1.,1.,1.,1.,1.,0.,0.,0.,0.,0.,0.,0.,0.,0.,0.,0.,0.,0.,
     10.,0./
C
C     INPUT GRID SIZE AND INTEGRATION TIME
C
      READ (5,72) L,M,IT
      L1=L-1
      M1=M-1
C
C     INPUT FININTE DIFFERENCE INCREMENTS
C
      READ (5,73) DX,DZ,DT
C
C     INPUT INITIAL CONDITIONS
C
      READ (5,82) UO,VO,TO,PO,AA,DTR
      H=50.
      TL(1)=TO
C
C     COMPUTE INITIAL VERTICAL TEMPERATURE DISTRIBUTION
C
      DO 1 J=2,7
1     TL(J)=TO+.001*H+DZ*.001*(J-2)
      DO 2 J=8,M
2     TL(J)=TL(7)-AA*DZ*(J-7)
      IDAY=1
      R=287.04
      F=.0001
      DZQ=DZ*DZ
      RCP=0.286
```

```
      DTG=DT*R/(2.*DX)
      DTX=DT/(2.*DX)
      DTF=DT*F
      DTZZ=DT/DZQ
      DTZ=DT/DZ
      GAR=9.8/(AA*R)
      GAR1=-9.8/(.001*R)
      PL(1)=PO
      DZX=DZ/(4.*DX)
C
C     COMPUTE INITIAL VERTICAL PRESSURE DISTRIBUTION
C
      DO 3 J=2,7
3     PL(J)=PL(1)*(TL(J)/TL(1))**GAR1
      DO 4 J=8,M
4     PL(J)=PL(7)*(TL(J)/TL(7))**GAR
C
C     COMPUTE INITIAL WATER VAPOUR DISTRIBUTION
C
      DO 5 J=1,7
5     QVL(J)=380./PL(J)*EXP(19.263-5262./TL(J))
      DO 6 J=8,M
6     QVL(J)=QVL(7)*(27-J)/20.
      DO 7 J=1,M
      UN(J)=UO
      DZR(J)=DZ*9.8/R
C
C     COMPUTE INITIAL VERTICAL POTENTIAL TEMPERATURE DISTRIBUTION
C
      TEL(J)=TL(J)*((100./PL(J))**.286)
C
C     INITIALIZE VECTORS AND MATRICES
C
      DO 7 I=1,L
      D(I)=0.
      T(I,J)=TL(J)
```

```
      QV1(I,J)=QVL(J)/1000.
      QV(I,J)=QVL(J)/1000.
      QW(I,J)=QWL(J)/1000.
      QW1(I,J)=QWL(J)/1000.
      V1(I,J)=0.
      U2(I,J)=0.
      U1(I,J)=0.
      U(I,J)=0.
      V(I,J)=0.
      W(I,J)=0.
      TE1(I,J)=0.
      TE(I,J)=0.
      P(I,J)=0.
      S(I,J)=0.
7     CONTINUE
      UN(1)=0.
      ZO=.02
      BETA1=2.5*ALOG((H+ZO)/ZO)
      BETA2=1./(.4*(H+ZO))
      ALPHA=(H**(-.3333)-ZO**(-.3333))/((H+DZ)**(-.3333)-ZO**(-.3333))
      CONST=1./(3.*(ZO**(-.333333)-(H+DZ)**(-.333333)))
      HOUR=0.
      K1=0
      K2=0
      DZR(1)=1.70708
      C(1)=0.
      DO 8 I=2,L
8     C(I)=1./(2.-C(I-1))
      WRITE (6,88)
      WRITE (6,89) L
      WRITE (6,90) M
      WRITE (6,91) DX
      WRITE (6,92) DZ
      WRITE (6,93) DT
      WRITE (6,94)
      WRITE (6,95) AA
```

```
      WRITE (6,96) UO
      WRITE (6,97) VO
      WRITE (6,98) TO
      POU=PO*10.
      WRITE (6,99) POU
      WRITE (6,100)
      WRITE (6,101)
      DO 9 K=1,M
      PLK=10.*PL(K)
      HI=H+(K-2)*DZ
      IF (K.EQ.1) HI=0.
      WRITE (6,102) K,TL(K),TEL(K),PLK,HI,QWL(K),QVL(K)
    9 CONTINUE
      DZQXQ=DZQ/(DX*DX)
      DTFC=DT*1.0616017E-4
      NK=L/2+2
      NV=NK+2
      NK1=NK-1
      ZXW=DZ/(8.*DX)
      DXQ=DX*DX
      DTZW=DT/(2.*DZ)
      DGZ=DT*R/(2.*DZ)
      M2=M-2
      L2=L-2
      CN=DZ*2.
      DZ2=2.*DZ
      PI1=3.14159265/180.
      PARA=H/(H+DZ)
      AB=4./3.
      DT2=DT
      E=8.0
      O=8.0
      RIA=9.8*(H+DZ)*(H+DZ)*(.00976-AA)/(UO*UO+VO*VO+1.E-5)
      AAA=(BETA1-DZ/(DZ+H)*(BETA1-H*BETA2)*.03*RIA)/(BETA1+BETA2*DZ)
      IF (RIA.GT.33.) AAA=PARA
      UN(2)=AAA*UO
```

```
      NK2=NK-2
      DTL=DT2/DX
10    E1=(K1*DT/3600.)
      DO 11 J=1,3
      DO 11 I=1,L
C
C     COMPUTE TOTAL HORIZONTAL WIND SPEED
C
      U2(I,J)=SQRT((U(I,J)+UO)**2+(V(I,J)+VO)**2)+1.E-5
11    TR(I,J)=TE(I,J)+TEL(J)
      TEBR=(TR(I,3)+TR(I,1))/2.
      DO 12 I=1,L
C
C     CALCULATE GRADIENT RICHARDSON NUMBER
C
      RI(I)=9.8/TEBR*(TR(I,3)-TR(I,1))*(H+DZ)/(U2(I,3)**2)
12    CONTINUE
      DO 14 I=1,L
      IF (RI(I).GT.-.03) GO TO 13
C
C     COMPUTE BOUNDARY LAYER PARAMETERS (UNSTABLE REGIME)
C
      Z(I)=SQRT(9.8*CONST/TEBR*(TR(I,1)-TR(I,3)))*((H+ZO)**AB)
      DTZ1(I)=-Z(I)/((M-2)*DZ)*DT2
      U2(I,2)=ALPHA*U2(I,3)
      TR(I,2)=ALPHA*TR(I,3)+(1.-ALPHA)*TR(I,1)
      QW(I,2)=ALPHA*QW(I,3)+(1.-ALPHA)*QW(I,1)
      QV(I,2)=ALPHA*QV(I,3)+(1.-ALPHA)*QV(I,1)
      U(I,2)=U2(I,2)/U2(I,3)*(U(I,3)+UO)-UN(2)
      V(I,2)=U2(I,2)/U2(I,3)*(V(I,3))
      TE1(I,2)=TR(I,2)-TEL(2)
      TE(I,2)=TE1(I,2)
      GO TO 14
13    CONTINUE
C
C     COMPUTE BOUNDARY LAYER PARAMETERS (STABLE REGIME)
```

```
C
      Z(I)=((.4*(H+ZO)*(1.-.03*RI(I)))**2)*U2(I,3)/(H+DZ)
      IF (RI(I).GT.33.) Z(I)=1.
      DTZ1(I)=-Z(I)/((M-2)*DZ)*DT2
      AA1=(BETA1-DZ/(DZ+H)*(BETA1-H*BETA2)*.03*RI(I))/(BETA1+BETA2*DZ)
      IF (RI(I).GT.33.) AA1=PARA
      AA2=1.-AA1
      U2(I,2)=U2(I,3)*AA1
      TR(I,2)=TR(I,3)*AA1+TR(I,1)*AA2
      QW(I,2)=QW(I,3)*AA1+QW(I,1)*AA2
      QV(I,2)=QV(I,3)*AA1+QV(I,1)*AA2
      U(I,2)=U2(I,2)/U2(I,3)*(U(I,3)+UO)-UN(2)
      V(I,2)=U2(I,2)/U2(I,3)*(V(I,3))
      TE1(I,2)=TR(I,2)-TEL(2)
      TE(I,2)=TE1(I,2)
14    CONTINUE
C
C     APPLY HORIZONTAL SMOOTHER TO WIND FIELD
C
      DO 15 I=2,L1
      DO 15 J=2,M1
      W(I,J)=.5*W1(I,J)+.25*(W1(I+1,J)+W1(I-1,J))
      U1(I,J)=.5*U(I,J)+.25*(U(I+1,J)+U(I-1,J))
15    V1(I,J)=.5*V(I,J)+.25*(V(I+1,J)+V(I-1,J))
C
C     APPLY LATERAL BOUNDARY CONDITIONS TO AUXILLARY FIELDS
C
      DO 16 J=2,M1
      U1(L,J)=U1(L1,J)
      V1(L,J)=V1(L1,J)
      QV1(1,J)=QV1(2,J)
      QW1(1,J)=QW1(2,J)
      V1(1,J)=V1(2,J)
      QV1(L,J)=QV1(L1,J)
      QW1(L,J)=QW1(L1,J)
      TE1(L,J)=TE1(L1,J)
```

```
      TE1(1,J)=TE1(2,J)
16    U1(1,J)=U1(2,J)
      DO 17 J=1,M1
      DO 17 I=1,L
      N=M-J
C
C     COMPUTE TEMPERATURE
C
      T(I,N)=(TE(I,N)+TEL(N))*((PL(N)+P(I,N)+P1(I,N)+G1(I,2))/100.)**RCP
C
C     COMPUTE HYDROSTATIC PRESSURE PERTURBATION
C
17    P(I,N)=(DZR(N)*(PL(N)/TL(N)-PL(N)/T(I,N))-P(I,N+1))/(DZR(N)/T(I,N)
     1-1.)
C
C     COMPUTE VERTICAL VELOCITY AT Z=H
C
      DO 18 I=2,L1
      W(I,2)=-ZXW*(U(I+1,2)-U(I-1,2))
18    W1(I,2)=W(I,2)
C
C     COMPUTE PHASE CHANGES DUE TO VERTICAL MOTION
C
      DO 20 I=2,L1
      DO 20 J=3,M1
      QS=.38/(PL(J)+P(I,J)+P1(I,J)+G1(I,2))*EXP(19.263-5262./T(I,J))
      IF (W(I,J).GE.0..AND.QV(I,J).LT.QS) GO TO 19
      IF (W(I,J).LT.0..AND.QW(I,J).LE.0.) GO TO 19
      S(I,J)=.034*QS*((39.77-.0264*T(I,J))/(336400.*QS+.0264*T(I,J)*T(I,
     1J)))*W(I,J)
      GO TO 20
19    S(I,J)=0.
20    CONTINUE
C
C     USE PREDICTION EQUATIONS MINUS NON-HYDROSTATIC PRESSURE AND ADVECT
C
```

```
      DO 26 J=3,M1
      DO 26 I=2,L1
      W1(I,J)=W(I,J)
      W1(I,J)=W1(I,J)+DTFC*U1(I,J)
      U(I,J)=U1(I,J)+DTF*V1(I,J)-DTFC*W(I,J)-DTG*T(I,J)/(PL(J)+P(I,J)+P1
     1(I,J)+G1(I,2))*(P(I+1,J)-P(I-1,J))+DTZZ*(U1(I,J+1)+UN(J+1)+U1(I,J-
     21)+UN(J-1)-2.*U1(I,J)-2.*UN(J))*Z(I)*(M-J)/(M-2)+DTZ1(I)*(U1(I,J+1
     3)+UN(J+1)-U1(I,J-1)-UN(J-1))/CN
      V(I,J)=V1(I,J)+DTZZ*(V1(I,J+1)+V1(I,J-1)-2.*V1(I,J))*Z(I)*(M-J)/(M
     1-2)+DTZ1(I)*(V1(I,J+1)-V1(I,J-1))/CN
      QW(I,J)=QW1(I,J)+S(I,J)*DT+DTZZ*(QW1(I,J+1)+QW1(I,J-1)-2.*QW1(I,J)
     1)*Z(I)*(M-J)/(M-2)+DTZ1(I)*(QW1(I,J+1)-QW1(I,J-1))/CN
      QV(I,J)=QV1(I,J)-S(I,J)*DT+DTZZ*(QV1(I,J+1)+QV1(I,J-1)-2.*QV1(I,J)
     1)*Z(I)*(M-J)/(M-2)+DTZ1(I)*(QV1(I,J+1)-QV1(I,J-1))/CN
      TE(I,J)=TE(I,J)+S(I,J)*2416.67*DT+DTZ1(I)*(TE1(I,J+1)+TEL(J+1)-TE1
     1(I,J-1)-TEL(J-1))/DZ2+DTZZ*(TE1(I,J+1)+TEL(J+1)+TE1(I,J-1)+TEL(J-1
     2)-2.*(TE1(I,J)+TEL(J)))*Z(I)*(M-J)/(M-2)
      IF (W(I,J)) 21,21,22
21    U(I,J)=U(I,J)-W(I,J)*(U1(I,J+1)-U1(I,J))*DTZ
      V(I,J)=V(I,J)-W(I,J)*(V1(I,J+1)-V1(I,J))*DTZ
      QV(I,J)=QV(I,J)-W(I,J)*(QV1(I,J+1)-QV1(I,J))*DTZ
      QW(I,J)=QW(I,J)-W(I,J)*(QW1(I,J+1)-QW1(I,J))*DTZ
      W1(I,J)=W1(I,J)-DTZ*W(I,J)*(W(I,J+1)-W(I,J))
      TE(I,J)=TE(I,J)-W(I,J)*(TE1(I,J+1)+TEL(J+1)-TE1(I,J)-TEL(J))*DTZ
C
C     USE UPSTREAM DIFFERENCES FOR ADVECTION TERMS
C
      GO TO 23
22    U(I,J)=U(I,J)-W(I,J)*(U1(I,J)+UN(J)-U1(I,J-1)-UN(J-1))*DTZ
      V(I,J)=V(I,J)-W(I,J)*(V1(I,J)-V1(I,J-1))*DTZ
      QV(I,J)=QV(I,J)-W(I,J)*(QV1(I,J)-QV1(I,J-1))*DTZ
      QW(I,J)=QW(I,J)-W(I,J)*(QW1(I,J)-QW1(I,J-1))*DTZ
      W1(I,J)=W1(I,J)-DTZ*W(I,J)*(W(I,J)-W(I,J-1))
      TE(I,J)=TE(I,J)-W(I,J)*(TE1(I,J)+TEL(J)-TE1(I,J-1)-TEL(J-1))*DTZ
23    CONTINUE
      IF ((U1(I,J)+UO)) 25,24,24
```

```
24      TE(I,J)=TE(I,J)-(U1(I,J)+UO)*(TE1(I,J)-TE1(I-1,J))*DTL
        V(I,J)=V(I,J)-DTL*(V1(I,J)-V1(I-1,J))*(U1(I,J)+UO)
        QV(I,J)=QV(I,J)-DTL*(QV1(I,J)-QV1(I-1,J))*(U1(I,J)+UO)
        QW(I,J)=QW(I,J)-DTL*(QW1(I,J)-QW1(I-1,J))*(U1(I,J)+UO)
        U(I,J)=U(I,J)-DTL*(U1(I,J)-U1(I-1,J))*(U1(I,J)+UO)
        W1(I,J)=W1(I,J)-DTL*(U1(I,J)+UO)*(W(I,J)-W(I-1,J))
        GO TO 26
25      TE(I,J)=TE(I,J)-(U1(I,J)+UO)*(TE1(I+1,J)-TE1(I,J))*DTL
        V(I,J)=V(I,J)-DTL*(V1(I+1,J)-V1(I,J))*(U1(I,J)+UO)
        QV(I,J)=QV(I,J)-DTL*(QV1(I+1,J)-QV1(I,J))*(U1(I,J)+UO)
        QW(I,J)=QW(I,J)-DTL*(QW1(I+1,J)-QW1(I,J))*(U1(I,J)+UO)
        U(I,J)=U(I,J)-DTL*(U1(I+1,J)-U1(I,J))*(U1(I,J)+UO)
        W1(I,J)=W1(I,J)-DTL*(U1(I,J)+UO)*(W(I+1,J)-W(I,J))
26      V(I,J)=V(I,J)-DTF*U1(I,J)
C
C       COMPUTE MOISTURE CORRECTION TERMS
C
        DO 28 I=2,L1
        DO 28 J=3,M1
        QS=.38/(PL(J)+P(I,J)+P1(I,J)+G1(I,2))*EXP(19.263-5262./T(I,J))
        DRDT=T(I,J)*T(I,J)/(QS*5262.)
        IF (QV(I,J).GE.QS) GO TO 27
        IF (QW(I,J).LE.0.) GO TO 28
        CQN=AMIN1(QS-QV(I,J),QW(I,J))
        QW(I,J)=QW(I,J)-CQN
        TE(I,J)=TE(I,J)-DRDT*CQN
        QV(I,J)=QV(I,J)+CQN
        GO TO 28
27      QW(I,J)=QW(I,J)+QV(I,J)-QS
        TE(I,J)=TE(I,J)+DRDT*(QV(I,J)-QS)
        QV(I,J)=QS
28      CONTINUE
C
C       APPLY TEMPERATURE WAVE TO LAND SURFACE
C
        DO 29 I=NK,L
```

```
      VAR=(I-NK1)*.5
      IF (I.GT.NV) VAR=2.
29    TE(I,1)=(5.+VAR/3.)*SIN(PI1*15.*(E1+O+16.))
C
C     APPLY TEMPERATURE WAVE TO SEA SURFACE
C
      DO 30 I=1,NK2
30    TE(I,1)=.5+SIN(PI1*15.*(E1+22))
      DO 32 I=1,L
      IF (QW(I,1).LE.0.) GO TO 31
      QV(I,1)=.38/(PL(1)+P(I,1)+P1(I,1)+G1(I,2))*EXP(19.263-5262./T(I,1)
     1)
      QW(I,1)=QWL(1)/1000.+QVL(1)/1000.-QV(I,1)
      GO TO 32
31    QW(I,1)=0.
      QV(I,1)=QWL(1)/1000.+QVL(1)/1000.
      QS=.38/(PL(1)+P(I,1)+P1(I,1)+G1(I,2))*EXP(19.263-5262./T(I,1))
      IF (QV(I,1).GT.QS) QW(I,1)=QV(I,1)-QS
      IF (QV(I,1).GT.QS) QV(I,1)=QS
32    CONTINUE
      TE(NK1,1)=.5*(TE(NK,1)+TE(NK-2,1))
C
C     APPLY BOUNDARY CONDITIONS TO FORECAST FIELDS
C
      DO 33 I=1,2
      NN=(L-3)*I-(L-5)
      N=L1*(I-1)+1
      DO 33 J=2,M1
      U(N,J)=U(NN,J)
      V(N,J)=V(NN,J)
      QW(N,J)=QW(NN,J)
      QV(N,J)=QV(NN,J)
33    TE(N,J)=TE(NN,J)
      DO 34 I=1,L
      DO 34 J=1,M1
      QW1(I,J)=QW(I,J)
```

```
      QV1(I,J)=QV(I,J)
34    TE1(I,J)=TE(I,J)
      DO 35 I=1,L
      G1(I,1)=1.25*U(I,M1)/18.25
      DO 35 J=2,M2
35    G1(I,1)=G1(I,1)+U(I,J)/18.25
      DO 36 I=2,L1
36    D(I)=(1.E-3*DX/DT*(G1(I-1,1)-G1(I,1))+D(I-1))*C(I)
      DO 37 I=2,L1
      N=L-I+1
37    G1(N,2)=G1(N+1,2)*C(N)+D(N)
      DO 38 I=2,L1
      DO 38 J=3,M1
38    U(I,J)=U(I,J)-DT/(DX*1.E-3)*(G1(I+1,2)-G1(I,2))
C
C     COMPUTE DIVERGENCE OF AUXILLARY VELOCITY FIELD
C
      DO 39 I=2,L1
      DO 39 J=3,M1
39    G2(I,J)=(U(I+1,J)-U(I-1,J))/(2.*DX)+(W1(I,J+1)-W1(I,J-1))/(2.*DZ)
      DO 40 I=2,L1
      DO 40 J=2,M1
40    G2(I,J)=G2(I,J)*DZQ*4.*(P(I,J)+PL(J)+P1(I,J)+G1(I,2))/(R*DT*T(I,J)
     1)
C
C     RELAX NON-HYDROSTATIC PRESSURE TO DIVERGENCE OF AUXILLARY VELOCITY
C
      ITER=0
      EPS=1.E-7
      ALAMDA=.7
41    K=0
      DO 42 I=3,L2
      DO 42 J=4,M2
      RES=P1(I,J+2)+P1(I,J-2)-(2.+2.*DZQXQ)*P1(I,J)+DZQXQ*(P1(I+2,J)+P1(
     1I-2,J))-G2(I,J)
      IF (ABS(RES).LT.EPS) GO TO 42
```

```
      P1(I,J)=P1(I,J)+(1.+ALAMDA)*RES/(2.+2.*DZQXQ)
      K=K+1
42    CONTINUE
      DO 45 I=3,L2
      RES=P1(I,5)-(1.+2.*DZQXQ)*P1(I,3)+DZQXQ*(P1(I+2,3)+P1(I-2,3))-G2(I
     1,3)
      IF (ABS(RES).LE.EPS) GO TO 43
      P1(I,3)=P1(I,3)+(1.+ALAMDA)*RES/(1.+2.*DZQXQ)
      K=K+1
43    RES=P1(I,M1-2)-(1.+2.*DZQXQ)*P1(I,M1)+DZQXQ*(P1(I+2,M1)+P1(I-2,M1)
     1)-G2(I,M1)
      IF (ABS(RES).LE.EPS) GO TO 44
      P1(I,M1)=P1(I,M1)+(1.+ALAMDA)*RES/(1.+2.*DZQXQ)
      K=K+1
44    CONTINUE
45    CONTINUE
      DO 47 J=4,M2
      RES=P1(2,J+2)+P1(2,J-2)-(2.+DZQXQ)*P1(2,J)+DZQXQ*P1(4,J)-G2(2,J)
      IF (ABS(RES).LE.EPS) GO TO 46
      K=K+1
      P1(2,J)=P1(2,J)+(1.+ALAMDA)*RES/(2.+DZQXQ)
46    RES=P1(L1,J+2)+P1(L1,J-2)-(2.+DZQXQ)*P1(L1,J)+DZQXQ*P1(L-3,J)-G2(L
     11,J)
      IF (ABS(RES).LE.EPS) GO TO 47
      K=K+1
      P1(L1,J)=P1(L1,J)+(1.+ALAMDA)*RES/(2.+DZQXQ)
47    CONTINUE
      RES=P1(2,5)-(1.+DZQXQ)*P1(2,3)+DZQXQ*P1(4,3)-G2(2,3)
      IF (ABS(RES).LE.EPS) GO TO 48
      K=K+1
      P1(2,3)=P1(2,3)+(1.+ALAMDA)*RES/(1.+DZQXQ)
48    RES=P1(2,M-3)-(1.+DZQXQ)*P1(2,M1)+DZQXQ*P1(4,M1)-G2(2,M1)
      IF (ABS(RES).LE.EPS) GO TO 49
      K=K+1
      P1(2,M1)=P1(2,M1)+(1.+ALAMDA)*RES/(1.+DZQXQ)
49    RES=P1(L1,M-3)-(1.+DZQXQ)*P1(L1,M1)+DZQXQ*P1(L-3,M1)-G2(L1,M1)
```

```
      IF (ABS(RES).LE.EPS) GO TO 50
      K=K+1
      P1(L1,M1)=P1(L1,M1)+(1.+ALAMDA)*RES/(1.+DZQXQ)
50    RES=P1(L1,5)-(1.+DZQXQ)*P1(L1,3)+DZQXQ*P1(L-3,3)-G2(L1,3)
      IF (ABS(RES).LE.EPS) GO TO 51
      K=K+1
      P1(L1,3)=P1(L1,3)+(1.+ALAMDA)*RES/(1.+DZQXQ)
51    CONTINUE
      ITER=ITER+1
C
C     ITER GREATER THAN 50 CAUSES TERMINATION OF PROGRAMME
C
      IF (ITER.GT.50) GO TO 54
      IF (K.GT.0) GO TO 41
C
C     APPLY NON-HYDROSTATIC PRESSURE TERMS TO PREDICTION EQUATIONS
C
      DO 52 I=2,L1
      DO 52 J=3,M1
      W1(I,J)=W1(I,J)-DGZ*(P1(I,J+1)-P1(I,J-1))*T(I,J)/(P(I,J)+P1(I,J)+P
     1L(J)+G1(I,2))
      U(I,J)=U(I,J)-DTG*(P1(I+1,J)-P1(I-1,J))*T(I,J)/(P(I,J)+P1(I,J)+PL(
     1J)+G1(I,2))
52    CONTINUE
      DO 53 I=2,L1
      DO 53 J=2,M1
      U1(I,J)=U(I,J)
53    W(I,J)=W1(I,J)
54    CONTINUE
      K1=K1+1
      K2=K2+1
C
C     DISPLAY RESULTS EVERY TWO HOURS
C
      IF (K2.LT.IFIX(7200./DT)) GO TO 10
      K2=0
```

```
      HOUR=HOUR+2.
      TIME=HOUR+8.
      IF (TIME.GT.24.) TIME=TIME-24.
      IF (HOUR.GT.22.) IDAY=2
      WRITE (6,74) TIME,IDAY
      WRITE (6,75)
      N=L-21
      DO 55 I=N,L1
      DO 55 J=1,M
55    Q1NEW(I,J)=U(I,J)+UN(J)
      DO 56 K=1,M
      J=M+1-K
56    WRITE (6,76) (Q1NEW(I,J),I=N,L1)
      WRITE (6,77)
      DO 57 K=1,M
      J=M+1-K
57    WRITE (6,78) (V(I,J),I=N,L1)
      WRITE (6,105)
      DO 58 K=1,M
      J=M+1-K
58    WRITE (6,106) (QV(I,J),I=N,L1)
      WRITE (6,104)
      DO 59 K=1,M
      J=M+1-K
59    WRITE (6,106) (QW(I,J),I=N,L1)
      WRITE (6,79)
      DO 60 I=1,L
      DO 60 J=1,M
60    Q1NEW(J,I)=W(I,J)*100.
      C1=1.
      CALL MAPPA (Q1NEW,C1)
      DO 61 I=1,L
      DO 61 J=1,M
61    T(I,J)=T(I,J)-273.16
      WRITE (6,80)
      DO 62 I=1,L
```

```
      DO 62 J=1,M
62    Q1NEW(J,I)=T(I,J)
      C1=1.
      CALL MAPPA (Q1NEW,C1)
      DO 63 J=1,M
      DO 63 I=1,L
      W1(I,J)=P(I,J)+P1(I,J)+G1(I,2)+PL(J)
63    T(I,J)=T(I,J)+273.16
      WRITE (6,83)
      DO 64 K=1,M
      J=M+1-K
64    WRITE (6,81) (W1(I,J),I=N,L1)
      DO 65 I=2,L1
      DO 65 J=3,M1
      V1(I,J)=(W(I,J+1)-W(I,J-1))/(2.*DZ)+(U(I+1,J)-U(I-1,J))/(2.*DX)
      V1(I,J)=V1(I,J)*100.
      G2(I,J)=(U(I,J+1)-U(I,J-1))/(2.*DZ)-(W(I+1,J)-W(I-1,J))/(2.*DX)
65    U1(I,J)=(V(I+1,J)-V(I-1,J))/(2.*DX)
      DO 66 I=N,L1
      V1(I,2)=0.
      G2(I,2)=0.
66    U1(I,2)=0.
      WRITE (6,84)
      DO 67 K=1,M
      J=M+1-K
67    WRITE (6,87) (V1(I,J),I=N,L1)
      WRITE (6,85)
      DO 68 K=1,M
      J=M+1-K
68    WRITE (6,87) (G2(I,J),I=N,L1)
      WRITE (6,86)
      DO 69 K=1,M
      J=M+1-K
69    WRITE (6,87) (U1(I,J),I=N,L1)
      DO 70 I=1,L
      DO 70 J=1,M
```

```
      W1(I,J)=W(I,J)
      V1(I,J)=V(I,J)
70    U1(I,J)=U(I,J)
      IF (ITER.GT.50) GO TO 71
      IF (HOUR.LT.FLOAT(IT)) GO TO 10
71    CONTINUE
      WRITE (6,103)
      STOP
C
72    FORMAT (3I12)
73    FORMAT (3E12.4)
74    FORMAT (1H1,30X,5HHOUR=,F5.2,3X,3HDAY,I4//)
75    FORMAT (1X,20X,28HVELOCITY FIELD U (METER/SEC)//)
76    FORMAT (1H ,21F6.2/)
77    FORMAT ('1',20X,28HVELOCITY FIELD V (METER/SEC)//)
78    FORMAT (1H ,21F6.2/)
79    FORMAT (1H1,20X,28HVERTICAL VELOCITY W (CM/SEC))
80    FORMAT (1H1,20X,17HTEMPERATURE FIELD)
81    FORMAT (1H ,21F6.2/)
82    FORMAT (6E12.4)
83    FORMAT (1H1,20X,14HPRESSURE FIELD//)
84    FORMAT ('1',15X,38HDIVERGENCE OF THE WIND FIELD          //)
85    FORMAT ('1',15X,38HVORTICITY COMPONENT IN THE Y DIRECTION//)
86    FORMAT ('1',15X,38HVORTICITY COMPONENT IN THE Z DIRECTION//)
87    FORMAT (1H ,4P21F6.1/)
88    FORMAT ('1',22HFINITE DIFFERENCE DATA///)
89    FORMAT (1X,34HNUMBER OF HORIZONTAL GRID POINTS  ,I7/)
90    FORMAT (1X,34HNUMBER OF VERTICAL GRID POINTS    ,I7/)
91    FORMAT (1X,34HHORIZONTAL INCREMENT (METERS)     ,F7.1/)
92    FORMAT (1X,34HVERTICAL INCREMENT (METERS)       ,F7.1/)
93    FORMAT (1X,34HTIME STEP (SECONDS)               ,F7.1/////)
94    FORMAT (1X,18HINITIAL CONDITIONS//)
95    FORMAT (1X,34HLAPSE RATE (DEG./M.)              ,F7.4/)
96    FORMAT (1X,34HU COMPONENT (M./SEC.)             ,F7.1/)
97    FORMAT (1X,34HV COMPONENT (M./SEC.)             ,F7.1/)
98    FORMAT (1X,34HSURFACE TEMPERATURE               ,F7.1/)
```

```
99     FORMAT (1X,34HSURFACE PRESSURE                    ,F7.1/)
100    FORMAT ('1',14HINITIAL FIELDS///)
101    FORMAT (1X,3HROW,15X,11HTEMPERATURE,7X,15HPOTENTIAL TEMP.,3X,8HPRE
      1SSURE,10X,6HHEIGHT,12X,12HLIQUID WATER,6X,12HWATER VAPOUR//)
102    FORMAT (1X,I2,15X,F6.1,12X,F6.1,11X,F7.1,11X,F7.1,12X,F7.1,15X,F7.
      12/)
103    FORMAT ('1')
104    FORMAT ('1',12HLIQUID WATER/)
105    FORMAT ('1',12HWATER VAPOUR/)
106    FORMAT (1X,3P21F6.2/)
       END
```

```
      SUBROUTINE MAPPA (Q1NEW,C1)
      DIMENSION Q1NEW(30,30), ANS(2,121), IANS(120), LE(11)
      DATA LE/1H0,1H1,1H2,1H3,1H4,1H5,1H6,1H7,1H8,1H9,1H /
      I=19
      NZ=28
      N=6
      JB=6
1     L=I+1
      WRITE (6,11) (L,(Q1NEW(L,J),J=N,NZ))
      DO 2 J=N,NZ
      XDIF=(Q1NEW(I+1,J)-Q1NEW(I,J))/3.0
      JX=1+5*(J-JB)
      ANS(2,JX)=Q1NEW(I,J)+XDIF
2     ANS(1,JX)=ANS(2,JX)+XDIF
      DO 3 J=N,NZ
      JX=1+5*(J-JB)
      DO 3 L=1,2
      YDIF=(ANS(L,JX+5)-ANS(L,JX))/5.0
      M1=JX+1
      M6=JX+4
      DO 3 M=M1,M6
3     ANS(L,M)=ANS(L,M-1)+YDIF
      DO 9 L=1,2
      DO 8 M=1,120
      IF (ANS(L,M)) 4,6,6
4     AANS=(-1.0)*ANS(L,M)
      KANS=C1*AANS
      IF (MOD(KANS,2).EQ.0) GO TO 7
5     KANS=KANS-10*(KANS/10)
      IANS(M)=LE(KANS+1)
      GO TO 8
6     KANS=C1*ANS(L,M)
      IF (MOD(KANS,2).EQ.0) GO TO 5
7     IANS(M)=LE(11)
8     CONTINUE
9     WRITE (6,12) (IANS(M),M=1,115)
```

```
      I=I-1
      IF (I-1) 10,1,1
10    CONTINUE
      L=1
      WRITE (6,11) (L,(Q1NEW(L,J),J=N,NZ))
      RETURN
C
11    FORMAT (I5,3X,23F5.1)
12    FORMAT (10X,115A1)
      END
```